International Workshop on Synchrotron High-Pressure Mineral Physics and Materials Science

December 6 and 7, 2007

Advanced Photon Source
Argonne National Laboratory
Argonne, Illinois USA

Organized by

Tetsuo Irifune
Geodynamics Research Center, Ehime University, Japan
Yanbin Wang
GSECARS, The University of Chicago, USA

Acknowledgments

This workshop is partly supported by the Center for Advanced Radiation Sources at The University of Chicago and by the Gakujutsu-sousei grant-in-aid from the Japan Society for the Promotion of Science to T. Irifune.

GeoSoilEnviroCARS (GSECARS) is supported by the National Science Foundation–Earth Sciences (EAR-0622171) and the U.S. Department of Energy–Geosciences (DE-FG02-94ER14466). Use of the Advanced Photon Source was supported by the U.S. Department of Energy, Office of Science, Office of Basic Energy Sciences, under Contract No. DE-AC02-06CH11357.

Contents

Acknowledgments ii
Getting to Argonne National Laboratory v
Special Issue of High Pressure Research vi

Program 1

Session I: Synchrotron High-pressure Facilities and Related Developments 7
New developments in diamond anvil cell facilities at GSECARS 8
Recently developed DAC technique at SPring-8 to study deep Earth materials 10
New progress in high-pressure research at HPCAT 12
Recent advances in large-volume high-pressure research at GSECARS 13
Development of Kawai-type MA with SD anvils and its application: Equation of state of MgSiO3-perovskite 14
Development of a CsCl pressure standard and its use in testing a series of multi-anvil cells 16
Ultrasonic measurements in multi-stage multi-anvil devices 18

Session II: Neutrons and New Techniques 21
Recent progress on high-pressure neutron beamline at J-PARC in Japan 22
Prospects for neutron diffraction under extreme pressure conditions at the new Spallation Neutron Source 24
Geophysics studies with high-resolution X-ray spectroscopy 25
Magnetic spectroscopy at high pressure using XMCD 26
Volumetric properties of amorphous materials at high pressure by computed tomography 27
A scanning angle energy-dispersive X-ray diffraction (SA-EDXD) technique for studying the structure of materials at high pressure in diamond anvil cells 28

Session III: Ultrahard and Other Materials 29
Synthesis of large and high-quality nano-polycrystalline diamond and its potential applications to high-pressure mineral physics 30
High-pressure and high-temperature experiments using nanocrystalline diamond anvil and laser heating 32
Precision laser machining of nano-polycrystalline diamond 34
High-pressure deformation study of nanocrystalline nickel 35
Electron-lattice interaction under high pressure examined by single-crystal diffraction study 36
New synchrotron-based single-crystal methods for structural mineral physics and materials science 38
Novel structural phase transition of vanadium under high pressure 40
Determination of the high-pressure phases (II′ and IV′) of CuGeO3 using single-crystal techniques 44
Equation of state and pressure-induced transition(s) in B4C: Correlation of static high-pressure synchrotron XRD, Raman, and shock-wave data 47

Session IV: Mineral Physics Applications 49
Synchrotrons: A core business? 50
Effect of pressure on the melting behavior of the Fe-S system at moderate pressures 51
In situ observation of immiscible liquids in the Fe-O-S system at 3 GPa using an X-ray radiographic technique 52
Inelastic X-ray scattering experiments on liquids in diamond anvil cells 54
Time-resolved X-ray diffraction experiment of dehydration of serpentine at high pressure 56
Partitioning of iron between perovskite, post-perovskite, and ferropericlase up to 154 GPa and 2000 K 58
Ultrasonic measurements of polycrystalline MgO and standard-free pressure calibration at high pressures and high temperatures 60

Poster Abstracts 63
Materials Science 65
Mineral Physics 71
New Techniques 85

Author Index 105

Getting to Argonne National Laboratory

Argonne National Laboratory
9700 S. Cass Avenue, Argonne, IL 60439
630-252-2000

Argonne is located about 25 miles southwest of Chicago's Loop. Maps are available at http://www.anl.gov/Visiting/anlil.html.

To reach Argonne from O'Hare International Airport, take I-294 south to I-55. Exit west on I-55 (toward St. Louis) and continue for about four miles to Cass Avenue. Exit south on Cass and turn right at the Argonne sign on Northgate Road , immediately south of I-55. Follow Northgate Road to the Argonne Information Center.

To reach Argonne from Midway Airport, take Cicero Avenue north to I-55. Enter I-55 south and continue for about 14 miles to Cass Avenue. Exit south on Cass and turn right at the Argonne sign on Northgate Road, immediately south of I-55. Follow Northgate Road to the Argonne Information Center.

To reach Argonne by public transportation, take the Metra train to the Westmont Metra station. PACE bus #715 leaves the Burlington/Westmont station at 7:22 a.m. and 7:58 a.m., arriving at the Argonne Information Center at 7:35 a.m. and 8:14 a.m., respectively. In the evening, PACE bus #715 leaves the Argonne Information Center at 5:25 p.m., arriving at the Westmont Metra station at 5:42 p.m. Because the bus schedule is subject to change by PACE without notice, visitors planning on using public transportation to reach Argonne are advised to verify the bus schedule by calling PACE at 847-364-7223 or visiting the Pace home page, http://www.pacebus.com/.

Special Issue of High Pressure Research

We are pleased to announce that the research presented at the workshop will be featured in a special issue of the international journal *High Pressure Research*. The title of the issue will be "High-Pressure Mineral Physics and Materials Science with Synchrotron and Other Radiation Sources."

To be considered for publication in the special issue, we must receive your manuscript by **January 31, 2008**. All papers will be peer-reviewed. We expect to finish the review process by March 31, 2008, and the issue will be published within 2008.

Send manuscripts to Yanbin Wang, wang@cars.uchicago.edu.

Program

Wednesday, December 5, 2007

Registration: 4:00 – 6:00 PM (Argonne Guest House Lobby)

Thursday, December 6, 2007

Registration: 8:00 – 9:00 AM (Lobby, Bldg. 402, APS Conference Center)

Session I. Synchrotron High-pressure Facilities and Related Developments

(Bldg. 402, Room E1100/E1200)

Time	Speaker	Affiliation	Title
9:00	Rivers, Mark	GSECARS, Univ. Chicago, USA	Welcome and introduction to APS
9:10	Prakapenka, Vitali	GSECARS, Univ. Chicago, USA	New developments in the diamond cell facilities at GSECARS
9:35	Ohishi, Yasuo	JASRI, SPring-8, Japan	Recently developed DAC technique at SPring-8 to study deep earth materials
10:00	Shen, Guoyin	HPCAT, CIW, USA	New progress in high-pressure research at HPCAT
10:20	Coffee Break		
10:40	Wang, Yanbin	GSECARS, Univ. Chicago, USA	Recent advances in large-volume high-pressure research at GSECARS
11:00	Tange, Yoshinori	GRC, Ehime Univ., Japan	Development of Kawai-type MA with SD anvils and its application: Equation of state of $MgSiO_3$-perovskite
11:20	Leinenweber, Kurt	Arizona State Univ., USA	Development of a CsCl pressure standard and its use in testing a series of multi-anvil cells
11:40	Mueller, Hans	GeoForschungsZentrum Potsdam, Germany	Ultrasonic measurements in multi-stage, multi-anvil devices
12:00	Lunch (Bldg. 402 Gallery, downstairs)		
13:00	Group photo and APS tour		

Section II. Neutrons and New Techniques

(Bldg. 402, Room E1100/E1200)

Time	Speaker	Affiliation	Title
14:00	Kagi, Hiroyuki	Tokyo Univ., Japan	Recent progress on high-pressure neutron beamline at J-PARC in Japan
14:25	Tulk, Chris	ORNL, USA	Prospects for neutron diffraction under extreme pressure conditions at the new Spallation Neutron Source
14:50	Sturhahn, Wolfgang	APS, USA	Geophysics studies with high-resolution X-ray spectroscopy
15:10	Haskel, Daniel	APS, USA	Magnetic spectroscopy at high pressure using XMCD
15:30	Lesher, Charles	UC Davis, USA	X-ray microtomography at high pressure
15:50	Yang, Wenge	HPCAT, CIW, USA	A scanning angle energy-dispersive X-ray diffraction (SA-EDXD) technique for studying the structure of materials at high pressure in the diamond anvil cell
16:10	Poster overviews (2 min presentations in alphabetical order by last names)		
17:00	Posters and refreshment (Bldg. 402 Gallery, downstairs)		
19:00	Dinner (Argonne Guest House dinning room)		

Friday, December 7, 2007

Section III. Ultrahard and Other Materials

(Bldg. 402, Room E1100/E1200)

Time	Speaker	Affiliation	Title
9:00	Irifune, Tetsuo	GRC, Ehime Univ., Japan	Synthesis of large and high-quality nano-polycrystalline diamond and its potential applications to high-pressure mineral physics
9:25	Ohfuji, Hiroaki	GRC, Ehime Univ., Japan	High-pressure and high-temperature experiments using nanocrystalline diamond anvil and laser heating
9:45	Okuchi, Takuo	Nagoya Univ., Japan	Precision laser machining of nano-polycrystalline diamond
10:05	Wang, Yuejian	LANL, USA	High-pressure deformation study of nanocrystalline nickel

Section III. Ultrahard and Other Materials — Continued

(Bldg. 402, Room E1100/E1200)

Time	Speaker	Affiliation	Title
10:25	Coffee Break		
10:50	Yamanaka, Takamitsu	Geophysical Laboratory, CIW, USA	Electron-lattice interaction under high pressure examined by single-crystal diffraction study
11:15	Dera, Przemyslaw	GSECARS, Univ. Chicago, USA	New synchrotron-based single-crystal methods for structural mineral physics and materials science
11:30	Ding, Yang	HPSynC, USA	Novel structural phase transition of vanadium under high pressure
11:50	Borkowski, Lauren	UNLV/GSECARS, USA	Determination of the high-pressure phases (II′ and IV′) of $CuGeO_3$ using single-crystal technique
12:10	Manghnani, Murli	Hawaii Univ., USA	Equation of state and pressure induced transition(s) in B_4C: Correlation of static high-pressure synchrotron XRD, Raman, and shock-wave data
12:30	Lunch (Bldg 402 Gallery, downstairs)		

Section IV. Mineral Physics Applications

(Bldg. 402, Room E1100/E1200)

Time	Speaker	Affiliation	Title
14:00	Fiquet, Gillaume	Université Paris 6 et 7, France	Synchrotrons: A core business?
14.25	Chen, Bin	UIUC, USA	Effect of pressure on the melting behavior of the Fe-S system at moderate pressures
14:45	Tsuno, Kyusei	Bayreuth, Germany	In situ observation of liquid immiscibility in the Fe-O-S melt at high pressure using an X-ray radiographic technique
15:05	Alatas, Ahmet	APS, USA	Inelastic X-ray scattering experiments on liquids in diamond anvil cells
15:25	Coffee Break		
15:50	Inoue, Toru	GRC, Ehime Univ., Japan	Time-resolved X-ray diffraction experiment of dehydration of serpentine at high pressure
16:10	Sakai, Takeshi	Tohoku Univ., Japan	Partitioning between perovskite, post-perovskite, and ferropericlase up to 154 GPa and 2000 K
16:30	Kono, Yoshio	GRC, Ehime Univ., Japan	Ultrasonic velocity measurements of polycrystalline MgO and standard free pressure calibration at high pressures and high temperatures
16:50	Irifune, Tetsuo	GRC, Ehime Univ., Japan	Closing remarks
17:00	Adjourn		
18:00	No-host dinner (interested persons meet in Guest House lobby)		

Posters (Thursday, December 6, 2007)

Posters are displayed in the Building 402 Gallery (downstairs) and arranged in alphabetical order by surname within each topic section.

Presenter	Affiliation	Title
	Materials Science	
Yu, Tony	Stony Brook Univ.	Synthesis and strength measurement of superhard B_6O at high pressure and temperature
Kharlamova, Svetlana	APS	Pressure-induced phase transitions in gadolinium iron borate materials
Yusa, Hitoshi	NIRIM	Post-corundum phases in Ga_2O_3 and In_2O_3: X-ray diffraction experiments and theoretical computations
Zhang, Jianzhong	LANL	Elastic properties of $BaCe_{1-x}Y_xO_{3-0.5x}$ perovskite: effect of oxygen vacancy and pressure-induced softening
Zhao, Yusheng	LANL	Graphic derivations of high P-T thermo-mechanics for polycrystalline materials
	Mineral Physics	
Gao, Lili	UIUC	Magnetic transition and sound velocities of Fe_3C at high pressure
Lavina, Babara	GSECARS	Effect of cation ordering on the spinel elastic properties
Nakajima, Yoichi	Tokyo Institute of Technologies	Effect of hydrogen and carbon on the melting temperature of iron
Sanehira, Takeshi	GSECARS, Univ. Chicago	Density changes of pyrolite and MORB near the 660 km seismic discontinuity by in-situ X-ray diffraction measurements and chemical composition analyses
Scott, Henry	Indiana Univ., South Bend	Room temperature equation of state for Fe_2P
Shinmei, Toru	GRC, Ehime Univ.	Density and Fe-Mg partitioning changes in pyrolite to 50 GPa
Whitaker, Matthew	Stony Brook Univ.	Combined in situ synchrotron X-ray diffraction and ultrasonic interferometry study of epsilon-FeSi at high pressure and temperature

Presenter	Affiliation	Title
	New Techniques	
Arakawa, Masashi	Univ. Tokyo	Vibrational spectroscopic analysis of CO_2 fluids at high pressure
Higo, Yuji	JASRI, SPring-8	Elastic wave velocity measurements under the condition of lowermost mantle transition region
Knight, Jason	LBNL	The study of binary chemical reactions at high pressure and high temperature using an imaging system and laser heated diamond anvil cell
Liu, Haozhe	Harbin Institute of Technology, China	High-pressure diamond anvil cell studies using synchrotron micro-tomography and high energy X-ray scattering techniques
Nishiyama, Norimasa	GRC, Ehime Univ.	Concept of a new large volume D-DIA: MADONNA
Odake, Shoko	Univ. Tokyo	Development of spectroscopic three-dimensional stress imaging technique around mineral inclusions in diamond
Rivers, Mark	GSECARS, Univ. Chicago	Gas loading system
Sanehira, Takeshi	GSECARS, Univ. Chicago	Johnson noise thermometry at high pressure
Urakawa, Satoru	Okayama Univ.	Development of high-pressure and high-temperature X-ray tomography technique: Application to sessile drop interfacial energy measurement
Zhai, Shuangmeng	ISEI, Okayama Univ.	Pressure generation and observation of post-perovskite phase in MnGeO3 and MgGeO3 by in situ X-ray diffraction using sintered diamond anvils
Zhao, Jiyong	APS	Nuclear resonant scattering under simultaneous high pressure and high temperature at 3-ID, APS

Session I:

Synchrotron High-pressure Facilities and Related Developments

New developments in diamond anvil cell facilities at GSECARS

Vitali PRAKAPENKA (University of Chicago, USA, prakapenka@cars.uchicago.edu), Mark RIVERS (University of Chicago, USA, rivers@cars.uchicago.edu), Steve SUTTON (University of Chicago, USA, sutton@cars.uchicago.edu)

1. Introduction

The main goal of the diamond anvil cell (DAC) program at GSECARS is to address key geochemical and geophysical problems across the entire pressure-temperature range of the Earth and other terrestrial planets. The DAC experiments cover all the major aspects of in-situ studies of minerals and non-crystalline materials at extreme conditions utilizing the wide range of experimental techniques available at GSECARS: micro-X-ray diffraction with monochromatic radiation, inelastic X-ray scattering (X-ray Raman), X-ray emission spectroscopy, X-ray fluorescence microprobe, X-ray absorption and radiography [1].

To maintain the GSECARS high pressure instrumentation as state-of-the-art research tools we are continuously investing in the latest technological tools to help the high pressure user community perform their research at the highest potential. This talk summarizes a few new developments in the diamond anvil cell facilities at GSECARS, sector 13 at the Advanced Photon Source.

2. Results and discussion

Laser heating plays an essential role for in-situ high pressure high temperature studies of physical-chemical properties of minerals in the DAC at relevant Earth mantle-core conditions. Working in the multi-Mbar pressure range, that requires very small samples, especially stable and controllable laser beams are crucial. To accomplish this, we have replaced the old lasers heating system based on lump pumped lasers with a new class of fiber lasers. The new laser heating system at GSECARS is based on the two diode pumped single mode CW Ytterbium fiber lasers with total output power up to 200W and wavelength of 1064nm. Special beam shaping optics combined with the unique properties of the fiber laser (feedback enforced power control and pointing stability, nearly ideal beam shape for TEM00 (M2 < 1.1) mode, extremely low divergence etc) allow us to control focused laser beam size and shape (flat top) at the sample position in DAC resulting in superior stability and laser heating uniformity at extreme conditions (Fig. 1).

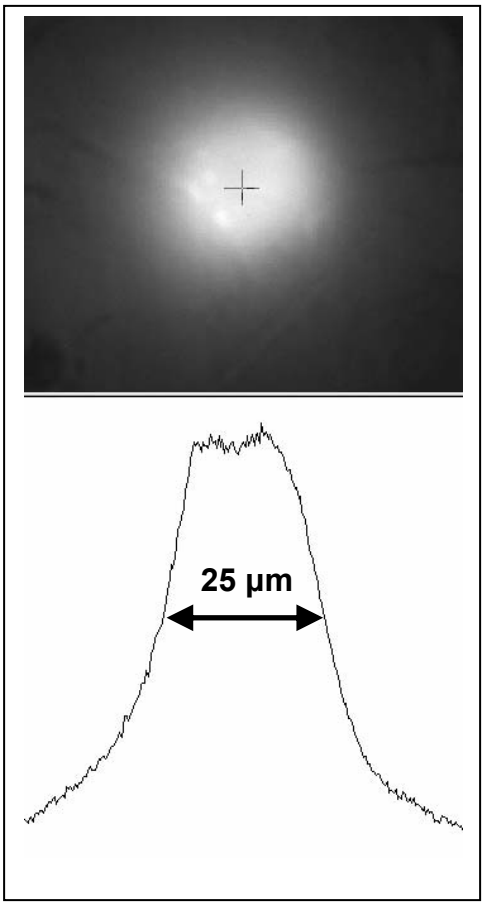

Fig. 1. The typical image and profile of the flat top laser heated spot on the Pt foil.

Significant improvements have been achieved for high-pressure micro-diffraction measurements by (1) reducing stray radiation background, (2) cleaning and tightly focusing the brilliant synchrotron beam, and (3) replacing WC seats in the DAC with X-ray transparent cubic BN. As a result, the very challenging DAC experiments at multi-Mbar pressures can be routinely conducted in-situ at high temperatures with double-side laser heating. Diffraction patterns uncontaminated by any additional reflections from high-Z gaskets can be collected from low-Z samples in the DAC with gasket holes down to 25 microns in diameter – a typical size for experiments in the Mbar pressure range.

Installation of a CO_2 laser heating system in 13ID-D at GSECARS is being supported by COMPRES as an infrastructure project for studying transparent materials (oxides, Mg-silicates) which cannot be efficiently heated with our existing near-infrared fiber lasers. At the moment, the on-line CO_2 laser heating system is in process of undergoing commissioning.

The main advantage of combining Brillouin spectroscopy with X-ray diffraction is the ability for simultaneous measurements of velocities and bulk modulus Ks (by Brillouin), and the volume/density (by XRD) independent of any pressure standard. A Brillouin spectroscopy system has been installed in the 13BM-D station which opens a new area of *in-situ* studies for materials at extreme conditions [2]. With this system that is unique in the world, it is now possible to measure sound velocities and densities of materials simultaneously, resulting in an absolute pressure scale and determinations of important material properties (e.g., equations of state and elasticity) as a function of pressure and temperature. High resolution X-ray diffraction and Brillouin spectroscopy collected simultaneously from the same sample area and in the same pressure-temperature environment provide information essential for interpreting seismic observations and constraining models of the composition and evolution of the Earth.

In addition to the existing Brillouin system in 13BM-D station we have installed a spectrometer covering a wide optical spectral range from 500nm to 1600nm that can be used for on-line low and high temperature measurements, Raman spectroscopy, and pressure determination using the ruby luminescence method. Thus, the full spectroscopic characterization of a sample is possible in-situ at extreme high pressure/temperature conditions with the powerful combination of X-ray diffraction, laser heating, Brillouin and Raman spectroscopy applied to a single point on the sample in a DAC at 13BM-D station.

Sample preparation is a crucial aspect of high pressure research and plays an important role in stable and controllable heating in the DAC, especially at multi-Mbar pressures. A vital part of successful sample loading in the DAC is selecting an appropriate pressure medium. The rare gases are preferred pressure media owing to the following properties: hydrostatic over a wide pressure range, low thermal conductivity, optical transparency, chemically inert, etc. Recently, with financial support from COMPRES, we have designed and built a gas-loading system at GSECARS, which allows loading of DACs with various high-pressure gases (including low-Z gases such as H_2, He), gas mixtures, or liquid-gas mixtures at room temperature. The system is currently undergoing commissioning.

References

[1] Shen, G., V. B. Prakapenka, P. J. Eng, M. L. Rivers, S. R. Sutton (2005), J. Synchrotron Rad., 12:642-649.

[2] Sinogeikin, S., J. Bass, V. Prakapenka, D. Lakshtanov, G. Shen, C. Sanchez-Valle, and M. Rivers. (2006), *Rev. Sci. Instrum.*, **77:** 103905-11.

Recently developed DAC technique at SPring-8 to study deep Earth materials

Yasuo OHISHI (JASRI/SPring-8, Japan, ohishi@spring8.or.jp), Naohisa HIRAO (JASRI/SPring-8, Japan, hirao@spring8.or.jp), Motohiko MURAKAMI (Okayama Univ., Japan, mthk@misasa.okayama-u.ac.jp), Kei HIROSE (kei@geo.titech.ac.jp)

1. Introduction

Recent advance in DAC technique has extended drastically the upper the pressure limit, approaching 400GPa, which corresponds to pressure of the Earth center. In succeeding years, a lot of X-ray techniques using DAC and third generation synchrotron radiation facilities have been developed. The beamline BL10XU of SPring-8 is a conventional synchrotron radiation -ray diffraction station for high pressure DAC experiments, and technological upgrades at BL10XU has been continuing, such as improvements of an X-ray micro-focusing optics, a laser-heating system, a double-crystal mono-chromator, an undulator X-ray source for higher energy X-rays, and several experimental environ-ments. Especially, high-flux X-ray diffraction and laser-heating system of BL10XU brought us the excellent discovery of post–perovskite structural phase transition of $MgSiO_3$.

Recently, in order to obtain complex structural parameters and to perform accurate/efficient high pressure experiments, we have installed various simultaneous measurement systems of X-ray diffraction combined with the Brillouin scattering, the Raman scattering spectroscopy, the electrical conductivity measurement, and so on. The Brillouin scattering measurement system combined with XRD and laser heating system at BL10XU, allows us to successfully obtain the high quality sound velocity data and density data under high pressure and high temperature conditions relevant to that of Earth's deep interior [1].

Other advanced synchrotron radiation X-ray techniques using DAC, X-ray absorption spectroscopy, X-ray Raman spectroscopy, nuclear resonant scattering, and high resolution X-ray inelastic scattering, are attractive to study the Earth's materials. Mössbauer spectroscopy is one of the most important techniques to reveal the electronic and magnetic properties of iron and iron compounds in deep Earth. Recently developed energy-domain synchrotron radiation (SR) Mössbauer spectroscopy [2], which is different method from the time resolved technique, enabled us to easily achieve multimagabar measurements using a DAC.

We will present two recent attractive techniques in order to investigate the deep Earth's materials, which are newly developed Brillouin scattering and X-ray diffraction simultaneous measurement system with laser-heating and advanced energy-domain SR Mössbauer spectroscopy method.

2. Combined Brillouin Scattering Spectroscopy and X-ray Diffraction Measurement System

In order to model the Earth's interior, we have to understand elastic properties of minerals under the conditions of the Earth's interior. From Brillouin scattering spectroscopy (BLS), we can directly measure the sound velocities of the Earth's materials. With the density data of the materials from X-ray diffraction (XRD), we can calculate the shear modulus and bulk modulus of the materials under extreme conditions.

A combined measurement system of BLS and XRD has been equipped recently and is currently in operation in APS [3]. However, a major barrier for resistive heating of sample in DAC is the technical difficulties to generate the relevant temperature conditions of the lower mantle, which generally reaches ~1500 K at most. Our new developed Brillouin scattering measurement system is combined with an infrared laser (CO_2 laser) heating technique. The system consists of three optical components of BLS (a Fabry-Perot interferometer, a diode laser (532 nm), optics, and DAC stages), XRD (incident X-ray optics and X-ray CDD) and infrared laser heating (CO_2 laser, optics and spectroradiometric temperature monitor).

We have succeeded to obtain the Brillouin scattering spectra at high pressures and high temperatures during infrared laser heating for both solid polycrystalline and liquid phases. This technique enables us to investigate the elastic properties and seismic wave velocity data for deep Earth's materials, providing the strong constraints on the Earth mantle models.

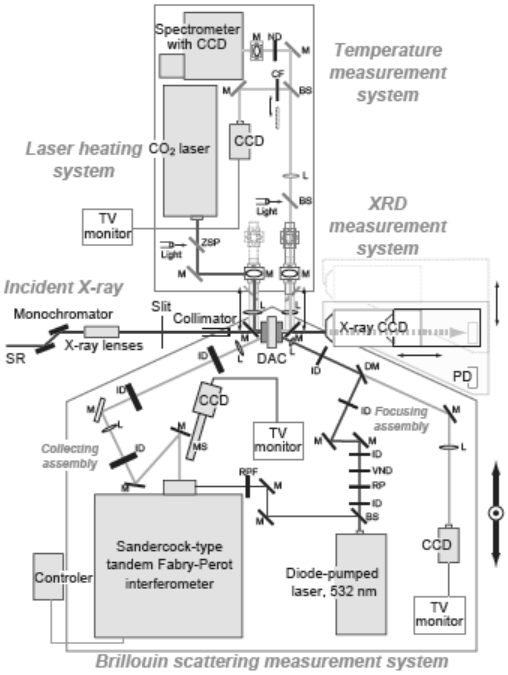

Fig. 1. Schematic layout of the Brillouin scattering measurement system combined with synchrotron radiation XRD and laser heating system at BL10XU.

3. Energy-Domain SR ^{57}Fe-Mössbauer Spectroscopy with DAC

The ^{57}Fe-Mössbauer spectroscopy is a powerful method for studying the electronic and magnetic properties of iron-containing materials. The new energy-domain SR ^{57}Fe-Mössbauer spectroscopy method has been developed at BL11XU of SPring-8 [3]. The Mössbauer absorption spectrum is observed by using the single-line 14.4 keV ^{57}Fe-Mössbauer beam with the bandwidth of neV order that is generated with a pure nuclear Bragg reflection from a $^{57}FeBO_3$ single crystal at the Néel temperature. The new system is suitable for high-pressure experiments because of very small beam, high photon flux, and no requisition of the bunch operation of the storage ring.

With a focusing X-ray device, we can perform ^{57}Fe-Mössbauer measurements with a DAC in multi-megabar pressure ranges where such measurements have not been realized in a conventional Mössbauer spectroscopy method using a radioisotope source. With multimegabar techniques, ^{57}Fe-Mössbauer measurements up to a pressure of 2.5 Mbar have been carried out on ^{57}Fe-containing Earth's materials [4]. In future, the newly developing system of the Doppler-shifted single-line ^{57}Fe-Mossbauer radiation [5] allows us to perform Mössbauer experiments under extreme conditions of high pressures and temperatures from cryogenic states to thousands of degrees, providing new discoveries and fundamental and important phenomena in Earth and planetary science, physics, and material sciences.

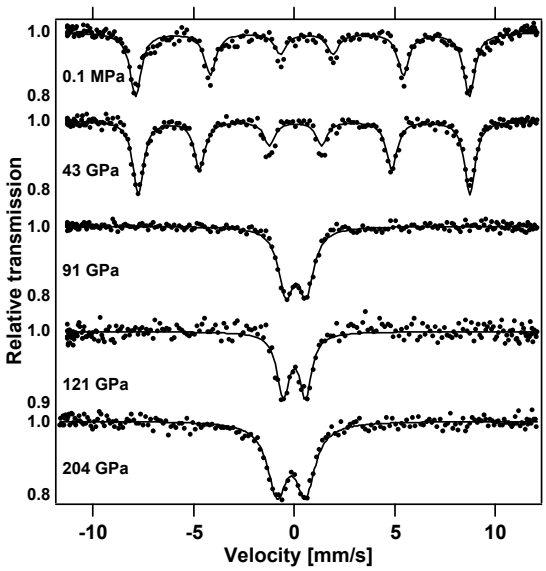

Fig. 2. Typical Mössbauer spectra of Fe_2O_3 at high pressure.

References

[1] Murakami et al., submitted.

[2] Mitsui et al. (2007a) Jpn. J. Appl. Phys., 46: 821–825.

[3] Sinogeikin et al. (2006) Rev. SCi. Instrum., 77:103905.

[4] Mitsui et al. (2007b) Jpn. J. Appl. Phys., 46: L382–L384.

[5] Mitsui et al. (2007c) Jpn. J. Appl. Phys., 46: L703–L705.

New progress in high-pressure research at HPCAT

Guoyin Shen (HPCAT and Geophysical Laboratory, Carnegie Institution of Washington

High Pressure Collaborative Access Team (HPCAT) operates an APS sector dedicated for high pressure researches. Four beamlines have been established for simultaneous operation: two undulator beamlines and two bending magnet beamlines. The developed high-pressure synchrotron techniques include X-ray scattering in meV and sub-eV energy resolution, X-ray spectroscopy (emission and absorption), and X-ray diffraction (polycrystalline, single crystal, high resolution, EDXD, ADXD). A number of high pressure equipments have been established in the experimental stations for pressure-temperature generation and measurement, and for sample characterization by optical spectroscopy. These include a double sided laser heating system, various cryostats, on-line ruby/Raman systems, and membrane control systems for pressure control. An overview of HPCAT developments, together with a few highlights in science and technology, will be discussed.

Recent advances in large-volume high-pressure research at GSECARS

Yanbin WANG (GSECARS, University of Chicago, USA, wang@cars.uchicago.edu), Takeshi SANEHIRA (GSECARS, University of Chicago, USA, sanehira@cars.uchicago.edu), Norimasa NISHIYAMA* (GSECARS, University of Chicago, nishiyama@sci.ehime-u.ac.jp), Mark L. RIVERS (GSECARS, University of Chicago, USA, rivers@cars.uchicago.edu)

* Now at Geodynamics Research Center, Ehime University Japan

Recent developments in large-volume press (LVP) high-pressure techniques at GSECARS have transformed our LVP systems into a versatile user facility. Many pressure modules have been developed, such as the DIA-, the Kawai-, the Drickamer-, and the torroidal-type apparatuses (e.g., Fig. 1). These devices allow a wide range of studies at high pressures combined with synchrotron radiation, ranging from equations of state to phase relations, ultrasonic to deformation, and crystal structure to microstructure. In many cases, the use of X-ray transparent materials (e.g., cubic boron nitride, cBN, and sintered diamond, SD) allows direct radiographic imaging of the sample, in addition to diffraction. Both white and monochromatized radiations are available for diffraction and imaging. The large Si (111) double-bounce monochromator makes it possible to switch between the white and monochromatic mode of operation during an experiment. Various pressure modules can be quickly switched from one to another to best suit users' specific needs. Highlights of scientific results include (1) monochromatic diffraction and imaging for controlled deformation experiments using the deformation DIA (D-DIA) for flow law determination up to 20 GPa, (2) combined monochromatic imaging and monochromatic diffraction for computed microtomography on millimeter sized samples to over 10 GPa and well over 1000C, using a Drickamer- or a torroidal-type device, (3) 2D monochromatic diffraction in the T-cup using SD anvils for determination of melting curves, (4) ultrasonic measurements combined with diffraction and imaging to 25 GPa and 2000K, and (5) CAESAR diffraction in the torroidal apparatus for crystalline and non-crystalline structural studies. Additional new developments will be discussed.

Fig. 1. Various large-volume high pressure devices for experiments in the 250 T press in 13-BM-D.

Acknowledgments

GeoSoilEnviroCARS is supported by the NSF–Earth Sciences (EAR-0622171) and DOE–Geosciences (DE-FG02-94ER14466). Use of the Advanced Photon Source was supported by the U.S. Department of Energy, Office of Science, Office of Basic Energy Sciences, under Contract No. DE-AC02-06CH11357.

Development of Kawai-type MA with SD anvils and its application: Equation of state of $MgSiO_3$-perovskite

Yoshinori TANGE (Ehime University, Japan, tan@sci.ehime-u.ac.jp), Tetsuo IRIFUNE (Ehime University, Japan, irifune@dpc.ehime-u.ac.jp), Ken-ichi FUNAKOSHI (Japan Synchrotron Research Institute, Japan, funakosi@spring8.or.jp)

1. Introduction

It is generally accepted that magnesium silicate perovskite, (Mg,Fe)SiO_3-Pv, is the most dominant phase in the Earth's lower mantle, and the *P-V-T* equation of state and thermoelastic parameters are essentially important to constrain the chemical composition and temperature of the lower mantle from seismic observations. $MgSiO_3$ is an abundant end component, which accounts for ~95 mol%. High-pressure and high-temperature in-situ X-ray diffraction studies of $MgSiO_3$-Pv have been carried out number of times, and the thermoelastic parameters have been increasingly well-constrained using synchrotron radiation source (e.g. [1,2,3,4]). However, systematic high-*T* experiments have been limited up to ~30 GPa, and precise *P-V-T* measurements at >30 GPa are needed to constrain *P-T* concerned parameters. Hence we carried out *P-V-T* measurements for $MgSiO_3$-Pv up to 62 GPa and 1500 K based on sintered diamond multi-anvil techniques.

2. Experimental

High-pressure and high-temperature experiments were performed by Kawai-type multi-anvil apparatus (SPEED-Mk.II [5]) with sintered diamond second-stage anvils. We used the sintered diamond anvils of 14.0 mm cube with truncated corners of 1.5 mm in the edge length (TEL = 1.5 mm). In order to generate ultra high-pressure, semi-sintered ceramics of Al_2O_3 was employed as pressure media and heat-treated pyrophyllite was used for gaskets. To produce a stable and uniform high-*T* condition, cylindrical resistance furnace of $LaCrO_3$ was used, and set into the center of the pressure media. $LaCrO_3$ has low transparency to X-ray, so graphite windows were set on the X-ray path to obtain brilliant XRD profiles. Temperature was measured by W/Re3-25 thermo-couple, of which the junction was and directly touched sample inside of the furnace. Sample container was made from graphite. $MgSiO_3$-Pv sample was synthesized in-situ from pure Mg_2SiO_4-forstelite, which decomposed to $MgSiO_3$-Pv and MgO. Au powder was mixed to the starting material as an internal pressure standard. Additionally MgO synthesized at high *T* was used as a pressure standard.

High *P-T* in-situ X-ray diffraction (XRD) measurements were conducted at a beamline, BL04B1 in SPring-8. Using bright white X-ray, energy dispersive XRD measurements were carried out with a SSD. The XRD profiles were collected only in the *T*-decreasing stage after sample syntheses, in order to ensure hydrostatic conditions in a series of the experiments. XRD profiles were acquired for 600-3600 seconds.

3. Results and Discussion

Four high *P-T* experiments were carried out in the range of 27-62 GPa and 300-1500 K. We obtained a precise *P-V-T* dataset, and errors in measurements were 0.3 GPa, 0.1 Å^3, and 2 K at most. A fit of the *P-V-T* dataset (based on Speziale's MgO-scale [6]) to high-*T* third-order Birch-Murnaghan equation of state yields a bulk modulus K_{T0} = 247.3(18) GPa, with a pressure derivative K'_{T0} = 4.20(9), and a temperature derivative $(\partial K_T/\partial T)_P$ = -0.030(3) GPaK^{-1}. In this analysis, V_0 was fixed as 162.35 Å^3. Defining thermal expansion as $\alpha_T = \alpha_0 + \alpha_1 T$ at 1atm, we obtained thermal expansion coefficients, α_0 = 2.47(14) 10^{-5}K^{-1} and α_1 = 1.05(15) 10^{-8}K^{-2}. Reproducibility of the fitting are shown in Fig. 1.

We obtained relatively small bulk modulus (e.g. 259.5 GPa in [4]), which is consistent with a recent result of Brillouin scattering measurement, K_{S0} = 253(3) GPa [7]. In the thermal expansion, we obtained larger thermal expansion coefficients than previous studies (e.g. α_0 = 2.18(12) 10^{-5}K^{-1}, and α_1 = 0.11(8) 10^{-8}K^{-2} in [4]). The large thermal expansivity increases $\Delta\rho$ as a function of ΔT, and accelerates the thermal convection of the lower mantle. However, the obtained thermoelastic parameters strongly depend on the "pressure-scale." In order to discuss the thermoelastic properties of Pv in the lower mantle and the effect on the mantle dynamics, it is most essential to construct the external pressure-scale.

References

[1] Wang et al. (1994) J. Geophys. Res., 83: 13-40.

[2] Funamori et al. (1996) J. Geophys. Res., 101: 8257-8269.

[3] Fiquet et al. (1998) Phys. Earth Planet. Int., 105: 21-31.

[4] Fiquet et al. (2000) Geophys. Res. Lett., 27: 21-24.

[5] Katsura et al. (2004) Phys. Earth Planet. Int., 143-144: 497-506.

[6] Speziale et al. (2001) J. Geophys. Res., 106: 515-528.

[7] Sinogeikin et al. (2004) Geophys. Res. Lett., 31: L06620.

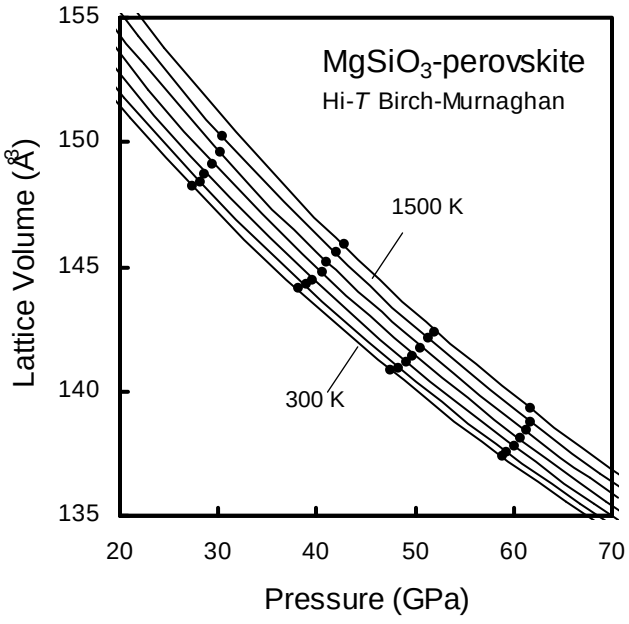

Fig. 1. Isothermal compression curves of $MgSiO_3$-Pv at 300-1500 K, where intervals are 200 K. Obtained P-V-T *data is fitted to high-*T *Birch-Murnaghan equation of state. Errors in* P-V *are smaller than symbol. Pressure is calculated using an EOS of MgO [6].*

Development of a CsCl pressure standard and its use in testing a series of multi-anvil cells

Kurt LEINENWEBER (Arizona State University, USA, kurtl@asu.edu), Emmanuel SOIGNARD (Arizona State University, USA, Emmanuel.Soignard@asu.edu), Yanbin WANG (University of Chicago GSECARS, USA, wang@cars.uchicago.edu)

1. Introduction

Pressure standards are fundamental to high-pressure research, and accurate and sensitive pressure standards are continually sought after.

The COMPRES (Consortium for Materials Properties Research in Earth Sciences) project includes an effort to design new multi-anvil cell assemblies which can be used by interested laboratories for their high pressure research. During the development of these assemblies, it was also wished to acquire in situ data on their performance and pressure calibration, which would give a great deal more information than the fixed-point calibrations that are normally used. For this purpose, we wanted to use the exact assemblies that we use in our laboratories, without X-ray windows or other modifications. In this case, it is very difficult to use standards such as MgO, because of the small number of peaks and low scattering, and poor results were obtained in initial tests. We decided to try CsCl because it is a good scatterer, and since it is simple cubic in its unit cell symmetry, it has a larger number of peaks defined by only one unit cell parameter so the fit to a weak pattern can be less ambiguous. Also, it has a very low bulk modulus, $K_0 = 16.7$ [1], compared to MgO, which has a compressibility of $K_0 = 162.5$ [2], so it is potentially ten times more pressure-sensitive. Finally, it has a significantly higher melting point than NaCl at pressures over 1 GPa because the melting curves cross at that pressure and the CsCl melting curve is unusually steep for an alkali halide [3]. CsCl was first suggested by Decker [4] as a pressure standard, but has not been used much primarily because it is also a strong X-ray absorber. We did not find this to be a problem when using a third-generation source, and indeed it was the only standard that worked well with our highly absorbing cells.

A related effort was undertaken to cross-reference the unit cell volume of CsCl against three other materials: MgO, Au and W. This helps to evaluate the P-V-T behavior of CsCl, and allows CsCl to be used with greater confidence as a pressure indicator, because it is referenced against more familiar standards, especially Au and MgO.

2. Experimental

CsCl was mixed with W and BN in a ratio of 6:1:6 by weight. The BN was used as a dispersant to stop recrystallization, and also to reduce absorption. MgO (ground single crystal) and Au were mixed in a ratio of 10:1. The two samples were layered into a BN capsule with a BN disc separating them. These samples were run in two different assemblies, a 14/8 and a 10/5 assembly, both with X-ray windows for access. The cell parameters of all four materials were collected in four fully functional experiments ranging from 10 GPa to 20 GPa at temperatures up to 1800°C.

Energy-dispersive X-ray diffraction was used with a two theta angle of near 6.1°, and a useful energy range of 20-70 KeV for cells with windows, and 45-70 KeV for cells without windows.

For data analysis, the program Crystal Cracker [5] was used. Peaks were fit with a pseudo-Voight fitting function. In the fittings, all peaks from all phases were fit simultaneously, and the fluorescence peaks of atoms in the beam path (Cs, Pb, W, Ta) were also included, with constraints on the intensities based on the fluorescence yields. This method is fast, helps eliminate ambiguous peak assignments in deriving cell parameters, corrects for the interference due to fluorescence, and also allows the standard errors in the parameters to be calculated systematically.

The Decker equation of state for CsCl could then be corrected using the unit cell information as a function of pressure and temperature. A modified Decker equation, and then a Mie-Gruneisen equation, both describing the same P-V-T data, are derived. The Mie-Gruneisen equation is more standard now than the Decker equation. There is also more study of how the Mie-Gruneisen equation performs under conditions of extrapolation. So, this equation may be preferred for consistency with the modern equations for MgO, Au, etc.

For the calibrations of the COMPRES multi-anvil cells, the cells (14/8 Bayreuth, 14/8 box heater, 10/5 and 8/3) were loaded with various W + CsCl + BN mixtures and run without X-ray windows. The

optimal mixture for these absorbing cells turned out to be the same, 6:1:6.

3. Results and discussion

For its age, the Decker equation for NaCl does quite well, although it has been found to be off by a few percent in its stated range of validity [6] and as much as 12% at higher pressures [7]. Our findings indicate that the Decker equation for CsCl may be better than that for NaCl. Well beyond its stated limit of 10 GPa and 1000°C, pressures derived from the Decker equation for CsCl remain fairly close to those from the Speziale [2] equation for MgO, which was recently suggested as an anchor standard for comparison to others [8]. The pressures derived from the Decker equation for CsCl are everywhere about 3% lower than those from Speziale's MgO, with the difference fairly independent of temperature. This is within the current uncertainties of pressure standards, but the MgO equation is based on more modern physical ideas and includes primary pressure measurements at room temperature, unlike the Decker equation.

The parameters of the Decker equation may be modified slightly to accommodate the shifts in pressure. Alternatively, the Decker equation can be re-fitted to a Mie-Gruneisen type equation, and then the new data can be used to correct the parameters in that equation. Given the modern preference for a Mie-Gruneisen approach, the latter is the most consistent and most easily compared to other equations. Both of these approaches will be discussed at the workshop.

There are concerns about such things as the transfer of the form of an EOS from a pressure standard to a sample. An erroneous functional form in a standard will be mapped to all the samples that are measured against it, biasing all the results. In the current case, the Speziale equation of state for MgO uses a certain form for q and γ, which may or may not be physically real. The question is, when other materials are measured against MgO, does the particular form for q and γ "transfer" to the other phase? This can happen any time the precision of the pressure measurement exceeds the accuracy of the pressure standard.

4. Conclusion

Overall, we may conclude that the simple relationship of CsCl-derived pressures to MgO-derived pressures shows that CsCl is a well-behaved material in this pressure range and could be used as a reliable pressure standard. CsCl also demonstrates great precision and sensitivity to small pressure changes, which makes it useful for studies where small changes in pressure are important. The further development of the CsCl pressure standard would benefit greatly from primary pressure measurements (i.e., measurements of the bulk modulus versus volume) for CsCl both at room temperature and high temperature.

References

[1] Kohler, U.; Johannsen, P.G.; Holzapfel, W.B. (1997). J. Phys.: Condens. Matter 9: 5581-5592.

[2] Speziale et al. (2001) J. Geophys. Res. 106, 515-528.

[3] Clark, S.P. (1959) J. Chem. Phys. 31: 1526-1531.

[4] Decker, D.L. (1971) J. Appl. Phys., 42: 3239-3244.

[5] Leinenweber, K. (in prep).

[6] Brown, J.M. (1999) J. Appl. Phys., 86: 5801-5808]

[7] Li, B.; Kung, J.; Uchida, T.; Wang, Y. (2005) J. Appl. Phys. 98: 013521-1.

[8] Fei, Y. et al. (2004) Phys Earth Planet Int 143-144, 516-526.

Ultrasonic measurements in multi-stage multi-anvil devices

Hans J. MUELLER (GeoForschungsZentrum Potsdam in der Helmholtz-Gemeinschaft, Germany, Hans-Joachim.Mueller@gfz-potsdam.de), Frank R. SCHILLING (at the same place, fsch@gfz-potsdam.de), Michael WEHBER (at the same place, michael.wehber@desy.de), Christian LATHE (at the same place, christian.lathe@fesy.de)

1. Introduction

A promising way to increase the maximum pressure of multi-anvil devices is "multi-staging," i.e., implementing an additional set of "sub-anvils" between anvils and sample resulting in a better distribution and limitation of the stress inside the anvils. Contrary to the common opinion of overshooting the maximum crushing strength most of the anvils fail in high pressure experiments due to the exceeding of the maximum tensile stress as a result of the lateral deformation. Utsumi *et al.*, 1986 published a technique to reach 60 GPa pressure by using sintered diamond anvils as second stage in a single-stage DIA-type multi-anvil apparatus. Li, 2001 published a peak pressure of more than 26 GPa for a single-stage DIA even though the diamond anvils had been broken. Wang & Utsumi, 2005 (pers. comm.) reported similar experiments performed in a deformation-DIA (D-DIA).

2. Experimental

Our experiments with two LVPs installed at DESY-HASYLAB also showed more than a pressure doubling in comparison to the original single-stage and double-stage configurations, i.e. 25 GPa at MAX80 and nearly 50 GPa at MAX200x (Mueller *et al*., 2006, 2007. The first ultrasonic experiments in this configuration were performed at MAX80. The top sub-anvil was acoustically coupled to the upper anvil equipped with a triple-mode ultrasonic transducer by a platinum disk of the same diameter as the cylindrical shaft of the sub-anvil. From acoustical point of view the travel path has 3 buffer rods—top MAX80 anvil, platinum disk, upper internal opposed anvil—and the bottom internal opposed anvil as reflector. As a result of preparatory experiments we had found the upper cut-off frequency for the existing transducer-TC-anvil system at about 320 MHz. An excitation function representing the bandwidth of 100 to 300 MHz was calculated and used in the data transfer function (DTF) ultrasonic interferometry experiments.

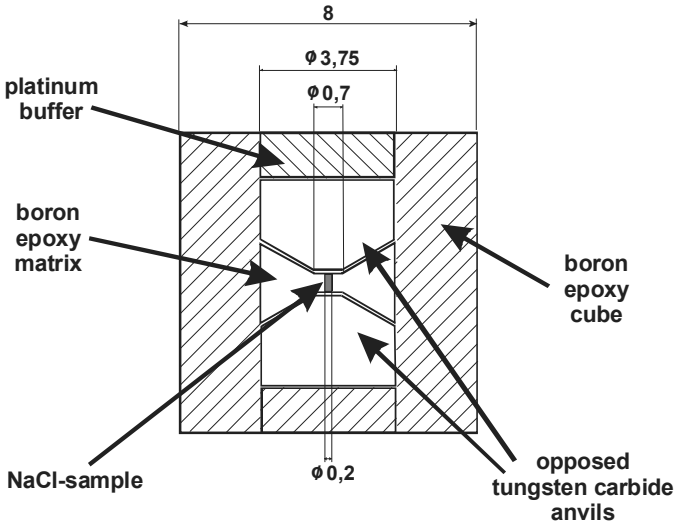

Fig. 1. Opposed anvil set-up for single-stage multi-anvil devices.

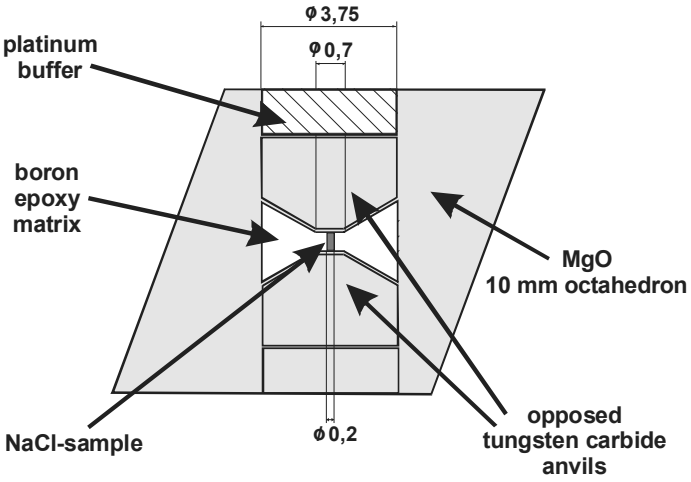

Fig. 2. Opposed anvil set-up as third stage for double-stage multi-anvil devices.

3. Results and discussion

NaCl was simultaneously used as pressure calibrant, using the EoS of Decker (1971), and sample for ultrasonic interferometry (Mueller *et al*., 2003, 2005). The compressibility results, derived from the ultrasonic data, are compared with static compression data up to 30 GPa (Birch, 1986) using experimental data from Boehler & Kennedy (1980) and Fritz *et al*. (1971). First evaluations indicate an increasing deviation at pressures exceeding 6 GPa. At 25 GPa the pressure derived from ultrasonic interferometry is about 13% higher than that inferred from the Decker (1971) pressure scale. Our results correspond to the data of Li *et al.* (2005) for a Mg_2SiO_4 wadsleyite sample surrounded by a mixture of NaCl and BN.

References

[1] Utsumi, W. *et al*. (1986) *J. Appl. Phys.,* **60:** 2201-2204.

[2] Li, B. (2001), *APS Report 01*: 192-193.

[3] Wang, Y & Utsumi, W. (2005) *COMPRES Annual Meeting 2005*, New Paltz.

[4] Mueller, H.J. *et al*. (2006) *High Pressure Research*, **26**: 529-537.

[5] Mueller, H.J. *et al*. (2007) *GSA Special Paper,* **421**: 207-226.

[6] Decker, D.L. (1971) *J. Appl. Phys*., **42**: 3239-3244.

[7] Mueller, H.J. *et al*. (2005) *Advances in High Pressure Technology for Geophysical Applications, Chapter 4:* 67-94.

[8] Mueller, H.J. *et al*. (2005) *Advances in High Pressure Technology for Geophysical Applications, Chapter 21:* 427-449.

[9] Birch, F. (1986) *J. Geophys. Res.*, **91**: 4949-4954.

[10] Boehler, R. & Kennedy, G.C. 1980) *J. Phys. Chem. Solids*, **41**: 517-523.

[11] Fritz, J.N. *et al*. (1971) *NBS Special Publ*., **326**: 201-208.

[12] Li, B. & Kung, J. (2005) *J. Appl. Phys*., **98**: 013521.

Session II:

Neutrons and New Techniques

Recent progress on high-pressure neutron beamline at J-PARC in Japan

Hiroyuki KAGI (Graduate School of Science, University of Tokyo, Japan, kagi@eqchem.s.u-tokyo.ac.jp)

1. Introduction

J-PARC (Japan Proton Accelerator Research Complex) project is under construction in Tokai village, Ibaraki prefecture, Japan, to be completed by 2008 with collaboration between JAERI (Japan Atomic Energy Research Institute) and KEK (High Energy Accelerator Research Organization). The J-PARC project involves a neutron science facility (JSNS), which will give us one of the strongest pulsed neutron flux in the world.

The high-pressure science community in Japan has submitted a proposal for the construction of a "high-pressure and high-temperature material science beamline" at JSNS. The proposal was already approved after scientific and technical reviews by the J-PARC committee. Crystal structures of hydrogen-bearing materials including hydrous minerals, order-disorder transitions of minerals, structure of light element liquid at high pressure, etc. will be targets of our facility. Among them, one of the main highlights in our proposal is an application of neutron science into understanding of magma processes featuring active geothermal events in Japan. Another direction is to challenge neutron scattering experiments at unexplored pressures.

To construct the new high-pressure beamline at J-PARC, we have submitted a couple of proposals to JSPS and MEXT, respectively, and one of them was accepted by JSPS in April, 2007. A target of the JSPS project is to achieve neutron diffraction experiments at pressures higher than 30 GPa. That involves development of a large-volume high-pressure apparatus, optimization of neutron optics for neutron scattering experiments at high pressures, and science of hydrous materials in the interiors of the earth and planets.

2. Development of large volume high-pressure cell

Neutron scattering (diffraction) experiments at high pressure restrict sample volume to be at least several tens of millimeters. This is because a neutron is an electrically neutral particle and makes very weak interaction with materials. To achieve high pressures for neutron scattering experiments, we have to develop a new high-pressure device with large sample volume. We are now testing two types of device to achieve this requirement. One is a Drickermer-type opposite anvil high-pressure device (see Fig. 1). Another type of device is a "palm cubic" high-pressure device being designed by Prof. Y. Uwatoko, a member of our JSPS project, and his colleagues [1]. As shown in Fig. 1, pulsed neutron beam is introduced through one of the anvils. We are going to use "HIME-DIA", an artificial sintered diamond developed by Irifune et al. (2003) as an anvil material [2]. "HIME-DIA" is very promising material for this purpose, because it is optically transparent and hard. In this cell configuration, we have to fabricate the hard polycrystalline diamond to be a truncated cone, which is a technical difficulty and a big challenge in our JSPS project.

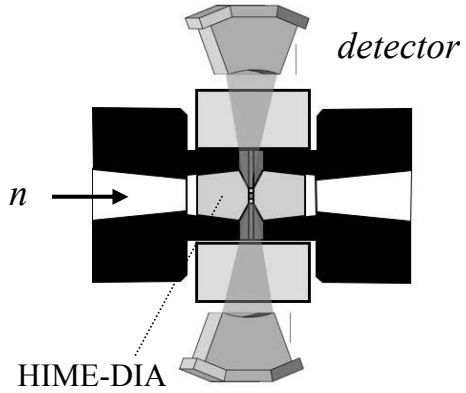

Fig. 1. Schematic view of Drickermer-type opposite anvil cell for neutron scattering experiments at high pressure.

3. Optimization of neutron optics

One of the experimental obstacles for neutron diffraction measurements under high-pressure conditions is weak signal from a tiny sample volume. Hence the high-pressure beamline needs optical devices to focus neutron beams into a small spot less than 1 mm with the energy resolution of 0.5% in $\Delta d/d$. For the purpose of designing "the high-pressure and high-temperature material beamline", several designs of super mirror guides were optimized by Monte Carlo simulation using the McStas software. The intensity, divergence and energy dependence for the tapered straight, elliptical and parabolic guides

compared with a linearly straight guide. The results are shown in Figs. 2 and 3.

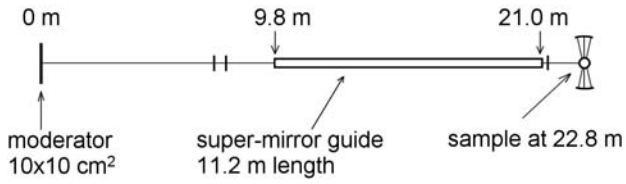

Fig. 2. Schematics of the beamline component for optimization of neutron optics.

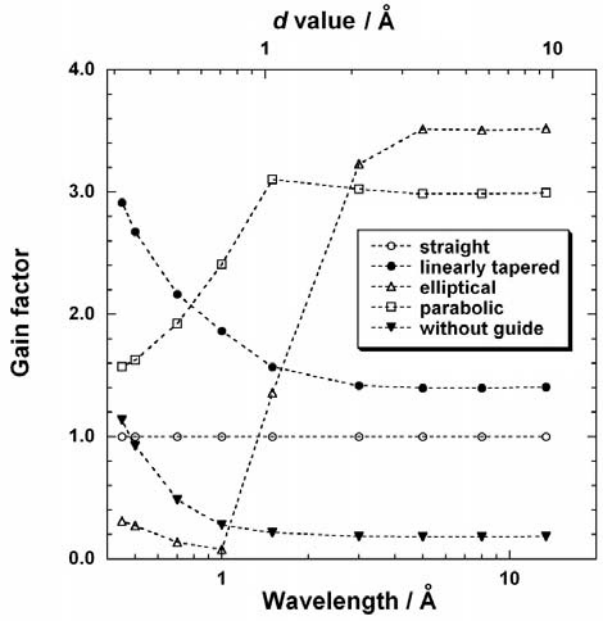

Fig. 3. Neutron intensities and gain factors at the sample position.

4. Material development and properties

One of the most important requirements for the application of HIME-DIA to the large-volume high-pressure apparatus is to grow the polycrystalline diamond as large as 6 mm or larger with maintaining the quality. We collaborate with Ehime University and Sumitomo Electric Industries, Co. Ltd. to improve growth conditions. As described in the previous section, the precise fabrication of the polycrystalline diamond (HIME-DIA) is a key technique to be developed in this project. We are trying to develop a laser fabrication technique for this purpose. Our colleague, Dr. Takuo Okuchi will present a detailed report in this workshop.

The surface of laser-treated diamond is covered by debris and laser-induced transformed layers. We are observing optical spectra and TEM images of laser-treated diamond surface.

4. Future plans

Our JSPS is now making progress on developments of high-pressure device and optimization of neutron optics. We ate going to finish the fabrication of the cell by FY2008 and neutron diffraction study will start from FY 2009. Our targets will be hydrous minerals, ices, hydrogen clathrate materials, etc. at pressures higher than 30 GPa. In FY2008, several beamlines at J-PARC will be already open for public users, but it is presumably difficult to construct the "high-pressure" dedicated beamline by that time. We are going to bring our newly developed high-pressure cell to the "TAKUMI" beamline (BL19), an engineering diffractometer and obtain scientific data during the duration of our JSPS project.

For the construction of the high-pressure beamline, we will submit a new proposal headed by Prof. Takehiko Yagi and the construction will start from FY2008 if the proposal is accepted.

Acknowledgments: This project is financially supported by a Grant-in-Aid for Scientific Research (Gakujutsu-sousei program; 19GS0205) from the Japan Society for Promotion of Science (JSPS). I am grateful to the project members: Hiroshi ARIMA, Hisako HIRAI, Kazuki KOMATSU, Tadashi KONDO, Takuo OKUCHI, Toyotaka OSAKABE, Shigeo SASAKI, Yoshiya UWATOKO, and Osamu YAMMURO. Special thanks are extended to Professor Tetsuo IRIFUNE, Hiroaki OHFUJI, Shoko ODAKE, Kazuaki IKEDA and Dr. Hitoshi SUMIYA.

References

[1] Koeda, M. et al. (2007) Joint 21st AIRAPT and 45th EHPRG International Conference on High Pressure Science and Technology (Abstract), 516, 2007.

[2] Irifune,T. et al. (2003) Nature 421: 599-601.

Prospects for neutron diffraction under extreme pressure conditions at the new Spallation Neutron Source

Chris A. Tulk (Oak Ridge National Laboratory)

The Spallation Neutron Source currently under construction at Oak Ridge National Laboratory in the United States has received first neutrons in the summer of 2006. The prospects for high pressure neutron diffraction are good with the completion of a dedicated high pressure user beamline this coming winter. Here the instrument parameters of the Spallation Neutrons And Pressure (SNAP) instrument will include a discussion of planned micro-diffraction capabilities. Specifically, recent progress in micro-focused neutron beams demonstrates that neutron diffraction from sub-100 micron samples held within "more standard" opposed gem anvil cells (e.g., DACS) are feasible. Examples of scattering from micro single crystal samples will be given.

Geophysics studies with high-resolution X-ray spectroscopy

Wolfgang STURHAHN (Argonne National Laboratory, USA, sturhahn@anl.gov)

The introduction of high-resolution (about 1 meV) inelastic X-ray scattering techniques to third generation synchrotron radiation facilities around the world has been very successful over the last decade. New opportunities for the study of vibrational properties of condensed matter have emerged for research areas like biophysics, geophysics, and nanoscience. In particular, the determination of phonon dispersion relations with momentum-resolved inelastic X-ray scattering (IXS), of vibrational density of states with nuclear resonant inelastic X-ray scattering (NRIXS), and of the determination of valences, spin states, and magnetic ordering with synchrotron Mössbauer spectroscopy (SMS), all under extreme conditions, provided novel and often remarkable results in the scientific area of geophysics, e.g., the study of iron metal in the Mbar regime [1,2]. In this contribution, the combination of high-resolution spectroscopy with diamond anvil cell technology and its impact on the geoscientific area will be discussed.

Nuclear resonant spectroscopies (NRIXS & SMS) under extreme conditions are key methods [3] to provide sound velocities and elasticity on iron, iron alloys, and iron oxides [2,4,5], to study valence and high-spin to low-spin transitions in lower mantle minerals [6,7], and to investigate melting of iron-bearing materials [8]. Its sensitivity in combination with isotope selectivity allowed investigations on materials under high pressures using diamond anvil cells and Laser heating. Examples will illustrate the present and potential future use of nuclear resonant spectroscopy in the Earth and planetary sciences. Even though ^{57}Fe has spawned the largest interest so far, we will also review the selection of other suitable nuclear resonances that could become important for future applications.

Momentum resolved IXS detects phonon dispersions and has been applied to Earth materials like iron metal [1,9] and MgO [10] under high pressure in diamond anvil cells. In single crystals, the dispersion of the acoustic phonons at low energies provides sound velocities for various directions and potentially the elastic tensor of the material [11].

The technical requirements for nuclear resonant and momentum resolved IXS methods have favored the diamond anvil cell for generation of high pressures. The X-ray energies are typically between 10 keV and 30 keV, and the high-pressure device has to accommodate sufficiently low absorption at those energies. In addition, momentum-resolved IXS needs access to a plane with 20-30 degree opening angle. NRIXS experiments require access to a significant solid angle. These conditions have been more readily met by diamond anvil cells. Here we will discuss the possibility of using a multi-anvil device instead and evaluate the conditions for IXS experiments in such apparatus.

This work is supported by the U. S. Department of Energy, Office of Science, Office of Basic Energy Sciences, under Contract No. DE-AC02-06CH11357 and by NSF through COMPRES.

References

[1] Fiquet, G. et al. (2001) Science, 291: 468-471.

[2] Mao, H.-K. et al. (2001) Science, 292: 914.

[3] Sturhahn, W. (2004) J. Phys.: Condens. Matter, 16: 914.

[4] Lin, J.-F. et al. (2005) Science, 308: 1892.

[5] Lin, J.-F. et al. (2006) Geophys. Res. Lett., 33: L22304.

[6] Jackson, J.M. et al. (2005) American Mineral., 90: 199.

[7] Lin, J.-F. et al. (2006) Phys. Rev. B., 73: 113107.

[8] Jackson, J.M. et al. (in preparation).

[9] Antonangeli, D. et al. (2004) Earth and Planet. Sci. Lett., 225: 243-251.

[10] Ghose, S. et al. (2006) Phys. Rev. Lett., 96: 035507.

[11] Antonangeli, D. et al. (2004) Phys. Rev. Lett., 93: 215505.

Magnetic spectroscopy at high pressure using XMCD

Daniel HASKEL (Magnetic Materials Group, Advanced Photon Source, Argonne National Laboratory)*

The imbalance in the electronic density of states between spin-up and spin-down electrons that occurs in ferro(ferri)-magnetic materials gives rise to dichroism in the absorption of circularly polarized X-rays with opposite helicity (XMCD). These dichroic effects are largest near element-selective atomic resonances and provide a unique window of opportunity to probe complex magnetic materials with element and electronic orbital selectivity. We describe the recent development of a high-pressure XMCD capability at Sector 4 of the APS for low temperature (10 K), high field (0.7 Tesla) experiments in a diamond anvil cell featuring perforated anvils (20 GPa). HP-XMCD experiments can be carried out in the 5-13 keV energy range allowing studies of transition metal (3d), rare-earth (4f) and (5d) magnetic systems. We illustrate this new capability with examples from recent experiments on half-metallic CrO_2, inverse-spinel Fe_3O_4 and magneto-caloric material $Gd_5(Si_xGe_{1-x})_4$.

* In collaboration with Y. C. Tseng, N. Souza-Neto, J. Lang, S. Sinogeikin, Y. Ding, Ho-Kwang Mao, N. Loh and A. Stampfl. Work at Argonne is supported by the U.S. Department of Energy, Office of Science, Office of Basic Energy Sciences, under Contract No. W-31-109-ENG-38.

Volumetric properties of amorphous materials at high pressure by computed tomography

Charles E. LESHER (UC Davis, USA; lesher@geology.ucdavis.edu), Sarah GAUDIO (UC Davis, USA; gaudio@geology.ucdavis.edu), Alisha CLARK (UC Davis, USA; clark@geology.ucdavis.edu), Yanbin WANG (GeoSoilEnviroCARS-APS, USA, wang@cars.uchicago.edu)

The volumetric properties of silicate glasses and supercooled liquid are examined at high pressures and temperatures using X-ray computed tomography and absorption. The high-pressure X-ray microtomography (HPXMT) system at the Advanced Photon Source, Argonne National Laboratory (GeoSoilEnvironCARS 13-BM-D beamline) consists of two opposing anvils compressed within an X-ray-transparent containment ring supported by thrust bearings and loaded using a 250-ton hydraulic press. This system permits the pressure cell to rotate under the load, while collecting radiographs through at least 180 degrees of rotation. The 13-BM-D beamline permits convenient switching between monochromatic radiation required for radiography and polychromatic radiation for pressure determination by energy dispersive diffraction. We report initial results on several refractory magnesium silicate glasses synthesized by levitation laser heating. Volume changes during room temperature compression of vitreous forsterite up to 4.2 GPa and $(MgO)_{62}(SiO_2)_{38}$ glass up to 11.5 GPa yield bulk moduli of 80-90 GPa for a K' of ~4. These values are consistent with ultrasonic measurements for more silica-rich glasses. The volumetric properties of vitreous enstatite at 2 GPa were examined on heating up to 1000ºC. Passage through the glass transition region is characterized by marked changes in volume. From these data we estimate a coefficient of thermal expansion for supercooled $MgSiO_3$ liquid of ~20 x 10^{-5}/degrees. Our results illustrate the capabilities of HPXMT for studies of refractory glasses and liquids at high pressure and offer strategies for future work on materials relevant to the Earth's mantle and core at even higher P and T.

A scanning angle energy-dispersive X-ray diffraction (SA-EDXD) technique for studying the structure of materials at high pressure in diamond anvil cells

Wenge Yang (HPCAT, Geophysical Laboratory, Carnegie Institution of Washington), Guoyin Shen (HPCAT, Geophysical Laboratory, Carnegie Institution of Washington), Yanbin Wang (GSECARS, University of Chicago), and Ho-kwang Mao (HPCAT, Geophysical Laboratory, Carnegie Institution of Washington)

A scanning angle diffraction technique with an energy-dispersive solid-state detector and white synchrotron radiation has been developed for high pressure structure studies in diamond anvil cell (DAC). The main feature of the technique is the well defined collimation in the beam pass to the detector, which improves the signal to noise ratio significantly comparing to routine monochromatic angle-dispersive powder diffraction. This is particularly useful and essential for low-scattering material, amorphous and liquid diffraction/scattering studies using DAC. The SA-EDXD technique provides an important new tool in amorphous and liquid study. Besides the good signal to noise ratio, the use of white beam up to 110 keV covers a large Q-range (>20 $Å^{-1}$); the SA-EDXD data are two dimensional, having angle dispersive data with all energies, with which partial and full structural factors could be obtained. We will present case studies for both crystalline and amorphous materials.

Session III:

Ultrahard and Other Materials

Synthesis of large and high-quality nano-polycrystalline diamond and its potential applications to high-pressure mineral physics

Tetsuo IRIFUNE (GRC, Ehime University, Japan; irifune@dpc.ehime-u.ac.jp), Takeo OHNISHI (GRC, Ehime University, Japan; tohnishi@sci.ehime-u.ac.jp), Toru SHINMEI (GRC, Ehime University, Japan; shinmei@sci.ehime-u.ac.jp), Hiroaki OHFUJI (GRC, Ehime University, Japan; ohfuji@sci.ehime-u.ac.jp), Hitoshi SUMIYA (Electoronics & Materials R&D Laboratories Sumitomo Elect. Indust., Japan, sumiya@sei.co.jp)

1. Introduction

We firstly reported synthesis of pure polycrystalline diamond by direct conversion from graphite at pressures above 12 GPa and temperatures of 2000-2700°C, depending on pressure, using multianvil apparatus [1-4]. Thus synthesized diamond bodies were found to possess a peculiar nano-structure with mixed granular and lamellar crystals. Moreover, they have extremely high Knoop hardness of Hk=120-145 GPa [4], which is equivalent to or even higher than those of single crystal diamonds (generally, Hk=60-130 GPa, depending on the crystallographic plane and direction) and much harder than commercially available sintered diamond composites (Hk=50~70 GPa).

As the synthesis of the nano-polycrystalline diamond (NPD; or what is called HIME-DIA, Highly Incompressible and Mechanically Endurable Diamond) requires quite high pressure of above ~12 GPa [2], its volumetric dimension has been limited to less than a few millimeters. Moreover, the quality of thus synthesized NPDs remained insufficient to be used as anvils for high-pressure apparatus, as they are accompanied by some major cracks and also often show the presence of some impurities of metastable hexagonal diamond and/or compressed graphite formed in the process of increasing temperature under pressure.

We developed techniques to produce stable temperature generation exceeding 2300°C at pressures greater than 15 GPa in larger sample volumes in multianvil apparatus for synthesis of NPDs with substantially larger dimensions than our earlier studies. Moreover, effort has been also directed to synthesize high-quality NPDs without any cracks and impurities to meet the requirements for the anvils for high pressure apparatus.

2. Experimental

We used a cell assembly for NPD synthesis, as shown in Fig. 1, to stably maintain temperatures of 2000-2500°C in larger sample volume at pressures above 15 GPa. Tungsten carbide cubes of 36 mm with a TEL = 11 mm are used as the second stage anvils. An octahedral pressure medium of semi-sintered MgO doped with 10% CoO is divided into three pieces, and the sample is placed in the middle part of the octahedron so that a larger volume can be used. A rhenium foil is used as the tube heater, in which the sample capsule enclosed in a semi-sintered MgO sleeve is inserted. The heater is surrounded by an $LaCrO_3$ tube, which is used as the thermal insulator. We used polycrystalline graphite rod (99.99%), which was enclosed in a metal capsule and placed in the MgO sleeve. Synthesis of NP was made at a fixed P, T conditions of 15 GPa and 2300°C,with typically 10-20 minute heating time.

Fig. 1. A schematic illustration of the cell assembly used for synthesis of NPD.

3. Results and discussion

Highly transparent NPDs with a diameter of near 4 mm and thickness of 0.5-2 mm were synthesized after the heating, the dimensions having been reduced by about 20%, but we sometimes noted the presence of major cracks in thus synthesized NPD. The occurrence of such cracks was greatly reduced by releasing pressure while the temperature was kept at modest temperatures [5], and we obtained crack-free NPDs as shown in Fig. 2.

X-ray diffraction and Raman spectroscopic measurements demonstrated that the sample was of pure cubic diamond. The Raman band for diamond at about 1332 cm^{-1} was generally sharper than those

reported in earlier studies [2], suggesting that the grain sizes of thus formed diamond are larger than those observed in earlier studies with smaller sample dimensions. TEM observations on some of the NPD samples demonstrated that the granular grains of cubic diamond are in fact significantly larger (typically ~50 nm) than those in earlier studies (10-20nm [1,3]). The reason for the grain growth in the present large NPD relative to earlier samples with smaller dimensions are unclear, but it may be related to the purity of the starting material we used in these experiments, as we used graphite starting material with higher purity (99.9995%) in the earlier studies.

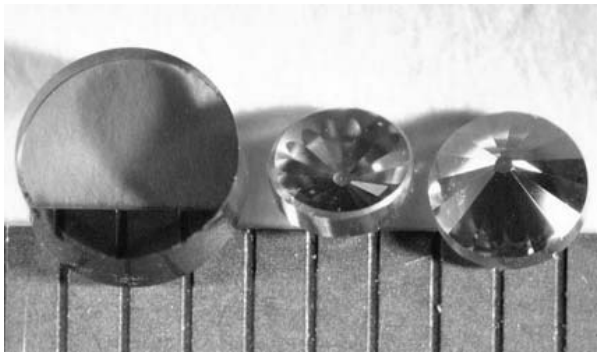

Fig. 2. NPDs with various shapes for industrial applications and high-pressure mineral physics.

The NPD was found to be transparent to optical lights with a wide range in wave lengths and possess thermal conductivity of about one order of magnitude lower than those of single crystal diamonds. Moreover, it is found that NPD maintains its hardness even at high temperatures of ~1000K. Initial attempts to apply the NPDs for high-pressure generation in both multianvil apparatus and diamond anvil cell are highly encouraging, suggesting the potential importance of this new ultrahard material for mineral physics studies at ultrahigh pressures.

References

[1] Irifune, T., Kurio, A., Sakamoto, S., Inoue, T., and Sumiya, H. (2003) Ultrahard polycrystalline diamnd from graphite, Nature, 421, 599-600.

[2] Irifune, T., Kurio, A., Sakamoto, S., Inoue, T., Sumiya, H. and Funakoshi, K. (2004) Formation of pure polycrystalline diamond by direct conversion of graphite at high pressure and high temperature, Phys. Earth Planet. Inter. 143, 593-600

[3] Sumiya, H., Irifune, T., Kurio, A., Sakamoto, S. and Inoue, T. (2003) Microstructure features of polycrystalline diamond synthesized directly from graphite under static high pressure, J. Mat. Sci., 39, 445-450.

[4] Sumiya, T. and Irifune T. (2004) Indentation hardness of nano-polycrystalline diamond prepared from graphite by direct conversion, Diamond Relat. Mater., 13, 1771-1776.

[5] Gwanmesia, G. D. and Liebermann, R. C. (1992) Polycrystals of high-pressure phases of mantle minerals: Hot-pressing and characterization of physical properties. In: High-Pressure Research: Application to Earth and Planetary Sciences (eds. Y. Syono and M. H. Manghnani), Terra Pub/AGU, Tokyo/Washington, D. C., pp. 117-135.

High-pressure and high-temperature experiments using nanocrystalline diamond anvil and laser heating

Takehiko YAGI, Taku OKADA (ISSP, University of Tokyo, Japan), *Hiroaki OHFUJI, Tetsuo IRIFUNE (GRC, Ehime University, Japan), Takumi KIKEGAWA (KEK, Japan), Nagayoshi SATA (JAMSTEC, Japan)

* Presenter: OHFUJI (ohfuji@sci.ehime-u.ac.jp)

1. Introduction

In the past decades, significant progress has been made in ultra-high pressure and temperature experiments using laser-heating diamond anvil cell (LHDAC). One of the most important outcomes of the LHDAC experiments is probably the discovery of the perovskite/post-perovskite phase transition under the conditions of the Earth's lowermost mantle [1, 2]. However, it has not been successful in generating high pressure-temperature conditions of the Earth's deep core mainly due to failure of diamond anvils during laser-heating at such very high pressures, and also to ineffective thermal insulation of the highly flattened sample. A potential method to overcome this issue is the use of nano-polycrystalline diamond (NPD, HIME-Dia) anvils for LHDAC experiments. NPD consists of a number of nano-sized (~100 nm) diamond crystals and therefore has practically no cleavage [3]. Its Noop hardness is equivalent or somewhat higher than that of single crystal diamond (IIa-type) even at high temperatures. It is also known that the thermal conductivity of NPD is about 15 times lower than that of single crystal diamond. This in turn means that the thermal insulation is better in NPD. Thus, all of these physical features suggest a capability of NPD for LHDAC experiments at extreme high pressure and temperature. In this report, we present results of the first attempt to generate high pressure and temperature using the NPD anvil cell and laser heating.

2. Experimental

A pair of beveled anvils with culet size of 300-100 μm (Fig. 1) were prepared from NPD blocks (synthesized at 21GPa, 2400°C at Ehime University). The first experiment was conducted using a pair of NPD anvils, whereas the second one was carried using a NPD anvil and a single crystal diamond anvil (hereafter called "hybrid cell"). We utilized a gasket composed of a diamond powder layer and a stainless steel or rhenium sheet to obtain better thermal insulation in the sample chamber, particularly, at high pressures [4,5]. Laser heating was performed using Nd-YAG, YLF, fiber lasers, and in situ X-ray measurements were done at Photon Factory and SPring-8.

3. Results and discussion

In the first experiment using a pair of NPD anvils, metallic iron was loaded into a sample chamber in a stainless steel + diamond powder gasket. It was compressed to 50 GPa and heated by a fiber laser from one side of the DAC. Continuous emission of visible light was first observed when the laser power increased to 12W. Fig. 2 shows a X-ray diffraction pattern of the sample after quenching to room temperature. Although the diffraction lines from the NPD anvils are considerably strong, peaks from the sample itself are also clearly seen. The sample was further compressed to 110 GPa and heated again, but no visible emission was observed even when the laser power increased to 60W. During the heating the culet of one of the anvils was seriously damaged and we ended the experiment.

In the second experiment using the hybrid cell, a mixture of $MgGeO_3$ ortho-pyroxene and Pt powers was loaded in Re + diamond powder gasket. When compressed to 52 GPa, the sample was heated by YLF laser from the both sides of the cell. We first observed continuous emission of light on the both sides when the power increased to 5W. Constant emission of light indicating high temperature generation > 2000K was also observed at 76 and 92 GPa with laser powers of 12 and 15W, respectively (Fig. 3). The experiment was suddenly ended when further pressurized to 120 GPa due to failure of the both anvils.

The present study showed that the NPD anvils are indeed capable of laser heating to generate high temperature (> 2000K) at the sample under high pressures (~100 GPa). However, these pressure-temperature conditions are not really higher than our initial prospective, and a couple of problems that need to be solved are also pointed out. Nevertheless, we believe that this would be the first big step for ultra-high pressure and temperature generation which is absolutely necessary for studying the Earth's deep interior.

References

[1] Murakami, T. et al. (2004) Science, 344: 855.

[2] Oganov, A.R. and Ono, S. (2004) Nature, 430: 445.

[3] Irifune, T. et al. (2003) Nature, 421, 599.

[4] Boehler, R et al. (1997) Phys. Rev. Let., 78: 4589.

[5] Zou, G. et al. (2001) Rev. Sci. Instrum., 72: 1298.

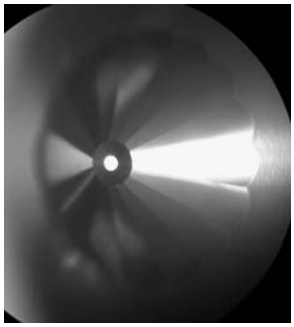

Fig. 1. Optical micrograph of a nano-polycrystalline diamond anvil.

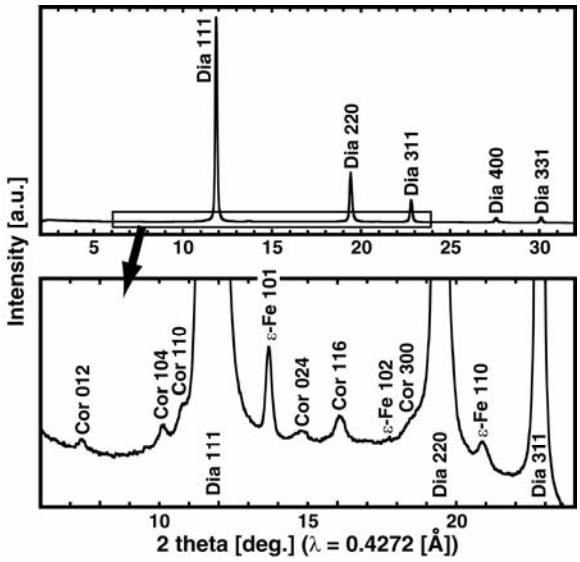

Fig. 2. Integrated XRD profiles of the sample (Fe) at 50 GPa after heating.

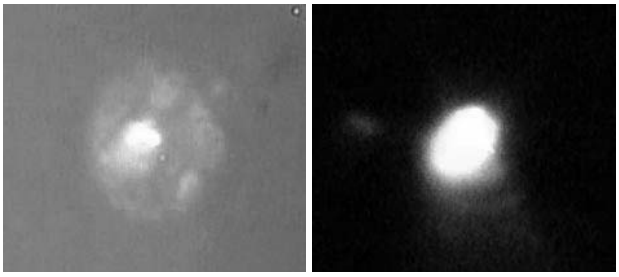

Fig. 3. Optical micrographs of the sample region in a hybrid DAC during heating (left: with light, right: without light).

Precision laser machining of nano-polycrystalline diamond

Takuo OKUCHI (Nagoya University, Japan, okuchi@eps.nagoya-u.ac.jp), Shoko ODAKE (University of Tokyo, Japan, odk@eqchem.s.u-tokyo.ac.jp), Hiroaki OHFUJI (Ehime University, Japan, ohfuji@sci.ehime-u.ac.jp), Mitsuru SUGATA and Shouhei NAGATOMO (Laser Solutions Co., Ltd., Japan, mitsuru.sugata@laser-solutions.co.jp and syohei.nagatomo@laser-solutions.co.jp), Hitoshi SUMIYA (Sumitomo Electric Industries, Ltd., Japan, sumiya@sei.co.jp), and Hiroyuki KAGI (University of Tokyo, Japan, kagi@eqchem.s.u-tokyo.ac.jp)

1. Introduction

Nano-polycrystalline diamond (NPD) is an alternative form of diamond material that is synthesized from graphite by direct conversion under excessively high pressure [1]. NPD consists of diamond grains with several tens of nanometers in size orienting in random directions. Therefore NPD has higher hardness than single-crystal diamond (SCD). In addition, it shows neither cleavage feature nor anisotropy of hardness those are weak points of SCD when it is used to generate excessively high pressure. The NPD also has higher fracture toughness than SCD [2].

One of the most important tasks to make further use of NPD in science and engineering applications is its precise machining into desired shapes. Polish-machining of NPD is much more difficult than that of SCD, although it is possible. The polishing of NPD is time-consuming so that NPD anvils could not be mass-produced, in spite of its proved capacity to generate multi-megabars [2].

The motivation of this study is thus to develop an alternative method for precise machining of NPD. Laser- processing may become an answer because results of laser- drilling of SCD showed that diamond can be machined very precisely [3]. We expect that laser also works well for NPD.

2. Experimental

NPD samples for machining, with typical thickness of 0.5 to 1 mm, were provided by T. Irifune at Ehime University and by Sumitomo Electric Industries. They were grooved or cut with RAPYULAS laser micro- processing system at Laser-solutions Co. Ltd, Kyoto, Japan. The light source was diode-pumped solid state laser with frequency multiplier for THG (355 nm wavelength). We controlled important processing parameters to find suitable conditions for precise machining; those are (1) averaged laser power, (2) frequency of the Q-switch, and (3) work sending velocity against the beam.

The grooved and cut surfaces of NPD were observed by field-effect scanning electron microscope (FE-SEM) and by transmission electron microscope (TEM), both at Ehime University. FE-SEM is suitable to observe the shape and size of excavated debris from the grooves and cut surfaces, while TEM gave information about spatial distribution of various carbon phases under the cut surface those are transformed from diamond. From these observations we found that the machining involves several distinct process- es such as (1) absorption of light energy and its conversion to heat, (2) thermal cracking, (3) thermochemical reaction with air, (4) carbon evaporation and recondensation, and (5) solid-solid phase transformation. These processes changes their significance with the machining conditions described above. The problem here is how to reduce mechanical and thermal damages of the cut surface while keeping the processing fast enough, which will be discussed in detail in the presentation.

References

[1] Irifune, T. *et al*. (2003) Nature, 421, 599-600.

[2] Nakamoto, Y. *et al*. (2007) Japan. J. Appl. Phys., 46, L640-L641.

[3] Okuchi, T. *et al*. (2007) Phys. Rev. B, 75, 144104.

Acknowledgments

We thank T. Irifune for providing NPD test pieces as well as giving useful comments. This work is supported by MEXT Grant-in-Aid for Creative Scientific Research entitled “Material sciences at ultra-high pressure using the strongest spallation neutron source.”

High-pressure deformation study of nanocrystalline nickel

Yuejian WANG (yuejianw@lanl.gov)[1], Jianzhong Zhang (jzhang@lanl.gov)[1], Yusheng ZHAO (yzhao@lanl.gov)[1], Sven C. VOGEL[1], Norimasa NISHIYAMA[2], and Yanbin WANG[2]

[1]LANSCE-Division, Los Alamos National Laboratory, USA; [2]Center for Advanced Radiation Sources, University of Chicago, Chicago, Illinois, USA

Nanocrystalline nickel has received significant attention, both experimentally and theoretically, due to its erotic plastic deformation and super mechanical property. Its recoverable srain broadening in conventional tensile test brings a new perspective to understanding the nanocrystalline plasticity [1]. Furthermore, nanocrystalline nickel exhibits much higher strength than its coarse-grain counterpart [2]. However, the study of uni-axial deformation of nano-nickel under different confining pressures has not been reported.

The deformation experiments were carried out at beamline 13-BM-D of the Advanced Photon Source, Argonne national Laboratory, with monochromatic X-rays and a 2-D radiographic imaging system. The detailed description of the D-DIA setups and experimental routines were published elsewhere [3-4]. In our experiment, the nano-nickel powders, with a median particle size of 12 nm, were prepared by mechanical milling technique. We investigated the uni-axial deformations of nano-Ni in both compression and extension cycles at confining pressures 16, 32, and 50 tons.. The total percent strain was derived from the sample length which can be measued from the X-ray radiograph. The differential lattice strains were determined from the lattice distortion along azimuth dimension. The differential strains were converted to differential stresses using elastic constant.

The deformation under each confining pressure is addressed and the yield strength is determined by the graphic derivation method. Furthermore, the mechanism underlying the deformation will be discussed.

References

[1] Zeljka Budrovic, Helena Van Swygenhoven, Peter M. Derlet, Steven van petegem, and Bernd Schmitt (2004) "Plastic deformation with reversible peak broadening in nanocrystalline nickel." *Science* **304**, 273-276.

[2] Yusheng Zhao, Jianzhong Zhang, Bjorn Clausen, T. D. Shen, Geory T. Gray III, and Liping Wang (2007) "Thermomechanics of nanocrystalline nickel under high pressure-temperature conditions." Nano letters 7, 426-432.

[3] Yanbin Wang, William B. Durham, Ivan C. Getting, Donald J. Weidner (2003) "The deformation-DIA: A new apparatus for high temperature triaxial deformation to pressures up to 15 GPa." *Review of Scientific Instruments* **74**, 3002-3011

[4] Takeyuki Uchida, Yanbin Wang, Mark L. Rivers, and Steve R. Sutton (2004) "Yield strength and strain hardening of MgO up to 8 GPa measured in the deformation-DIA with monochromatic X-ray diffraction." *Earth and Planetary Science letters* **226**, 117-126.

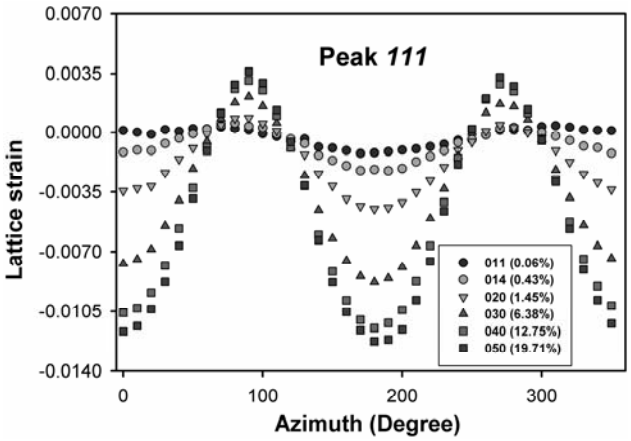

Fig. 1. An example of the azimuthal distortion of lattice strain for peak 111 taken from the deformation cycle at 16 ton. The legend shows the data file number with total strains in brackets. The hydrostatic strain and differential lattice strain were obtained by fitting each reflection distortion.

Electron-lattice interaction under high pressure examined by single-crystal diffraction study

Takamitsu YAMANAKA, Ho-Kwang MAO (Carnegie Institute of Washington, Geophysical Laboratory)

1. Introduction

Developments of high-pressure apparatus have enhanced *in situ* investigations of Earth's interiors under extreme conditions. Crystal structures analyses together with physical properties of earth materials under nonambient conditions are one of the significant subjects to understand geophysical phenomena, because many minerals in the crust and mantle undergo structure changes such as phase transformation, lattice deformation, decomposition cation ordering and amorphization under high-pressure conditions, Synchrotron radiation (SR) facilities have accelerated high-pressure crystal-lography, because of their great advantages for diffraction study at nonambient conditions using DAC [1]. Phase transitions under compression due to lattice instability, electronic state change and magnetic spin change can be elucidated by X-ray diffraction, absorption and resonance phenomena using DAC together with X-ray inelastic measure-ments. These experiments provide the significant insight of pressure effect on electron-lattice or spin-lattice interactions such as Jahn-Teller transition, Mott transition, charge displopornation, density of state change, high-low spin transition, spin Peierls transition etc. Structure analysis of high-pressure phases with super structure, incommensurate struc-ture, defused structure and polytype structure can be solved only by single-crystal diffraction study.

2. Experimental

High-pressure diffraction studies using DAC often encountered several difficulties for *in situ* intensity measurement. We have made significant progresses in the high-pressure generation system and efficient equipment for single-crystal diffraction study up to megabar region [2].

Developments of various types of detectors and SR accelerate kinetic studies and dynamical studies of these changes. The diffraction study using hard X-ray under compression at high temperatures generated by electric resistive heater or laser and at low tempera-tures using cryostat.

Maximum entropy method (MEM) can visualize electron density distribution using diffraction intensity observed at high pressure. MEM can ignore termination effect induced from small aperture angle of DAC [3]. Electron orbital distribution of *d*-electrons of transition metal elements, localization of electron, bonding electron (σ, π-bond) are elucidated by MEM [4].

High flux hard X-ray provided by SR has a big advantage for measurement of X-ray emission spectra (XES). High-low spin transition was observed by XES at APS [5].

Combination of optical investigations by Raman and infrared spectroscopy is efficient to comprehend the electronic state under high pressure.

3. Result

I. Anisotropy of electric conduction of $FeTiO_3$ ilmenite under high pressure

The high-pressure diffraction studies of $FeTiO_3$ have been conducted up to 8.2GPa using SR in PF at Tsukuba with DAC. The deformations of FeO_6 and TiO_6 octahedra were reduced with pressure. In order to elucidate the electric conductivity change with pressure, electron density distribution of $FeTiO_3$ has been executed by MEM using single-crystal diffraction intensity data. MEM based on $F_{obs}(hkl)$ more clearly shows electron density than the difference Fourier synthesis $F_{obs}(hkl)$-$F_{calc}(hkl)$. The radial distribution of the electron density indicates electron localization around the cation positions. The bonding electron density is lowered with pressure. Neither charge transfer nor electron hopping between Fe and Ti along the *c* axis in $FeTiO_3$ is possible under high pressure. But the electric conductivity due to electron super-exchange in Fe-Fe and Ti-Ti has been clarified by the MEM electron density distribution. The anisotropy in the electric conductivity has been clarified.

II. Jahn-Teller distortion of Fe_2TiO_4 ulvospinel at high pressure and low temperature

Structure refinements using single-crystals were executed under high pressures up to15GPa at room temperature and under low-temperature condition down to -170˚C at ambient pressure. The transition from cubic totetragonal is induced from the tetragonal distortion due to the Jahn-Teller effect of Fe^{2+}at the tetrahedral site. The phase-transition takes place at 9 GPa and –110˚C. The c/a ratio is 0.9982(4) at 11.43 GPa and 1.0035(5) at –170˚C. Degeneracy of e_g orbital of $^{IV}Fe^{2+}$ under the high-pressure and

low-temperature condition is different and the former prefers electronic state d_{x2-y2} and the latter d_{z2} orbital. Difference Fourier maps and MEM maps on (100) and (001) planes of Fe_2TiO_4 reveal the electron density of e_g electrons of $^{IV}Fe^{2+}$. Spin configuration of low temperature JT and High-pressure JT are expressed by A and B in the figure, respectively. Orthorhombic structure of Fe_2TiO_4 at 30 GPa determined by Rietveld method was $CaTi_2O_4$ type structure by powder diffraction study. In addition, we found another new higher-pressure polymorph at 45 GPa.

III. Mn_2O_3 bixbyite transforms to post-perovskite and further to monoclinic phase at high pressure

Bixbyite $(Mn,Fe)_2O_3$ has a C-type rare-earth oxide structure with space group of $Ia\bar{3}$ and different from many A_2O_3 of 3d transition metal oxides, which have corundum structure $R\bar{3}c$. Single-crystal structure analyses and powder diffraction experiments were carried out using synchrotron radiation under high pressures up to 41.21GPa. Lattice constants and bond distances were elucidated as a function of pressure. Single crystal structure analysis under high pressures up to 9.64GPa has been executed using DAC. There are two octahedral Mn^{3+} sites show different compression curves. $M1O_6$ octahedron is less compressive than $M2O_6$ octahedron. $M1O_6$ octahedron is a largely distorted octahedron. Both octahedra do not show a noticeable Jahn-Teller distortion induced from Mn^{3+}. Transition to post-perovskite was confirmed at about 21 GPa with a large hysteresis. The transition is reversible and non-quenchable [6].

After laser heating the post-perovskite phase at 25GPa, powder diffraction study showed that the high-pressure phase changed the monoclinic new phase similar to structure of Gd_2O_3. However, XES confirmed no change at the structure transition, proving that the structure transition has no relation with the high-low spin transition.

The spin transition pressure will be much higher than 21GPa. It has been known the spin transition of Fe_2O_3 is about 50GPa. In the next experiment, the spin transition pressure will be clarified. The result can suggest the spin transition of the series of M_2O_3 with transition elements.

References

[1] Yamanaka T. GSA Special Paper 421 175-188, 2007

[2] Yamanaka T., Fukuda T., Hattori T. and Sumiya H. Rev.sci.Inst.42, 1458-1462, 2001

[3] Yamanaka T., Komatsu Y. and Nomori H. Phys. Chem. Minerals 34, 307-318, 2007

[4] Yamanaka T., OkadaA T., Komatsu Y and Nomori H. Jour. Synchrotron Rad. 12, 566-576, 2005

[5] JF Lin, VV Struszhkin, Jacobsen, G Shen, VB Prakapenka, HK Mao and RJ. Hemley. Synchrotron Radiation 12, 637-641 2005

[6] Yamanaka T., Nagai T. Okada T and Fukuda T. Zeit. Krist. 220, 938-945, 2005

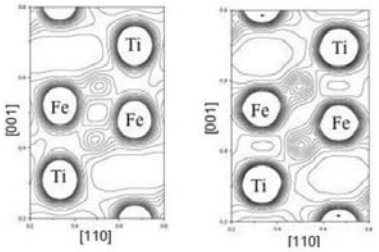

Fig. 1. Electron density on the (010) plane calculated by MEM at 0.1MPa and 8.2GPa. The data sets of $\sin\theta/\lambda < 0.90$ are used for MEM calculations. The contour lines are drawn from 0.2 to 4.0eÅ^{-3} with 0.2eÅ^{-3} intervals.

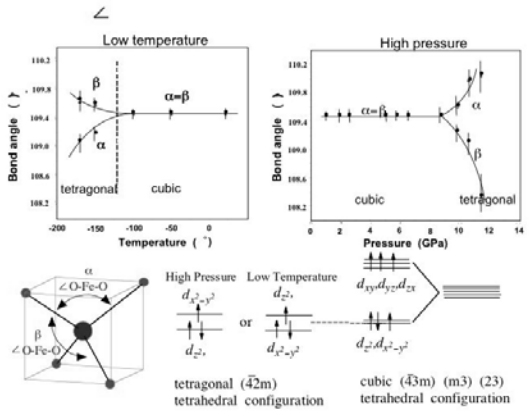

Fig. 2. Spin configuration and tetrahedral deformation in the tetrahedral phase of Fe_2TiO_4. A and B present the deformation and the spin configuration at high pressure and low temperature. Bond angle O-Fe-O is an indicator of the elongation and flattening of the unit cell with c/a.

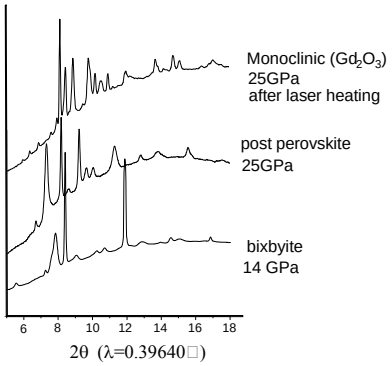

Fig. 3. High-pressure polymorphs of Mn_2O_3. It has a rare earth oxide C-type structure and transforms to $CaIrO_3$ type structure at 21GPa. After heating at 1400C and 25GPa, it further transforms to monoclinic Gd_2O_3.

New synchrotron-based single-crystal methods for structural mineral physics and materials science

P. Dera[1], B. Lavina[1,2], L.A. Borkowski[1,2], R.T. Downs[3], and M.F. Nicol[2]

[1]*CARS, University of Chicago;* [2]*HiPSEC and Department of Physics, University of Nevada, Las Vegas;* [3]*Department of Geosciences, University of Arizona, Tucson*

Introduction

Our understanding of the Earth deep interior and our ability to model its physical properties depend heavily on the understanding of phase diagrams and crystal structures of the mineral phases present in these environments.

The dominating crystal structure determination method used by modern high-pressure scientists is powder X-ray diffraction (PXD). This approach, while very valuable in determining compressibility of materials and qualitative identification of phase transitions, has very limited capabilities for full structure determination (applied to non quenchable phases of previously unknown structure type). The main reason for this shortcoming is the one-dimensional character of the PXD spectra, and notoriously broad diffraction peaks caused by strain in samples at very high pressures. Single-crystal X-ray diffraction (SXD) methods, which have been used with success for complete structure determination at ambient conditions, and have been introduced to high-pressure science in the 1970s, have thus far been limited to pressure of about 10 GPa.

The recent advances in synchrotron technology, offering incident beam sizes in a 5 μm range, much increased flux, and great incident energy tenability introduce new possibilities to modify and optimize SXD experimental methodology to better answer the needs of structure determination from micrograins (less that 10 μm) enclosed in Diamond Anvil Cells (DACs). Our group at the Advanced Photon Source, Argonne National Lab has developed and tested a range of novel methods involving both polychromatic as well as monochromatic radiation and different kinds of detectors for studying crystal structures of single crystals at high pressure [1-3]. This talk will focus on monochromatic SXD methods development at GSECARS.

Experimental

Series of full structure determination tests with micrograins (5-20 μm) of range of materials pressurized in DACs have been performed at Sectors 13 (GSECARS), of the Advanced Photon Source at Argonne National Lab. Maximum pressure reached in the experiments was 45 GPa. The data collection approach was monochromatic SXD. In the presentation the theoretical basis of monochromatic method will be briefly introduced, and a comparison of the capabilities, benefits, quality of the results, with other high-pressure SXD methods, as well as possible applications will be reviewed.

Results and discussion

Single crystal of zeolite mesolite ($Na_2Ca_2[Al_2Si_3O_{10}]_3 \cdot 8(H_2O)$) has been chosen as the test case of the monochromatic SXD method implemented in station 13IDD. Mesolite belongs to the NAT zeolite family, for which pressure-induced superabsorption has been observed [4] by means of powder diffraction. Preliminary results of compression study mesolite with a CCD detector clearly show volume expansion by 4.4% at ~1.8 GPa (Fig. 1), due to transport of pressure medium molecules inside the pores. The molecular transport through the channels is accompanied by appearance of diffuse scattering lines in the diffraction images. Upon pressure release the crystal retains much of absorbed solvent and exhibits symmetry different than the original one. Data collection time for complete wide oscillation image (Fig. 2) was 5 seconds. The mechanism of the osmotic compression determined for mesolite will be presented.

Acknowledgements

This project was supported by a grant from the Major Research Instrumentation Program, Division of Materials Research, National Science Foundation (NSF-DMR-0521179). GSECARS is supported by the National Science Foundation, the U.S. Department of Energy, the W.M Keck Foundation, the U.S. Department of Agriculture and the State of Illinois. Use of the APS was supported by DOE-BES, under Contract No. DE-AC02-06CH11357.

References

[1] Dera P., Prewitt C.T., Jacobsen S.D. J. Synchr. Rad. 12, 547-548, (2005).

[2] Ice G., Dera P. J. Synchr. Rad. 12, 608-617, (2005).

[3] Jacobsen, S.D., Lin, J.-F., Shen, G., Prakapenka, V., Dera, P., Angel, R.J., Mao, H.K. and Hemley, R.J. J. Synchr. Rad. 12, 577-584, (2005).

[4] Lee, Y. Hriljac, J.A., Vogt, T., Parise, J.B., Artioli, G. J. Am. Chem. Soc. 123, 12732-12733 (2001).

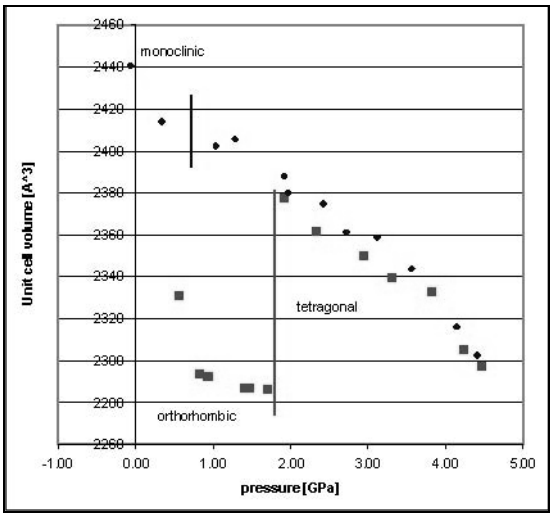

Fig. 1. Pressure dependence of the unit cell volume of mesolite during osmotic compression measured using monochromatic single diffraction method.

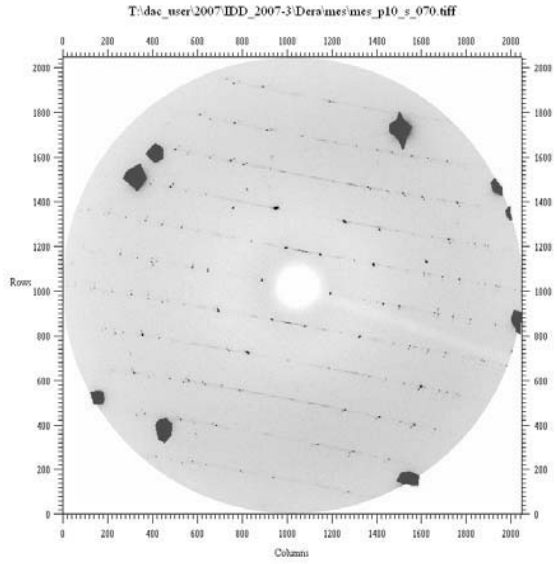

Fig. 2. Wide oscillation (60°) monochromatic X-ray diffraction image collected from a single crystal of mesolite in a DAC.

Novel structural phase transition of vanadium under high pressure

Yang DING (HPSynC-Carnegie Institution of Washington, USA, yangding@aps.anl.gov)

1. Introduction

Elucidating the structural stability trends and the underlying mechanisms in elemental metals is a fundamental topic in condensed matter physics. Of particular interest are the transition metals that exhibit the hcp (hexagonal close packed)-bcc (body centered cubic)-hcp-fcc (face centered cubic) sequence of structures with increasing either atomic number or pressure. The driving force behind such structural variations is typically attributed to the increasing *d*-band filling with increasing atomic numbers [1,2,3] or the pressure-induced *s-d* electronic transitions [4,5]. According to the structural sequence, the vanadium group metals (V, Nb and Ta) are commonly predicted to be stable in the bcc structure up to at least a couple of hundred GPa [1-5]. As no structural change has been reported so far [6], they now become standard examples demonstrating the success of applying first principles calculations for structural stability of elemental metals. However, the latest lattice dynamics calculations, aimed at understanding the T_c anomaly in vanadium around 120 GPa [7], suggested a possible shear instability due to phonon softening in vanadium [8,9]. This prediction prompted our interest to re-investigate the structural transition of vanadium under high pressure.

2. Experimental

Using diamond-anvil cell and synchrotron X-ray diffraction techniques, we report in this letter for the first time the observation of a transition from bcc to a rhombohedral phase in vanadium at 69 GPa. The vanadium sample displays the characteristics of a second order phase transition across which the pressure dependences of lattice parameters are continuous, but their slopes are discontinuous. This form of transition has never been reported in any transition metal or other pure element, and represents an entirely different trend from previous reports. Moreover, the discovery reveals that electronic structure features other than the *s-d* transition, such as Fermi surface nesting and electronic topological transition, could be the origin of structure variations, and provides essential information for proper re-evaluation of the T_c anomaly at 120 GPa which occurs in the new phase rather than the simple bcc vanadium.

Mao-type symmetric diamond-anvil cell with two beveled diamond anvils (80 μm central flat beveled at 8° angle from the 400 μm culet) was used to pre-indent Re gasket from the original thickness of 250 μm to 20 μm central thickness. A 50 μm diameter hole was drilled at the center of the gasket to form the sample chamber. Powder vanadium sample (purity 99.99% from Alfa Aesar) was loaded in the sample chamber without a pressure medium. A 3-5 μm platinum powder chip used as the pressure standard was added to a quadrant of the sample area. High-pressure angle-dispersive diffraction experiments were performed at 16ID-B station of the HPCAT Sector, Advanced Photon Source, Argonne National Laboratory. The monochromatic X-ray beam, operated at 29.21 and 30.87 KeV, was focused to ~20 μm in diameter at the sample position. The small beam was used to select specific sample areas. Areas that only contained pure vanadium diffraction pattern (*e.g.*, Fig. 1) were used for clear identification of phase transition without possible complications from the Pt and Re diffraction, and areas that contained both vanadium and Pt were used for pressure determination and confirmation of the vanadium diffraction. Pressure was determined from the equation of state of platinum [10, 11] based on three diffraction lines: 111, 200, and 220. The uncertainty in *d*-spacing measurements was estimated to be less than 0.007 Å, which corresponded to 4-5 GPa uncertainty around 100 GPa. The diffraction patterns were collected using a MAR345 image plate (pixel size 100 x 100 μm^2), and the exposure time was typically 30-600 *s*. The two dimensional diffraction rings on the image plate (Fig. 1) were integrated with the FIT2D program [12] to produce diffraction patterns of intensity versus 2θ (Fig. 2), and the lattice parameters were obtained from the refinement of diffraction patterns with the GSAS program [13].

3. Results and discussion

Experiments were carried out up to 155 GPa. Vanadium remained in the bcc structure until the 110 and 220 peaks split above 65 GPa, whereas the 200 diffraction stayed as a single sharp line up to the maximum pressure (Fig. 1). The changes evinced a transition from cubic to a rhombohedral lattice due to the elongation or contraction of a unit-cell body diagonal [111] relative to the other three body diagonals, similar to the B2-R phase transformation discovered in NiTi alloys [14]. Figure 2 shows the diffraction patterns of vanadium at 65, 90, and 155 GPa. The transformation from the bcc structure

($Im\bar{3}m$) into a rhomboheral structure ($R\bar{3}m$) is illustrated by the insert in Figure 2(b). The cubic unit cell with lattice parameter a_c can also be represented by a rhombohedral unit cell with lattice parameter a_R and α; the two unit cells are related by $a_R = \frac{\sqrt{3}}{2} a_C$ and $\alpha = 109.47^\circ$. When α deviated from 109.47°, the symmetry was reduced from cubic to rhombohedral. The cubic 110 diffraction peak was no longer degenerate but split into rhombohedral $1\bar{1}0$ and 100, and the cubic 211 split into rhombohedral $2\bar{1}0$, $2\bar{1}\bar{1}$, and 110. The rhombohedral α angle could thus be calculated from the splitting of the cubic 110 and 211 diffraction lines as shown in the inserts in Figure 2(c).

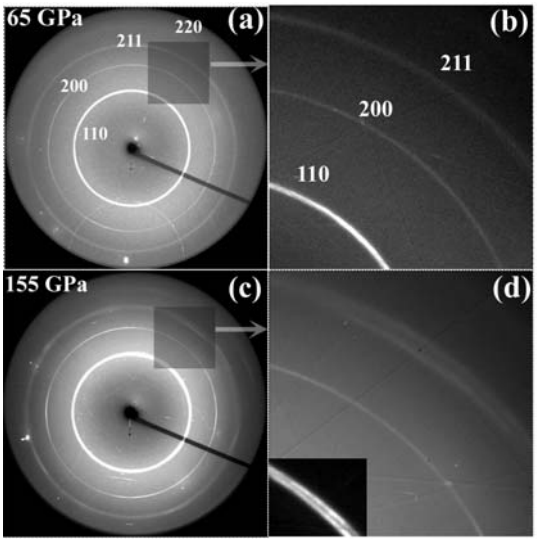

Fig. 1. (a) The diffraction pattern of vanadium recorded on an image plate at 65 GPa under non-hydrostatic conditions. The indexing is based on a bcc lattice. (b) The enlarged image of the shadowed area in (a). (c) The diffraction pattern of vanadium at 155 GPa. (d) The enlarged image of the shadow area in (c).

To eliminate the possibility of anisotropic broadening due to strong uniaxial stress [15], we performed an additional quasi-hydrostatic experiment to 76 GPa on vanadium powder sample using helium as pressure transmission medium [16]. As shown in Figure 3, in the quasihydrostatic experiment above the transition pressure, the 110, 211 and 220 reflections also split, whereas 200 remained as a single sharp peak, thus unambiguously confirming the phase transition from cubic to rhombohedral lattice.

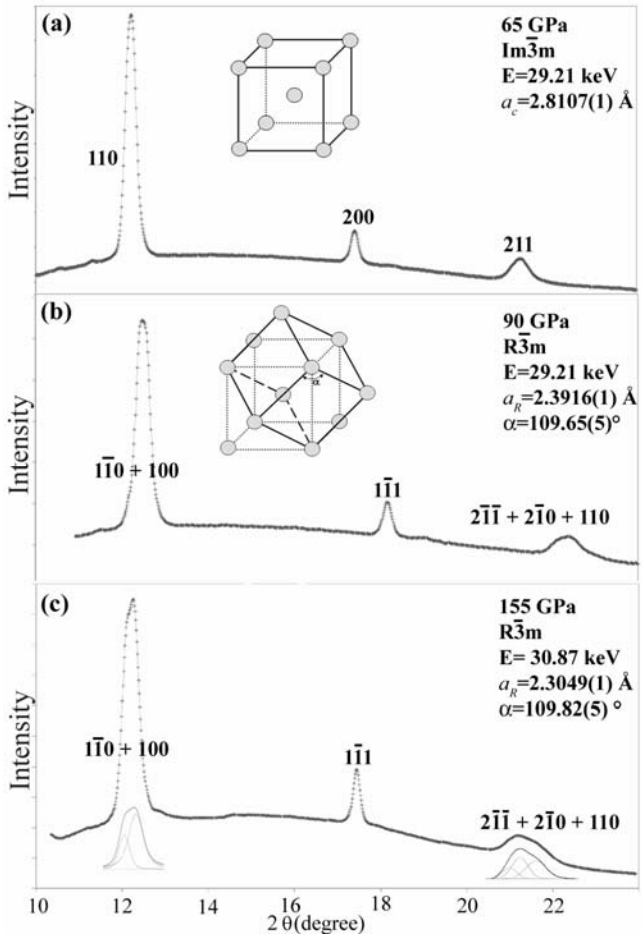

Fig. 2. Non-hydrostatic X-ray diffraction patterns of vanadium at (a) 65 GPa, (b) 90 GPa and (c) The 155 GPa. The insert in (b) demonstrates the transformation of vanadium from cubic to the rhombohedral structure. The inserts in (c) demonstrate the resolved splitting peaks according to refinement of rhombohedral structure model. E denotes the energy of X-ray photon used for diffraction.

Takemura studied X-ray diffraction of vanadium up to 154 GPa [6]. Although he did not claim any structural transition, the diffraction pattern of vanadium in his report at 154 GPa indeed showed a very broad 110 peak, a shoulder on the low angle side, and a sharp 200 peak that are consistent with the present conclusion of a bcc-rhombohedral transition.

The phase transition displayed a lattice distortion without a discontinuity in the pressure-volume plot (Figure 4a), thus characterizing a second-order displacive phase transition. For example, for the non-hydrostatic series, the deviation of α from 109.47° (cubic) at 65 GPa to 109.65° at 90 GPa, and to 109.82° at 155 GPa provides a direct measurement of

symmetry breaking strain. The transition pressure was analyzed based on Landau theory, in which the order parameter $<Q>$ was defined as $(\alpha/\alpha_0) - 1$ where α_0 is 109.47° for the cubic phase. $<Q>^2$ is proportional to spontaneous lattice strain [17]. The transition pressures P_c, obtained by fitting the equation $<Q> = C\ (P-P_c)^{1/2}$ where C is a constant, are determined to be 69(1) GPa for non-hydrostatic and 63(1) GPa for quasi-hydrostatic experiments (Figure 4(b)). The bulk moduli obtained from non-hydrostatic and quasi-hydrostatic experiments are K_0=195(3) GPa with K_0'=3.5(2) and K_0=158(1) GPa with K_0'=3.9(2) (Figure 4a) respectively, by fitting the third Birch-Murnaghan equation of the state to the pressure-volume data of bcc vanadium (Figure 4(a)). The quasi-hydrostatic results in our experiments agree well with K_0 = 162(5) GPa and K_0' = 3.5(5) from quasi-hydrostatic experiments by Takermura [6]. Our non-hydrostatic data points shift to slightly higher pressure side of the quasi-hydrostatic data points; this agrees with the well documented effect of non-hydrostaticity in high-pressure literatures, (for example. ref. [18]).

It is known that vanadium group metals display Kohn anomalies [19,20] in the transverse acoustic phonon branch along the [ξ00] direction, and the anomaly at $\xi = 1/4$ was predicted to soften under high pressure and eventually become imaginary at 130 GPa [8] (but the mechanism of softening was not discussed by the authors). This mode is related to the shear elasticity tensor by $C_{44} = \omega^2\rho/K^2$, where ω, ρ, and K are phonon frequency, density and phonon wave vector, in the long wavelength limit, and C_{44} is associated with a trigonal distortion of the cubic lattice. Consequently, the pressure induced rhombohedral transition in vanadium could be trigged by the C_{44} instability due to the phonon softening.

The *d*-band filling via *s-d* transition is typically regarded as a major driving force behind the pressure-induced structure transitions in transition metals. However, it is unlikely that the C_{44} softening in vanadium is driven by *s-d* transition. For instance, chromium ($3d^5 4s^1$) with two more electrons in the *d* band than vanadium ($3d^3 4s^2$) shows no softening but stiffening of C_{44} (C_{44} of vanadium is 43 GPa [21], while that of chromium is 100 GPa [22]), Therefore, other mechanisms must be considered.

Very recent *ab initio* calculations on bcc vanadium by Landa et al., employing full-potential linear muffin-tin orbitals (FPLMTO) [23] and exact muffin-tin orbital calculations (EMTO) [9] methods, show that C_{44} reaches a maximum and softens at pressures above 60 GPa and drops to zero at 120 (FPLMTO) to 180 GPa(EMTO). According to these calculations [9, 23], the Kohn anomaly at $\xi = 1/4$ along [ξ, 0 ,0] in the transverse acoustic phonon mode was a consequence of Fermi surface nesting in the third band. Upon compression, the nesting vector $\boldsymbol{q}_n = 0.48\ \pi/\alpha$ decreased and the effect of the Kohn anomaly on C_{44} increased. When $\boldsymbol{q}_n$ became zero, a minimum appeared in the shear elastic constant C_{44} due to an electronic topological transition in 3rd band. Meanwhile, the pressure induced *s-d* transition also introduced band Jahn-Teller effects on C_{44} softening, but this effect was secondary to those of Fermi surface nesting and electronic topological transition [9]. The physical meaning of the predicted trigonal elasticity tensor C_{44} instability at 120-180 GPa is an upper limit, above which a finite shear would lead to infinitely large strain in the bcc vanadium and cause the collapse of the structure; a phase transition must occur before reaching this limit. Our experimental observation of the rhombohedral transition at 63-69 GPa is consistent with the predicted upper limit.

References

[1] J. Duthie and D. Pettifor, Phys. Rev. Lett. **38**, 564 (1977).

[2] H. L. Skriver, Phys. Rev. B **31**, 1909 (1985).

[3] J. A. Moriarty, Phys. Rev. B **45**, 2004 (1992).

[4] A. K. McMahan, Physica, **139 & 140B**, 31 (1986)

[5] G. B. Grad, P. Blaha, J. Luitz, K. Schwarz, A. Fernández Guillermet, and S. J. Sferco, Phys. Rev. B **62**, 12743 (2000).

[6] K. Takemura *Sci. Technol.* High Pressure **443** (2000).

[7] M. Ishizuka, M. Iketani, and S. Endo, Phys. Rev. B **61**, R3823 (2000).

[8] N Suzuki and M Otani, J. Phys.: Condens. Matter. **14,** 10869 (2002).

[9] A. Landa, J. Klepeis, P. Söderlind, I. Naumov, L. Vitos, and A. Ruban, J. Phys: Condens. Matter **18**, 5079, (2006).

[10] N. C. Holmes, J. A. Moriarty, G.R. Gathers, and W. J. Nellis, J. Appl. Phys. **66**, 2962 (1989).

[11] H. Cynn and C. S. Yoo, Phys. Rev. B **59**, 8526 (1999).

[12] A. P. Hammersley, S. O. Svensson, M. Hanfland, A. N. Fitch, and D. Häusermann, High Press. Res. **14**, 235 (1996).

[13] A. C. Larson, and R. B. Von Dreele, General Structure Analysis System (GSAS), Los Alamos

National Laboratory Report No. LAUR, 86-748, (1994).

[14] J. Khalil-Allafi, W. W. Schmahl and T. Reinecke, Smart Mater. Struct. 14, S192, (2005)

[15] N. Funamori, M. Funamori, R. Jeanloz, and N. Hamaya, J. Appl. Phys. 82, 142 (1997), and references therein.

[16] Hydrostatic compression experiment with helium as transmission medium was conducted on vanadium powder from same batch as used in non-hydrostatic experiments. A compacted vanadium powder chip of 30 x 30 x 10 μm was loaded together with ruby and platinum pressure standards in a Mao-type symmetric diamond-anvil cell, and the vanadium sample was well separated from Pt pressure standard. Two beveled diamond anvils (200 μm flat beveled from a 400 μm culet at an angle of 8°) were used with a 90 μm hole on a 30 μm thick, pre-indented rhenium gasket. The diffraction experiments were performed at the 16ID-B station of HPCAT with a 5 x 7 μm^2 monochromatic X-ray beam operated at 30.57 keV. The sample and Pt diffraction peaks remain sharp, and the ruby fluorescence peaks remain well resolved, indicating hydrostatic condition.

[17] K. Aizu J. Phys. Japan **28,** 706, (1970)

[18] T. S. Duffy, G. Y. Shen, D. L. Heinz, J. F. Shu, Y. Z. Ma, H. K. Mao, R.J. Hemley, and A. K. Singh, Phys. Rev. B **60**, 15063 (1999)",

[19] Y. Nakagawa and A. D. B. Woods, Phys. Rev. Lett. **11**, 271 (1963)

[20] M. W. Finnis and K. L. Kear, Phys. Rev. Lett. **52**, 291 (1984)

[21] D. I. Bolef, J. Appl. Phys. **32**, 100, (1961)

[22] D.I. Bolef and J. de Klerk, Phys. Rev. **129**, 1063 (1963)

[23] A. Landa, J. Klepeis, P. Söderlind, I. Naumov, O. Velikokhatnyi, L. Vitos, A. Ruban, J. Phys. Chem. Solids, **67**,2056 (2006); J. Klepeis and P. Söderlind, Bulletin of the APS, *49*, 496 (2004).

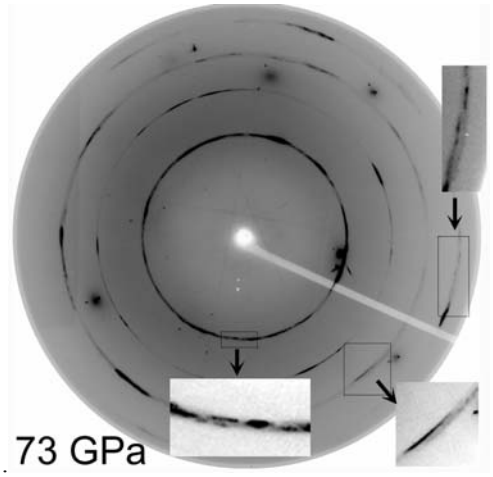

Fig. 3. The diffraction pattern of vanadium at 73 GPa under quasi-hydrostatic conditions recorded on an image plate. The diffraction rings are spotty because the sample-grinding was minimized in order to avoid the introduction of residual strain. From inside outward, the four rings are originally 110, 200, 211, and 220 reflections of the cubic phase. Inserts are zoomed images showing the splitting of 110, 211 and 220 rings after rhombohedral transition.

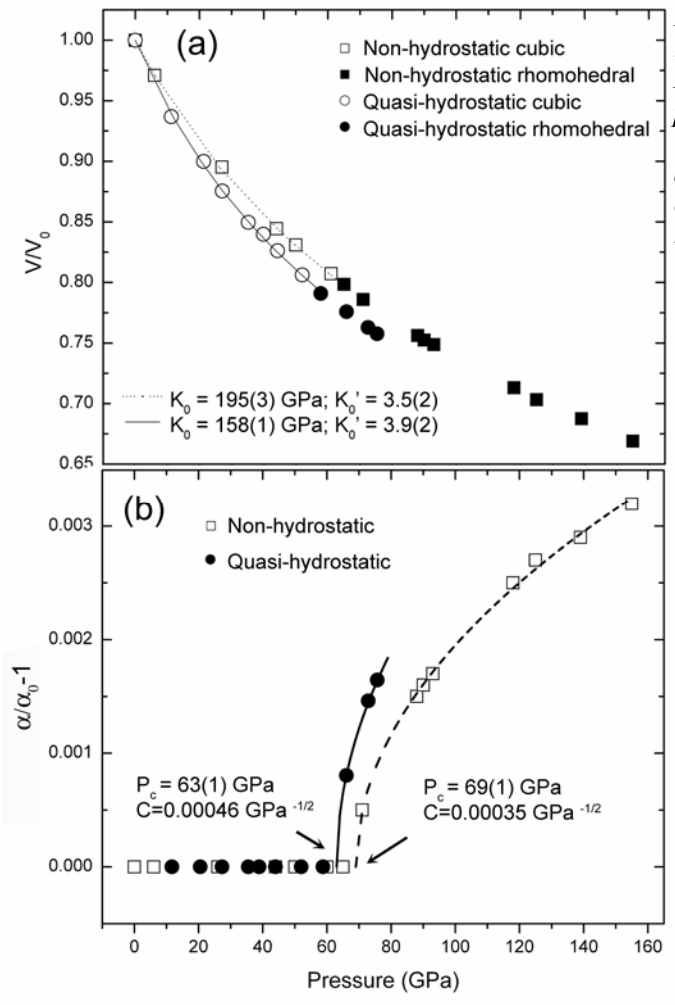

Fig. 4. (a) The pressure-volume data of vanadium. The lines represent the fitted results using 3rd Birch-Murnaghan equation of state. (b) The plot of order parameter $\langle Q \rangle$*, defined as* $(\alpha/\alpha_0) - 1$ *where* $\alpha_0 = 109.47°$*, versus pressure. The phase transition pressures determined from non-hydrostatic and quasi-hydrostatic experiments are 69(1) GPa and 63(1) GPa, respectively, using equation* $\langle Q \rangle = C(P-P_c)^{1/2}$.

Determination of the high-pressure phases (II′ and IV′) of $CuGeO_3$ using single-crystal techniques

Lauren BORKOWSKI (High Pressure Science and Engineering Center, UNLV, and GSECARS, USA, borkowski@cars.uchicago.edu), Barbara LAVINA (High Pressure Science and Engineering Center, UNLV and GSECARS, USA, lavina@cars.uchicago.edu), Przemyslaw DERA (GSECARS, USA, dera@cars.uchicago.edu), Hanns-Peter LIERMANN (HPCAT, Geophysical Laboratory, Carnegie Institution of Sciences, USA, pliermann@hpcat.aps.anl.gov)

1. Introduction

Copper metagermanate ($CuGeO_3$) is considered to be the first known inorganic material to display a spin-Peierls transition.[1] This property has attracted interest to such extent that the material has been studied under varying conditions, in particular at high pressure. Compression studies of this material have revealed two sets of phase transitions that are sensitive to the hydrostatic pressure conditions in the sample chamber.[2]

Compression studies under purely hydrostatic conditions reported that $CuGeO_3$ transforms first to a monoclinic phase (II) at 7 GPa,[3] then to an orthorhombic phase (II′) at 14 GPa, and finally to a tetragonal phase (VI) at 22 GPa.[4] All phases are unquenchable to ambient conditions. Thus, compressing $CuGeO_3$ under quasi-hydrostatic compression, will result in an alternative phase transition pathway starting with a quenchable orthorhombic phase (III) at 7 GPa,[5] proceeding to a monoclinic phase (IV) at 8 GPa, then to phase IV′ at 12.5 GPa, and finally to phase V at 18 GPa.[6] Previous studies provide us with the crystal structures of the low pressure phases (I, II, III and IV). Raman and powder X-ray diffraction studies provide estimates of the cell dimensions and space groups of the remaining higher pressure phases, although the crystal structures of phases II′, IV′, V and VI remain elusive.

2. Experimental

Crystals of $CuGeO_3$ were obtained from Dr. S.-W. Cheong of Lucent Technologies, Bell Laboratories. Suitable single crystals of phase I were selected and transformed to phase III by squeezing the crystals in a diamond anvil cell (DAC) using silicon oil as the pressure medium. The pressure was increased until the crystals changed color from a pale blue color to an intense blue. Careful pressure release allowed the recovery of metastable crystals of phase III. Single crystals of both starting phases (I and III) were loaded in the same DAC using Ne gas as the pressure medium and ruby as a pressure standard.

The crystals were studied using a combination of monochromatic single crystal X-ray diffraction (SXD) and polychromatic energy dispersive X-ray diffraction (EDX SXD) at GeoSoilEnviroCARS (sector 13, APS) and the High Pressure Collaborative Access Team (HPCAT, sector 16, APS), respectively. The EDX SXD technique is being developed by our group for the express purpose of determining the structures of high-pressure non-quenchable phases using single crystals.

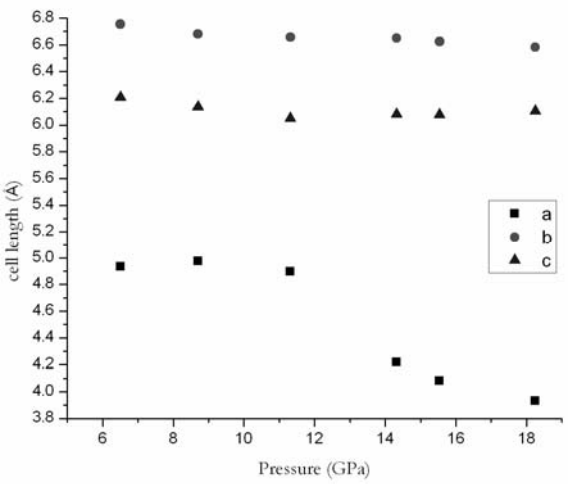

Fig. 1. Plot of lattice parameters versus pressure showing the II to II′ phase transition occurring at approximately 13 GPa.

3. Results and discussion

Using a combination of both methods, we were able to unambiguously determine the lattice parameters of phases II′ and IV′. In both cases there is a distinct decrease in the lattice parameters that precedes the phase transition and seem to be most pronounced in the **a** direction (Figs. 1 and 2). The lattice parameters of phase II′ from powder X-ray diffraction experiments reported by Ming, et. al.[4] do not agree with the lattice parameters determined in this study. We attribute this discrepancy to the higher quality and three-dimensional character of single crystal data. Presented herein will be the results of the $CuGeO_3$ studies as well as an up-date of the EDX SXD technique.

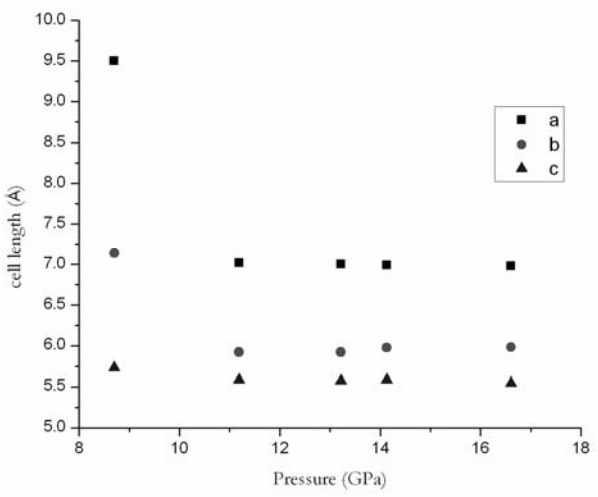

Fig. 2. Plot of lattice parameters versus pressure showing the III to IV' phase transition occurring between 8.7 and 11.2 GPa. It appears that we passed through the phase IV without measure the diffraction pattern.

Acknowledgments

Support from NSF and DOE (BES and NNSA) are gratefully acknowledged.

References

[1] Hase, M.; Terasaki, I.; Uchinokura, K. *Phys. Rev. Lett.* **1993**, *70*, 3651-3654.

[2] Jayaraman, A.; Sharma, S. K.; Wang, S. Y.; Cheong, S.-W. *Curr. Sci.* **1996**, *71*, 306-312.

[3] Yoshiasa, A.; Yagyu, G.; Ito, T.; Yamanaka, T.; Nagai, T. *Z. Anorg. Allg. Chem.* **2000**, *626*, 36-41.

[4] Ming, L. C.; Shieh, S. R.; Jayaraman, A.; Sharma, S. K.; Kim, Y. H. *J. Phys. Chem. Solids* **1999**, *60*, 69-81.

[5] Dera, P.; Jayaraman, A.; Prewitt, C. T.; Gramsch, S. *Phys. Rev. B* **2002**, *65*, 134105.

[6] Ming, L. C.; Sharma, S. K.; Jayaraman, A. J.; Kobayashi, Y.; Suzuki, E.; Endo, S.; Prakapenka, V.; Yang, D. *Spectrochim. Acta A* **2005**, *61*, 2418-2422.

Equation of state and pressure-induced transition(s) in B_4C: Correlation of static high-pressure synchrotron XRD, Raman, nd shock-wave data

Murli H. MANGHNANI (murli@soest.hawaii.edu)[1], George AMULELE[1], Przemyslaw DERA[2], Yuchang WANG[1], Yanbin WANG[2], Robert DOWNS[3], Anwar HUSHUR[1]

[1]University of Hawaii, Hawaii Institute of Geophysics and Planetology, USA; [2]University of Chicago, GSECARS, Advanced Photon Source, Argonne National Laboratory, USA; [3]University of Arizona, USA

1. Introduction

Synchrotron X-ray diffraction (XRD) and Raman spectroscopy measurements have been carried out on B_4C in a diamond-anvil cell to 60 GPa. These results, in conjunction with single-crystal XRD at ambient conditions and high-pressure ultrasonic measurements, are compared with shock wave data in order to understand the compression behavior, establish the equations of state, and explain the observed poor ballistic performance.

2. Experimental

Experimental details shall be orally presented.

3. Summary of results and discussion

Whereas the powder XRD data indicate no easily detectable discontinuous changes within the studied pressure range, the Raman spectroscopy, electrical conductivity measurements, and shock wave data suggest a more complex behavior. Motivated by this discrepancy, a detailed strain/stress analysis based on the peak profile broadening was performed, revealing two regions of discontinuous strain change, which cannot be explained by the transformations of pressure transmitting medium. These changes can be tentatively associated with electronic transformations and changes in bonding. Preliminary results from the electrical resistivity and optical measurements support this interpretation.

Session IV:

Mineral Physics Applications

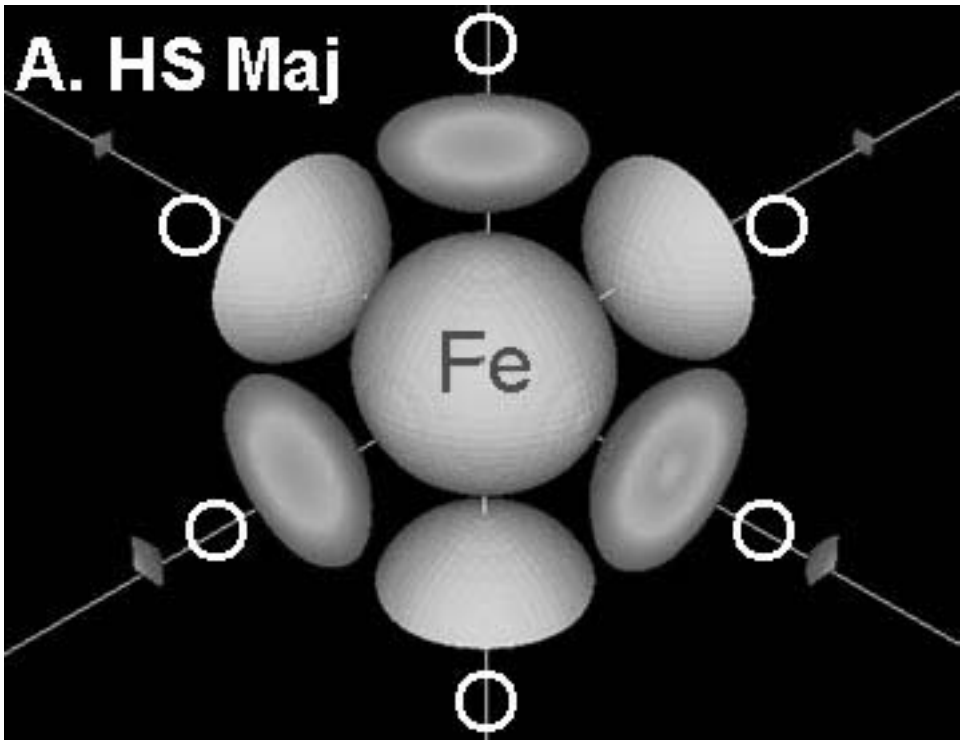

Synchrotrons: A core business?

Guillaume FIQUET (Institut de Minéralogie et de Physique des Milieux Condensés, Institut de Physique du Globe de Paris, France, guillaume.fiquet@impmc.jussieu.fr)

1. Introduction

Because the core is composed primarily of iron alloyed with light elements, the physics of iron and related alloys must be well understood to assess the effect of impurities on the properties the real core material could be made of. In this study, we focus on Fe_3C cohenite which further allows us to constrain the carbon content of the inner core.

In addition, the structure of iron at inner core conditions is still an open issue, since some theoretical calculations (e.g., [1]) or a recent experimental observation on a nickel-iron alloy indicate that a body centered cubic one could be more appropriate [2]. It is however still reasonable to envisage that iron adopts the hexagonal close packed structure (hcp) at Earth's inner core conditions. To answer both these questions, we present the results of two different studies carried out using synchrotron radiation at ESRF (Grenoble, France).

2. Experimental

The high-pressure and high-temperature behavior of iron has been investigated to 140 GPa and 3400 K with *in situ* synchrotron X-ray diffraction at beamstation ID27 of ESRF. I present series of experiments carried out on hot-pressed samples of iron and periclase in a laser-heated diamond-anvil cell, that were combined with ATEM examination of recovered samples.

We also measured compressional sound velocities of Fe_3C-cementite at high-pressure by very high resolution inelastic X-ray scattering.

3. Results and discussion

Among all structures proposed so far for pure iron samples, hcp-iron only is found to be present at the highest pressure and temperature investigated. In addition, these experiments allow us to better bracket the triple point between the fcc and hcp phases and the liquid, and to address the evolution of the c/a ratio with pressure and temperature and the related elastic anisotropy of iron at core conditions. Finally, a new thermal equation of state for iron at megabar pressures is proposed, with tighter constraints on the light element content of the inner core.

We show that Fe_3C follows Birch's law for the longitudinal acoustic velocity V_P, namely a linear dependence between velocity and density, as shown in the illustration hereafter.

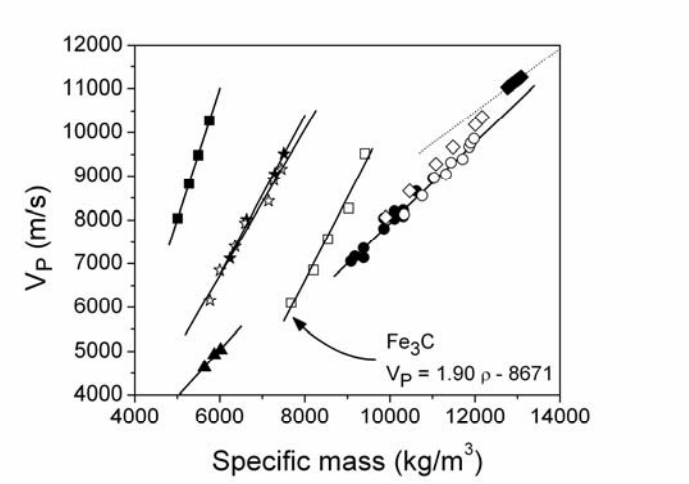

This dataset completes the previous sets recently established by [3] for FeO, FeSi, FeS, and FeS_2, and provides new mineralogical constraints on the composition of Earth's core. Our results, combined with data already obtained for other iron alloys are compared with seismic data, and suggest that a reduced carbon amount in the inner core could reasonably explain density and velocity differences between pure iron and seismic models. This conclusion, however, depends on the remaining uncertainty on magnetic structure for a very low carbon content in the iron alloy. It does not preclude the incorporation of another light element in the inner core, such as silicon.

References

[1] Belonoshko et al. (2003) Nature 424, 1032.

[2] Dubrovinsky et al. (2007) Science 316, 1880.

[3] Badro et al. (2007) Earth Planet. Sci. Lett., 254, 234.

Effect of pressure on the melting behavior of the Fe-S system at moderate pressures

Bin CHEN (University of Illinois at Urbana-Champaign, U.S.A., binchen2@uiuc.edu), Jie LI (University of Illinois at Urbana-Champaign, U.S.A., jackieli@uiuc.edu)

1. Introduction

On the ground of its siderophile (Fe-loving) nature and cosmochemical abundance, sulfur (S) is believed to be one of the most likely alloying light elements in Fe-rich planetary cores. Detailed studies on the phase relations in the Fe-S system at high pressures and temperatures are essential for our understanding of the thermal states and physical properties of sulfur-bearing iron cores. Previous experimental investigations on melting relations in the Fe-S system revealed that the formation of the intermediate Fe-S compounds Fe_3S_2 and Fe_3S changes the phase diagram significantly [Fei et al., 1997, 2000]. To date, the liquidus curves of the Fe-S system at moderate pressures have not been determined. We have conducted experiments to determine the liquidus curves of the Fe-S system at 10 and 14 GPa. We found a positive departure from ideal solution behaviour at 14 GPa resulting in substantial reductions in the liquidus temperatures of Fe-rich alloys under conditions found at intermediate depths in Mercury's core. The experimental results on the liquidus curves of Fe-S system are applied to Mercury in order to understand the physical states of its core.

2. Experimental

Using a 1000 US ton Walker-type multi-anvil apparatus, we measured the liquidus curves of the Fe-rich portions of the Fe-S system at 10 and 14 GPa. Stoichiometric mixtures of Fe and FeS were dried and packed into MgO capsules. High temperature was generated with a cylindrical rhenium furnace and monitored using a rhenium-tungsten thermocouple, without considering the pressure effect on the electro-motive force (emf). Pressures were calibrated from known phase transitions in Bi, ZnS, GaP at room temperature and in SiO_2, $CaGeO_3$ and $MgSiO_3$ at high temperatures. In each experiment, the assembly was compressed to the target pressure at room temperature and then heated to the target temperature. After equilibrating at high pressure and high temperature, the sample was quenched by shutting off the power to the furnace. Recovered samples were polished, carbon-coated, and analyzed with a Scanning Electron Microscope (SEM) and an Electron Probe Microanalyzer (EPMA).

3. Results and discussion

The liquidus curves of the Fe-rich portion of the Fe-S binary system at 10 and 14 GPa are constructed based on our experimental data together with melting temperature of iron and the eutectic temperatures [Fei et al., 1997, 2000; Boehler 1990]. At 10 GPa, the liquidus curve is relatively smooth, consistent with nearly ideal solution behavior. Upon the formation of the intermediate compound Fe_3S_2 at around 14 GPa, however, the liquidus curve shows a positive departure from ideal solution behaviour, indicating moderate repulsion between the Fe and Fe_3S_2 endmember components in the liquid. The non-ideal liquidus curve at 14 GPa leads to minimum in the liquidus gradient. The occurrence of this minimum, and a similar minimum in the pressure dependent eutectic temperature, coincide with the formation of the intermediate sulfide Fe_3S_2, suggesting that a substantial change in Fe-S interaction near 14 GPa.

References

[1] Fei, Y., Bertka, C. M. & Finger, L. W. High-pressure iron-sulfur compound Fe3S2, and melting relations in the system Fe-FeS. Science 275, 1621-1623 (1997).

[2] Fei, Y., Li, J., Bertka, C. M. & Prewitt, C. T. Structure type and bulk modulus of Fe3S, a new iron-sulfur compound. Am. Mineral. 85, 1830-1833 (2000).

[3] Boehler, R. Temperatures in the Earth's core from melting-point measurements of iron at high static pressures. Nature 363, 534-536 (1993).

In situ observation of immiscible liquids in the Fe-O-S system at 3 GPa using an X-ray radiographic technique

Kyusei TSUNO (Bayeriches Geoinsititut, Universität Bayreuth, Germany, kyusei.tsuno@uni-bayreuth.de)
Hidenori TERASAKI (Inst. of Mineral. Petrol. and Econ..Geo, Tohoku University, Japan, terasaki@mail.tains.tohoku.ac.jp),
Eiji OHTANI (Inst. of Mineral. Petrol. and Econ..Geo, Tohoku University, Japan, ohtani@mail.tains.tohoku.ac.jp)
Akio SUZUKI (Inst. of Mineral. Petrol. and Econ..Geo, Tohoku University, Japan, ohtani@mail.tains.tohoku.ac.jp)
Yuki ASAHARA (SPring-8, JASRI, Japan, asaharay@spring8.or.jp)
Keisuke NISHIDA (Inst. of Mineral. Petrol. and Econ..Geo, Tohoku University, Japan, nishidak@ganko.tohoku.ac.jp)
Tatsuya SAKAMAKI (Inst. of Mineral. Petrol. and Econ..Geo, Tohoku University, Japan, sakamaki@ganko.tohoku.ac.jp)
Ken-ichi FUNAKOSHI (SPring-8, JASRI, Japan, funakosi@spring8.or.jp)
Takumi KIKEGAWA (Photon Factory, KEK, Japan, takumi.kikegawa@kek.jp)

1. Introduction

It is important to investigate liquid immiscibility in the Fe-light element(s) systems in order to discuss the chemical composition and formation process of the planetary cores. In previous studies in the Fe-O-(S) [1-4], and Fe-S-Si system [5], investigations of the liquid immiscibility were based on the textural observation and chemical analysis of recovered products. However, there is no consensus on textural interpretation of the immiscible liquids in the Fe-O-(S) system [1-4]. Therefore, we have performed it situ experiments of the liquid immiscibility in the Fe-O-S system at high pressures and temperatures using a synchrotron X-ray radiographic technique.

2. Experimental

High pressure experiments were carried out using a Kawai-type multianvil press. We used a 1500-ton press on BL04B1 beamline at SPring-8, and a 700-ton press on BL14C2 beamline at KEK-PF. For performing X-ray radiography measurements, we used a white X-ray beam at SPring-8, and a monochromatic X-ray with 35 keV at KEK-PF. Direct X-ray beams passed through the cell assembly at high pressure, and transmitted X-rays were observed as radiographic images using CCD cameras with a YAG fluorescence screen.

Starting compositions were $Fe_{65}O_{27}S_8$, $Fe_{62}O_{23}S_{15}$, $Fe_{61}O_{19}S_{20}$, $Fe_{57}O_{16}S_{27}$, and $Fe_{54}O_{13}S_{33}$ (in atomic ratio). We used a Al_2O_3 sample container, graphite heater, MgO or boron-epoxy pressure medium, and boron epoxy windows sandwiched by pyrophyllite as gasket.

All experiments were performed at 3 GPa based on an equation of state of hBN, and temperatures were

monitored using a $W_{97}Re_3$-$W_{75}Re_{25}$ thermocouple. After the experiments, texture and chemical compositions of the recovered samples were analyzed using a SEM/EDX and an electron microprobe.

3. Results and discussion

Three types of melting and quench processes were observed in the in-situ measurements.

(1) Primary immiscible liquids were observed in radiographs, and were quenched as two separate phases, with a starting composition of $Fe_{65}O_{27}S_8$.

(2) Primary immiscible liquids became miscible with increasing temperature, and a miscible liquid was separated into two phases during quenching, with starting compositions of $Fe_{62}O_{23}S_{15}$ and $Fe_{61}O_{19}S_{20}$.

(3) A miscible liquid is observed above the liquidus temperature during heating, with a starting compositions of $Fe_{57}O_{16}S_{27}$, and $Fe_{54}O_{13}S_{33}$.

Here we show typical radiographic images of (2), with starting composition of $Fe_{62}O_{23}S_{15}$. That experiment was performed at SPring-8. Immiscible liquids were observed at temperatures of 1723-2003K (Fig. 1a). Beyond those temperatures, they became miscible (Fig. 1b). Two separated phases appeared during quenching from 2073K (Fig. 1c). The recovered product also shows the two phases (Fig. 1d).

The present results show that in-situ measurements are required for determination of the miscibility gaps in the Fe-light element(s) systems.

References

[1] Kato, T., Ringwood, A.E. (1989) Phys. Chem. Miner., 16: 524-538.

[2] Ringwood, A.E., Hibberson, W. (1989) Phys. Chem. Miner., 17: 313-319.

[3] Urakawa, S., Kato, M., Kumazawa, M. (1987) in High Pressure Research in Mineral Physics, Geophys. Monogr. Ser., vol. 39: pp.95-111.

[4] Tsuno, K., Ohtani, E., Terasaki, H. (2007) Phys. Earth Planet. Inter., 160: 75-85.

[5] Sanloup, C., Fei, Y. (2004) Phys. Earth Planet. Inter., 147: 57-65.

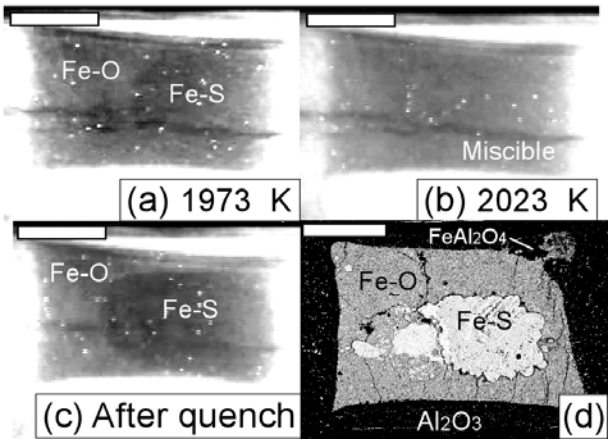

Fig. 1. X-ray radiographic images with a starting composition of $Fe_{62}O_{23}S_{15}$ (S1699) performed at SPring-8, (a) at 1973K, (b) at 2073K, and (c) after quench. The scale bars are 500 μm. (d) A back scatted electron image of the recovered product. The scale bar is 500 μm.

Inelastic X-ray scattering experiments on liquids in diamond anvil cells

Ahmet ALATAS , Harald SINN, Jiyong ZHAO, Ayman H. SAID, Bogdan M. LEU, Wolfgang STURHAHN, Ercan E. ALP (XSD, Advanced Photon Source, ANL, Alatas@aps.anl.gov), Guoyin SHEN (HPCAT - Carnegie Institution of Washington at Sector 16, APS), Vitali B. PRAKAPENKA (Consortium for Advanced Radiation Sources, University of Chicago)

Measurement of physical properties of solids or liquids under pressure at high temperatures is important in understanding the behavior of planetary materials. It is clear that any new methodology development will contribute greatly in solving some of the puzzles related to the structure of earth and other terrestrial planets, whether this interest originates from a condensed matter physics, mineral physics, or geology point of view.

Among the physical properties, the atomic structure is addressed by x-ray diffraction, and great progress has been made in the last two decades in incorporating special structure diamond-anvil-cells (DAC) to synchrotron radiation beamlines. A combination of laser heating or resistive heating has expanded our knowledge of the phase diagram and equation of state for many minerals and alloys at elevated temperatures and pressures reflecting the conditions in the lower mantle, down to the mantle-core boundary.

However, the progress in measuring thermo-elastic properties using various inelastic x-ray scattering (IXS) techniques under such extreme conditions has lagged behind, and only in the last few years has some progress been made. Among the successful attempts, one can mention direct measurement of phonon-density of states with Nuclear Resonant Inelastic X-Ray Scattering (NRIXS) [1] or phonon dispersion relations with momentum-resolved inelastic x-ray scattering (MRIXS) [2-4]. While the measurement of lattice dynamics is relevant to solids, knowledge of viscosity and thermal conductivity is equally relevant and significant to liquid core, as well as accurate determination of melting boundary for iron-alloys under core conditions.

The MRIXS measures momentum transfer (Q)-dependent position, width, and intensity of Brillouin and Rayleigh scattering. The strength of the Rayleigh (elastic) line is due to the presence of entropy fluctuations in a pure liquid and/or concentration fluctuations, while the Q dependence of the width of the central line is related to thermal conductivity. Similarly, the intensity of the Brillouin lines is due to the presence of sustained pressure fluctuations, while the position is related to sound velocity, and the Q-dependence of the width is related to dynamic viscosity. Furthermore, the detailed balance between Stokes and anti-Stokes lines would be a good measure of the temperature of the sample, directly measured at the intersection of x-ray beam and the laser beam.

MRIXS has been successfully used in extracting velocity of sound and viscosity of liquids at ambient pressure and temperature in water, alkali metal liquids, metal-ammonia solutions or noble element liquids [5,6], as well as at very high temperatures exceeding 2500K to study liquid sapphire, silicon, or boron [7]. However, to date there is not much progress in combining laser heating, DAC, and MRIXS techniques simultaneously.

Our early attempts using resistive heating and measuring the thermo-physical properties of liquid indium inside a DAC with resistive heating indicated a strong potential for this approach. We have encountered a strong elastic scattering background. As mentioned before, the Rayleigh (elastic) line is an important physical quantity in liquid studies and, therefore, this elastic scattering background affects the data quality. This problem does not exist in the NRIXS method since prompt counts that include this background are discriminated from delay counts with time discrimination electronics. The origin of this background is identified as coming from diamonds because it is in the path of scattering volume that is involved at the sample position. The way to avoid this background is to use the collimator system after the DAC; this will be implemented at the beamline soon.

For the experiment, we use the inelastic x-ray scattering spectrometer with four analyzers working with energy resolutions of about 2.2 meV at the Advanced Photon Source, 3ID beamline [8]. Incident beam was focused onto a sample by torodial mirror to an approximately 250 x 150 (Hor. x Ver.) micron beam size. Moreover, we have better focusing capability at sector 30, a newly developed beamline at the APS. Beam size at sector 30 is about 40 x 15 micron (hor. x ver.) using a KB mirror system.

The use of the Advanced Photon Source was supported by the U. S. Department of Energy, Office of Science, Office of Basic Energy Sciences, under Contract No. DE-ACO2-06CH11357.

References

[1] H. K. Mao et al., Science, 292, 914 (2001).

[2] G. Fiquet et al., Physics of the Earth and Planetary Interiors, 143-144, 5 (2004).

[3] D. Antonangeli et al., Earth and Planetary Science Letters, 225, 243-251 (2004).

[4] D. Antonangeli et al., Phys. Rev. Lett. 93, 215505 (2004).

[5] F. Sette et. al., PRL, 75, 850-853 (1995).

[6] A. H. Said et. al., PRB, 68, 104302 (2003).

[7] H.Sinn et al., Science, 299, 2047 (2003).

[8] H. Sinn et al., Nucl. Instrum. Methods Phys. Res. A 467-468, 1545 (2001).

Time-resolved X-ray diffraction experiment of dehydration of serpentine at high pressure

Toru INOUE (GRC, Ehime Univ., Japan, inoue@sci.ehime-u.ac.jp), Isamu YOSHIMI (GRC, Ehime Univ., Japan, yoshimi@sci.ehime-u.ac.jp), Akihiro YAMADA (GRC, Ehime Univ., Japan, a-yamada@sci.ehime-u.ac.jp), Tetsuo IRIFUNE (GRC, Ehime Univ., Japan, irifune@dpc.ehime-u.ac.jp), Takumi KIKEGAWA (KEK, Japan, kikegawa@post.kek.jp)

1. Introduction

Serpentine is the most abundant hydrous phase in subducted slab, and the descending slab transports water into the Earth's interior. Antigorite (Atg) is one of the polymorph of serpentine, and the dehydration of Atg at certain depth supplies free water, and the upward migration contributes to the generation of magma in the mantle wedge. To evaluate the ability of H_2O transportation into the deep Earth's mantle, it is important to know the dehydration rate of Atg at high P-T conditions. We have conducted time-resolved dehydration experiments of Atg at high pressure and high temperature by in situ X-ray diffraction using MAX-80 (AR-NE5C) at PF-AR, Japan.

2. Experimental

Natural Atg was used as a starting material, and the sample was sealed by Au or Pt lids plus diamond sleeve, which enabled us to get high quality of diffraction because of high X-ray transparency of diamond [1]. Experiments were conducted between 3 and 9 GPa and temperature up to 700°C. We gradually increased temperature to ~500°C, and then the diffraction data were collected at every 50°C with increasing temperature. In each temperature, the diffractions were collected in every 60 seconds for certain duration with checking the peak change.

3. Results and discussion

Atg dehydrated to forsterite (Fo) + enstatite (En) + fluid via small amount of "talc-like" phase (Tlc) formation with increasing temperature below ~6 GPa (Fig. 1). These results were almost consistent with Perrillat et al. (2005) [2], but the degree of "talc-like" phase formation was different. At 3 GPa, the rapid dehydration was occurred at 700°C in 15 minutes, and at 5 GPa, that was occurred at 650°C in 50 minutes (see Fig. 1). Comparing with the previous phase equilibrium studies of Atg [e.g., 3], our result shows that the dehydration of Atg quickly occurs when P-T path goes into the region of Fo +En + fluid. This shows that Atg in subducted slab should quickly dehydrate when the slab crosses the dehydration boundary of Atg. Thus metastable Atg can not exist in subducted slab at around 650-700°C and 3-5 GPa.

To clarify the dehydration mechanism of Atg, we tried to fit the data by Avrami model [4]. The detailed analysis at 3-6 GPa and 650°C, where was the dissociation condition of Atg, showed that the nucleation rate was quite high for enstatite, but low for forsterite (Fig. 1). This result also can be confirmed clearly from the observation that incubation periods exist for forsterite formation. And also the fitting of the dissociation of Atg showed that the slope (the n value of Avrami model) was changed with time; this indicates the nucleation rate is changed from high to low with increasing time. Thus, the dissociation mechanism of Atg is complicated because of the reaction with silicate-rich fluid.

Talc was formed above 6 GPa with dissociation of Atg, and then the formation of phase A was observed in the present experiments. These results are inconsistent with the previous phase equilibrium reports [e.g., 3].

Acknowledgment

We acknowledge Y. Kono, T. Kawamura, and M. Katsuda for helping the present high-pressure in situ X-ray experiment in PF.

References

[1] Inoue, T. (2005) PF Activity Report 2004 #22 Part B, 206.

[2] Perrillat, J.-P. et al. (2005) Earth Planet. Sci. Lett., 236: 899-913.

[3] Komabayashi, T. et al. (2005) Phys. Earth. Planet. Inter., 151: 276-289.

[4] Avrami, M. (1939) J. Chem. Phys. 7: 1103-1112.

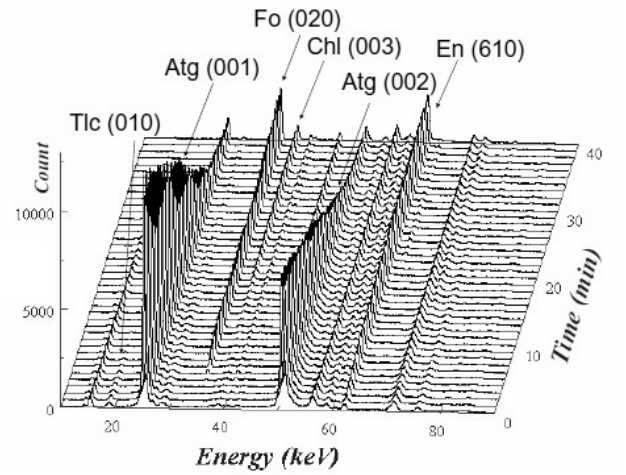

Fig. 1. An example of antigorite dehydration (AR068: 5.2 GPa, 650°C). The reaction "antigorite(Atg) → forsterite(Fo) + enstatite(En) + Fluid" occurred in this condition. Small amounst of talc (Tlc) and chlorite (Chl) can be seen.

Partitioning of iron between perovskite, post-perovskite, and ferropericlase up to 154 GPa and 2000 K

Takeshi SAKAI (International Advanced Research and Education Organization, Tohoku University, Japan, sakai@ganko.tohoku.ac.jp)
Eiji OHTANI (Inst. Mineral. Petrol. & Econ. Geol., Faculty of Sci., Tohoku Univ, Japan, ohtani@mail.tains.tohoku.ac.jp)
Masaaki MIYAHARA (Inst. Mineral. Petrol. & Econ. Geol., Faculty of Sci., Tohoku Univ, Japan, miyahara@ganko.tohoku.ac.jp)
Masahiko NISHIJIMA (Institute for Material Research, Tohoku Univ, Japan, ni_shi@imr.tohoku.ac.jp)
Hidenori TERASAKI (Inst. Mineral. Petrol. & Econ. Geol., Faculty of Sci., Tohoku Univ, Japan, terasaki@mail.tains.tohoku.ac.jp)
Tadashi KONDO (Graduate School of Science, Osaka Univ, Japan, tdskondo@ess.sci.osaka-u.ac.jp), Takumi KIKEGAWA (Photon Factory, Japan, kikegawa@post.kek.jp)
Naohisa HIRAO (Japan Synchrotron Radiation research Institute, Japan, hirao@spring8.or.jp)
Yasuo OHISHI (Japan Synchrotron Radiation research Institute, Japan, ohishi@spring8.or.jp)

1. Introduction

The lower mantle mainly consists of iron-bearing magnesium silicate perovskite and ferropericlase. The Fe-Mg partition coefficient between these minerals is important to understand the chemical and physical properties of the mantle. The lowermost 200 km of the mantle is called D″ layer and it is considered to be a thermal and chemical boundary layer between the silicate mantle and outer core. Recent high pressure studies [1] revealed that (Mg, Fe)SiO_3 perovskite transformed to post-perovskite phase at the pressure and temperature conditions of D″ layer. Thus, it is considered that (Mg, Fe)SiO_3 post-perovskite (PPv) phase and (Mg, Fe)O ferropericlase (Fp) are important minerals mainly constituting D″ layer. It is essential to clarify the Fe-Mg partition coefficient (K= (FeO/MgO)PPv/ (FeO/MgO)Fp in molar ratio) between post-perovskite and ferropericlase in order to understand the chemical and physical properties of this region.

2. Experimental

In this study, high pressure and high temperature partitioning experiments were performed up to 154 GPa at 2000K using a laser heated diamond anvil cell (LHDAC). Powdered or single crystalline Al-free San Carlos olivine ($Mg_{0.88}$, $Fe_{0.12})_2SiO_4$ was used as a starting material in order to avoid complicated compositional effects. The starting material was embedded in sodium chloride which is pressure medium. Pressures were determined by both the ruby fluorescence method [2] and the Raman shift of the first-order Raman spectra of diamond anvil [3]. Temperatures were measured by spectroradiometric method. Angle dispersive X-ray diffraction at high pressure was carried out using synchrotron radiation and an imaging plate (IP) at the BL18C at KEK-PF and at the BL10XU at SPring-8, Japan. Monochromatic X-rays of approximately 30 keV were collimated to 15-40 μm in diameter. X-ray diffraction patterns of the run products were collected at high pressure after heating and/or at ambient conditions after recovering the samples. The recovered samples were analyzed using the technique of combination of focused ion beam (FIB) method and analytical transmission electron microscopy (ATEM) (JEOL JEM-3000F (FEG TEM-STEM)).

3. Results and discussion

Post-perovskite and ferropericlase were identified at 154 GPa and 121 GPa after laser heating at 2000K. The lattice parameters of post-perovskite were a = 2.423(3) Å, b = 7.909(14) Å, c = 6.035(2) Å at 154 GPa and a = 2.468(5) Å, b = 8.055(15) Å, c = 6.161(8) Å at 121 GPa, respectively. The X-ray diffraction pattern of the recovered sample shows only ferropericlase because post-perovskite is unquenchable phase. The iron contents of ferropericlase was estimated from the relationship between the unit cell volume and iron contents suggested by Andrault (2001) [4]. Fe# of the recovered sample from 121 GPa was 0.21(2) and that from 154 GPa was 0.23(1). Here, Fe# was defined as FeO/(MgO+FeO) in the mole fraction. The iron contents of post-perovskite phase were calculated from the chemical mass balance using the composition of ferropericlase. The calculated Fe# of post-perovskite were 0.03 at 121 GPa and 0.01 at 154 GPa. The partition coefficients (K) of iron between post-perovskite and ferropericlase were 0.14 at 121 GPa and 0.02 at 154 GPa. The ATEM analysis shows that post-perovskite phase exhibits with very small

iron content of Fe# = 0.01 in the recovered sample from 140 GPa and 2000K. Therefore, the partition coefficient was K = 0.03, which indicates that iron prefers ferropericlase strongly rather than post-perovskite phase, which is consistent with the prediction of the ab initio calculation [5], and the high-spin/low-spin transition arguments of ferropericlase [6]. Kobayashi et al. (2005) [7] showed higher partitioning coefficient of K= 0.30 in spite of the lower temperature condition of 1600 K compared to the present experiment. They reported that significant iron depletion occurred in the sample heated at the high pressure condition, i.e. bulk Fe# reduced to 0.09 from 0.12. On the other hand, the bulk iron content of the present experiment conducted at 140 GPa and 2000 K does not show a significant iron depletion. Therefore, the difference in the partition coefficients between the present result and that by Kobayashi et al. may be caused by the compositional dependency of the partitioning behavior between post-perovskite and ferropericlase. Further study is necessary to clarify the compositional effect together with the effect of the spin transition on the partitioning behavior.

References

[1] Murakami et al (2004), Science, 304, 855-853.

[2] Mao et al (1978), J. Appl. Phys., 49, 3276-3283.

[3] Akahama Y., H. Kawamura (2004), J. Appl. Phys., 96, 3748-3751.

[4] Andrault, D. (2001), J. Geophys. Res., 106, 2079-2087.

[5] Iitaka et al (2004), Nature, 430, 442-445.

[6] Badro et al (2003), Science, 300, 789-791

[7] Kobayashi et al (2005), Geophys. Res. Lett., 32, L19301, doi:10.1029/2005GL023257

Ultrasonic measurements of polycrystalline MgO and standard-free pressure calibration at high pressures and high temperatures

Yoshio KONO (GRC, Ehime Univ., Japan, kono@sci.ehime-u.ac.jp), Yuji HIGO (JASRI, Japan, higo@spring8.or.jp), Toru INOUE (GRC, Ehime Univ., Japan, inoue@sci.ehime-u.ac.jp), Tetsuo IRIFUNE (GRC, Ehime Univ., Japan, irifune@dpc.ehime-u.ac.jp)

1. Introduction

Pressure is one of the most crucial uncertainties in high-pressure X-ray diffraction experiment, which should influence on precise determination of experimental values such as P-T conditions of phase transition and/or pressure derivative of physical properties. Pressure-volume-temperature equation of state of solid such as Au [1-3], Pt [3], MgO [3,4] and/or NaCl [5] has been used for determining pressure in high-pressure X-ray diffraction experiment, while the pressure in the equation of state depends on other equation of state and has not independently been solved because of the lack of direct measurement of sample pressure. Recently, Brillouin scattering and ultrasonic measurements in conjunction with high-pressure X-ray diffraction suggested standard-free pressure calibration [6-9]. In particular, Brillouin scattering measurement combined with X-ray diffraction study in diamond anvil cell [6] show standard-free pressure scale of MgO up to 55 GPa at 300K. However, these study determined pressure-volume equation of state only at 300K, and no standard-free pressure determination at high temperatures have been reported. Here we carried out in situ high pressure X-ray diffraction experiments combined with ultrasonic elastic wave velocity measurement at high pressures and high temperatures, and determined pressure-temperature-volume equation of state without pressure standard.

2. Experiment

High-pressure experiment was carried out using the 1500-ton Kawai-type multi-anvil apparatus (SPEED-1500) in BL04B1 beamline at SPring-8, Japan. Ultrasonic measurements and X-ray diffraction experiments were carried out up to 1650K and 17.5 GPa from Au scale [1]. The unit cell volume of MgO, Au, and NaCl and resultant their densities were determined from X-ray diffraction measurements. Elastic wave velocities of MgO were determined from elastic wave travel time and sample length. Ultrasonic elastic waves were generated and received by $LiNbO_3$ transducer, and the elastic wave travel time was determined from signals reflected at both ends of MgO sample. The sample length was directly measured using X-ray radiography.

3. Results and discussion

Compressional and shear wave velocities of MgO show quasi-linear pressure and temperature dependence without nonlinear behavior at high temperatures as observed in ringwoodite [10] and majorite with pyrolite minus olivine composition [11]. We also observed quasi-linear pressure and temperature dependence of adiabatic bulk modulus (Ks), which was determined using the observed compressional and shear wave velocities, and density. Zero pressure isothermal bulk modulus (K_{T0}) and its pressure (K'_{T0}) and temperature ($\partial K_T/\partial T$) derivatives were determined with fixed zero pressure thermal expansion coefficient [12], zero pressure Grüneisen parameter and its volume dependences [13] using the following regression equation:

$$Ks/(1+\alpha\gamma T) = K_{T0}(0,T)(1+2f)^{5/2}\{1+(3K'_{T0}-5)f\}$$
$$\alpha = \alpha_0 + \partial\alpha/\partial P \times P$$
$$K_{T0}(0,T) = K_{T0} + \partial K_T/\partial T \times T$$
$$f = \left\{(V_0/V)^{2/3}-1\right\}$$
$$V_0/V = \frac{V(0,T)/V(0,300)}{V(P,T)/V(0,300)} = \frac{\exp\left(\int_{300}^{T}\alpha(T)dT\right)}{V(P,T)/V(0,300)}$$

where α and γ are the thermal expansion coefficient and Grüneisen parameter, respectively. The equation was fitted with the difference of up to ~2% in isothermal bulk modulus at each pressure and temperature conditions. Pressure (P) at high temperature condition (T) was determined using the Birch-Murnaghan equation of state using the zero pressure thermal expansion coefficient, and observed zero pressure isothermal bulk modulus and its pressure and temperature derivatives as:

$$P = 3K_{T0}(0,T)(1+2f)^{5/2} f\{1+3(K'_{T0}-4)f/2\}$$

Our determined pressure below 20 GPa is consistent with those determined from the previously reported standard-free pressure-volume equation of state [6, 9] with the difference of less than 0.4 GPa. In particular, the differences of pressures between this study and Li et al. (2006) [6] are less than 0.1 GPa at 300K and <20 GPa. In contrast, we observed a significant difference of up to ~3 GPa between this study and

Zha et al. (2000) [9] if we extrapolate our equation of state to 55 GPa.

We compared our P-V-T equation of state of MgO with previously reported one [4]. The P-V relations at 300K and below 20 GPa are consistent but the pressure determined from the equation of state [4] at 1650K is slightly higher (~0.7 GPa at ~19-20 GPa) than that from our equation of state. We also compared our results with the pressure determined from equation of state of Au and NaCl using the simultaneously determined volume of Au and NaCl in our experiment. Both Au [1] and NaCl [5] scales show lower pressures than our estimation under high-pressure conditions. The difference increases with increasing pressure and reaches up to ~0.8 GPa at ~16-18 GPa. In contrast, our determined pressures at high temperatures are relatively consistent with those determined from Au scale [2] although the pressures at 300 K show marked difference above ~10 GPa.

In conclusion, we determined P-V-T equation of state of MgO without pressure standard under the pressure and temperature conditions up to ~18 GPa and 1650K. Our P-V relation at 300 K is consistent with previously determined standard-free P-V relations [6,9]. In contrast, present comparison of P-V-T equation of state between this study and previously published ones [1,2,4-5] shows marked differences in the estimated pressure. In order to evaluate more details for the previously reported equation of state and to establish absolute equation of state, we need further elastic wave velocity measurements combined with X-ray diffraction study at higher pressures and temperatures than present study.

Acknowledgment

We acknowledge A. Barnhoon and I. Jackson for supplying the MgO sample used here.

References

[1] Anderson, O. L., Isaak, D. G., and Yamamoto, S. (1989) J. Appl. Phys., 65: 1534-1543.

[2] Shim, S. H., Duffy, T. S. and Takemura, K. (2002), Earth Planet. Sci. Lett., 203: 729-739.

[3] Jamieson, J. C., Fritz, J. N. and Manghnani, M. H. (1982) High Pressure Research in Mineral Physics, eds. Manghnan, M. H. and Syno, Y., 427-437.

[4] Speziale, S., Zha, C. S. and Duffy, T. S. (2001) J. Geophs. Res., 106: 515-528.

[5] Decker, D.L. (1971) J. Appl. Phys., 42: 3239-3244.

[6] Zha, C. S., Mao, H. K. and Hemley, R. J. (2000) PNAS, 97: 13494-13499.

[7] Mueller, H. J., Schilling, F. R., Lauterjung, J. and Lathe, C. (2003) Eur. J. Mineral., 15: 865-873.

[8] Li, B., Kung, J., Uchida, T. and Wang, Y. (2005), J. Appl. Phys., 98: 013521.

[9] Li, B., Woody, K. and Kung, J. (2006) J. Geophys. Res., 111: B11206.

[10] Higo, Y., Inoue, T., Irifune, T., Funakoshi, K. and Li, B., in submitted to Phys. Earth Planet. Inter.

[11] T., Irifune, Higo, Y., Inoue, T., Kono, Y., Ohfuji, H. and Funakoshi, K., submitted to Nature.

[12] Dubrovinsky, L. S. and Saxena, S. K. (1997) Phys. Chem. Minerals, 24: 547-550.

Poster Abstracts

Materials Science

Synthesis and strength measurement of superhard B_6O at high pressure and temperature

Jiuhua CHEN (jiuhua.chen@fiu.edu)[1,2], Yunpeng YANG (yunpengmyang2002@hotmail.com)[2], Tony YU (tony.yu@sunysb.edu)[2], Jianzhong ZHANG (jzhang@lanl.gov)[3], Yusheng ZHAO(yzhao@lanl.gov)[3]

[1]CeSMEC and Mechanical and Materials Engineering, Florida International University, USA, [2]Mineral Physics Institute and the Department of Geosciences, Stony Brook University, Stony Brook University, USA, [3]LANSCE-Division, Los Alamos National Laboratory, USA

Boron compounds are of great interest in materials science because of their unique physical properties. Cubic boron nitride is the second hardest materials discovered so far in the world, next to diamond. A recently study reports that boron suboxide (B_6O) can be as hard as cubic boron nitride [1]. Similar to diamond and cubic boron nitride, B6O crystallizes at high pressures.

In our experiment, the B_6O sample is synthesize at 6 GPa and 1650^{o}C. Strength measurements are carried out using in situ X-ray diffraction at the X17B2 beamline of the National Synchrotron Light Source (NSLS). Energy dispersive diffraction patterns from the powdered sample are recorded as the sample is compressed. Upon compression, nonuniform contacts at grain boundaries build up microscopic differential stress in the sample, which gives rise to diffraction peak broadening. The differential stress is derived through deconvolution of the peak width. Analyses of diffraction peak (021) and (113) show anisotropic yielding in B_6O (Figure 1). The (021) orientation does not show yielding within the investigated pressure range (8 GPa) whereas the (113) orientation yielding at 6 GPa of sample pressure. During heating, significant weakening (yielding) was observed at temperatures above 400^{o}C. The yield temperature of boron suboxide is much lower than that of diamond, 1200^{o}C [2], similar to that observed in moissanite (SiC) [3].

Nanocrystalline B_6O was synthesized at a higher pressure, 30% increase in hardness in the nanocrystalline sample was observed.

References

[1] He, D., Y. Zhao, L. Daemen, J. Qian, T. D. Shen and T. W. Zerda (2002). "Boron suboxide: As hard as cubic boron nitride." *APPLIED PHYSICS LETTERS* **18**(4): 643-645.

[2] Weidner, D. J., Y. Wang and M. T. Vaughan (1994). "Yield strength at high pressure and temperature." *Geophysical Research Letters* **21**: 753 - 756.

[3] Zhang, J., Liping Wang, D. J. Weidner, T. Uchida and J.-A. Xu (2002). "The strength of moissanite." *American Mineralogist* **87**: 1005-1008.

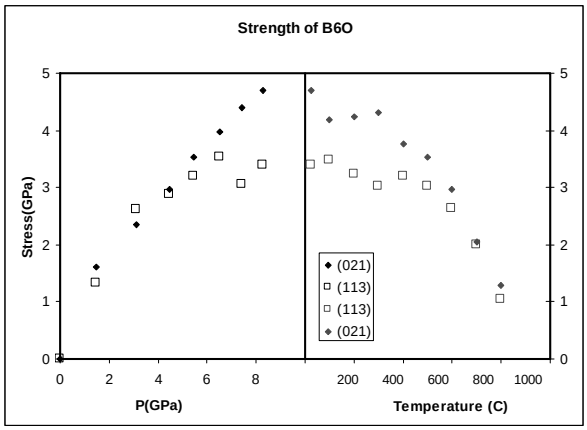

Fig. 1. Stress in the sample derived from peak broadening in the diffraction patterns collected during compression at ambient temperature (left) and during heating at the peak pressure (right). Different symbols indicate the data derived from different diffraction peaks.

Pressure-Induced Phase Transitions In Gadolinium Iron Borate

S.A. Kharlamova (kharlams@aps.anl.gov)[1,2], V. Struzhkin[3], S. Sinogeikin[3,4], A.G. Gavriliuk[5], D. Brown[6], T. Toellner[1], J. Zhao[1], M. Lerche[3], I.S. Lyubutin[7], S. Ovchinnikov[2], E.E. Alp[1] W. Sturhahn[1]

[1]IXN, Advanced Photon Source, Argonne National Laboratory; [2]Kirensky Institute of Physics, SB, Russian Academy of Sciences; [3]Geophysical Laboratory, Carnegie Institution of Washington; [4]HPCAT, Advanced Photon Source, Argonne National Laboratory; [5]Institute of High-Pressure Physics, Russian Academy of Sciences; [6]Northwestern University; [7]Shubnikov Institute of Crystallography, Russian Academy of Sciences, Russia

1. Introduction

An understanding of spin crossover (SC) dynamics is relevant to understanding of a role or participation of SC in natural systems including lower Mantle minerals, heme proteins as well as from fundamental science of view. For example, pressure-induced electronic spin transitions of Fe(III) and Fe(II) iron occur in silicate perovskite and magnesiowustite which are abundant minerals in the Earth's lower mantle [1-5]. Such a SC phenomenon has recently been observed in a number of magnetic materials $FeBO_3$ [6,7], $BiFeO_3$ [8], Fe_2O_3 [9]. In those cases, iron ions are in the trivalent state Fe^{3+} and the high-spin-low-spin (HS–LS) crossover is manifested as the collapse of the local magnetic moment and as the transition of the antiferromagnet to a paramagnetic state. For example, in $FeBO_3$ at low temperatures a spin - crossover and some magnetic transitions with two triple points were found [6,7]. Gadolinium iron borate, $GdFe_3(BO_3)_4$ is also a system with SEC and recently, we have reported on phase transitions in this material induced by high pressures at room temperature [11,12].

2. Experimental

The structural and magnetic behavior of $Gd^{57}Fe_3(BO_3)$ at high pressures up to 91 GPa and temperatures using a synchrotron Mössbauer spectroscopy technique have been studied. We used helium and neon gas as pressure mediums during structure investigation an NaCl as a pressure medium for magnetic measurements. The pressure was determined from R_1-fluorescence line of ruby or from X-ray diffraction of NaCl in different experiments.

3. Results and discussion

A structural phase transition with coexisting of two phases was observed in high-spin-low-spin crossover region at 52-70 GPa. The hyperfine parameters and results obtained from the experiments are discussed. Based on our experimental data and theoretical calculation a tentative magnetic pressure-temperature phase diagram and an equation of states of $Gd^{57}Fe_3(BO_3)$ are proposed. Important features of the phase diagram are a spin crossover, insulator-semiconductor transition and possible presence of two triple points where magnetic and paramagnetic phases of the high-spin and low-spin states coexist.

References

[1] J. Badro, et al. Science 305, 383 (2004).

[2] J. M. Jackson, et al. Amer. Min. 90, 199 (2005).

[3] J.-F.Lin, et al. Nature 43. 377 (2005)

[4] J.Li, et al. PNAS 101, 14027 (2004).

[5] W. Sturhahn, et al. Geophys. Res.Lett.32 L12307 (2005)

[6] I.A. Troyan, et al. JETP Lett. 74, 24 (2001).

[7] A.G. Gavriliuk, et al. JETP 100, 688 (2005).

[8] A.G. Gavriliuk, et al. JETP Lett. 82, 224 (2005).

[9] M.P. Pasternak, et al. Phys. Rev. Lett. 82, 4663 (1999).

[10] I.S. Lyubutin, et al. JETP Lett. 82, 702 (2005).

[11] A.G. Gavriliuk, et al. JETP Lett. 80, 426 (2004).

[12] A.G. Gavriliuk, et al. J. Phys.: Cond. Matt. 17 (2005)

Acknowledgments

This work was done at Advanced Photon Source supported by the U.S. Department of Energy, Office of Science, Basic Energy Sciences, under contract No. DE-AC02-06CH11357. We are grateful to I.S. Lyubutin, A. Gavriliuk, and V. Struzhkin for useful discussions. We thank V. Prakapenka (GSECARS) and S. Sinogeikin (HPCAT) for help and discussion.

Post-corundum phases in Ga_2O_3 and In_2O_3: X-ray diffraction experiments and theoretical computations

Hitoshi YUSA (NIMS, Japan, yusa.hitoshi@nims.go.jp), Taku TSUCHIYA (Ehime U.GRC, Japan, takut@sci.ehime-u.ac.jp), Nagayoshi SATA (JAMSTEC, Japan, sata@jamstec.go.jp), Yasuo OHISHI (JASRI, Japan, ohishi@spring8.or.jp)

1. Introduction

Group-IIIB sesquioxides, such as gallium oxide and indium oxide, have been widely surveyed as attractive semiconductive materials with a wide band gap. It has been reported that their dense phase is a corundum structure.[1,2] The high-pressure transitions of α-Al_2O_3 (corundum), the so-called "post-corundum phase," have attracted much attention from both theoretical and experimental high pressure studies over the past twenty years. For instance, the post-corundum phase influences the utilization of ruby (Cr^{3+}-doped α-Al_2O_3) pressure scale. Other than group-IIIB oxides, it is known that corundum is stable in the case of various sesqui-oxides such as Fe_2O_3, Cr_2O_3, V_2O_3, and Ti_2O_3 at ambient pressure. Among sesquioxides, the post phase of hematite (Fe_2O_3) has been actively studied for its significance in the Earth's interior.[e.g., 3,4] As a result of in-situ high-pressure experiments using a laser heated DAC, it is reported that corundum (Al_2O_3) and hematite (Fe_2O_3) transform to a Rh_2O_3(II)-type structure at 96 GPa[5] and to an orthorhombic perovskite ($GdFeO_3$-type) or Rh_2O_3(II)-type structure at 30 GPa,[4] respectively. In these studies, the post-corundum phases could not be recovered at ambient pressure. In-situ experiments were therefore indispensable for the discovery of these phases.

In the present study, to clarify the post-corundum phases in Ga_2O_3 and In_2O_3 as well as the high-temperature behavior of β-Ga_2O_3 and C-RES In_2O_3, we conducted in-situ X-ray diffraction experiments under high pressure and temperature. Theoretical computations of the phase stability of their post-corundum candidates, such as Rh_2O_3(II) and orthorhombic perovskite, were also performed in order to predict the transition pressure in advance of the high-pressure experiments.

2. Experimental

The powder-form samples of gallium oxide and indium oxide, mixed with a small amount of platinum or gold powder, for enhancing heat by lasers, were put into a hole in a rhenium gasket seated on a diamond anvil. A few small grains of ruby pressure marker were also enclosed in the hole. The high-pressure X-ray powder diffraction experiments were performed at BL10XU in SPring-8. A symmetrical DAC was used for double sided heating. The samples was heated by Nd:YLF or Nd:YAG laser beam (20 microns or 60 microns in diameter) after being compressed to the target pressure. A monochromatic X-ray (30 keV) was collimated to 20 microns in diameter on the sample. The uncertainties in temperature within the 20 microns area was about ±10%. Debye rings from diffracted X-rays were detected by an imaging plate and a charge-coupled device.

Computations were performed within the density functional theory (DFT) and the local density approximation (LDA). The transition pressures are determined from crossover points of the calculated static enthalpies of each phase.

3. Results and discussion

Using examples from DFT-LDA computations, first, to examine the Rh_2O_3(II) structure in Ga_2O_3, we set the target pressure beyond 50 GPa. The sample was compressed up to 65 GPa at room temperature. After the laser heating at 2300 ± 200K, the diffraction pattern changed to sharp peaks, and then the pressure drops to 52 GPa due to annealing effects under high temperature. Rietveld refinement was performed on the basis of both perovskite and Rh_2O_3(II) structures (Fig. 1). As a whole, the discrepancy between observed and fitted profiles is small in both cases (R_{wp} = 0.07 to 0.08). If a perovskite structure adopted, however, there are some local disagreements such as the absence of (110) reflection of *Pbnm* perovskite (Fig. 1a), and a large fitting errors at 2θ = 15 to 16 deg. (Fig. 1c). Moreover, according to DFT-LDA computation, if corundum to perovskite transition exists, the transition pressure would be located around 86 GPa, which is much higher than the pressure in the present experiments. Considering the structural resemblance between Rh_2O_3(II) and corundum, we conclude that the Rh_2O_3(II) structure is appropriate for the post-corundum phase in Ga_2O_3. To determine the transition pressure from corundum to Rh_2O_3(II), we repeatedly conducted high *P-T* experiments. As a result, the transition boundary is located around

37 GPa at high temperature. This result is consistent with 30 GPa from DFT-LDA computations.

The present computation results in In_2O_3 suggest that the transitions for corundum–Rh_2O_3(II), C-RES–Rh_2O_3(II), and C-RES–corundum would occur around 8 GPa in each case. The C-RES structure with peak broadening still remains after compression to 5.2 GPa. After that, the sample was irradiated by a Nd:YAG laser for a few minutes repeatedly. After the final heating, the pressure was elevated to 8.1 GPa, and the C-RES phase completely changed to Rh_2O_3(II) phase. We note the transient process until the C-RES phase completely disappears. After the first laser heating, the diffraction peaks of Rh_2O_3(II) (020), (112), and (200) had already emerged on the right side of a C-RES (222) peak. The peaks gradually grew by successive heating. When we carefully examined the diffraction profiles, we temporary observed a small peak corresponding to corundum (104). Although the pressures in the transient process were not measured at all stages, it seems that the stability field of corundum is limited to be very narrow. This result is consistent with that by computations, except for observation of the limited stability area of corundum phase, which does not exist in the computation results.

It is well known that the crystal structure of the sesquioxides is correlated with cation size, as typically shown in the rare-earth sesquioxides. Since the ratio of cation and anion sizes varies with pressure, the structure sequentially changes from C to B or A-RES structure with increasing pressure. In case of In_2O_3 and Tl_2O_3, belonging to IIIB sesquioxides, the corundum structure appears as a next phase of C-RES structure.[2] On the basis of cation coordination and density increase, the phase sequence: C → corundum → B was proposed at that time.[2]

Considering the volume-reduction ratio from C to B-RES phase, the volume reduction is assumed to be 8%, as the coordination of cations in the B-RES structure is closer to seven than six. In the present experiments on In_2O_3, the C-RES–Rh_2O_3(II) transition exhibits only 3.9% volume reduction at the transition pressure. This value is much smaller than 8%, which is expected in the C–B-RES transition. Despite further compression of Rh_2O_3(II) phase, yielding a volume reduction of more than 4%, the B-RES phase did not appear. This result might predict a higher oxygen-coordinated phase than B-RES as the post Rh_2O_3(II) phase in In_2O_3. Further structural evolution of Ga_2O_3 and In_2O_3 will be presented at the workshop site.

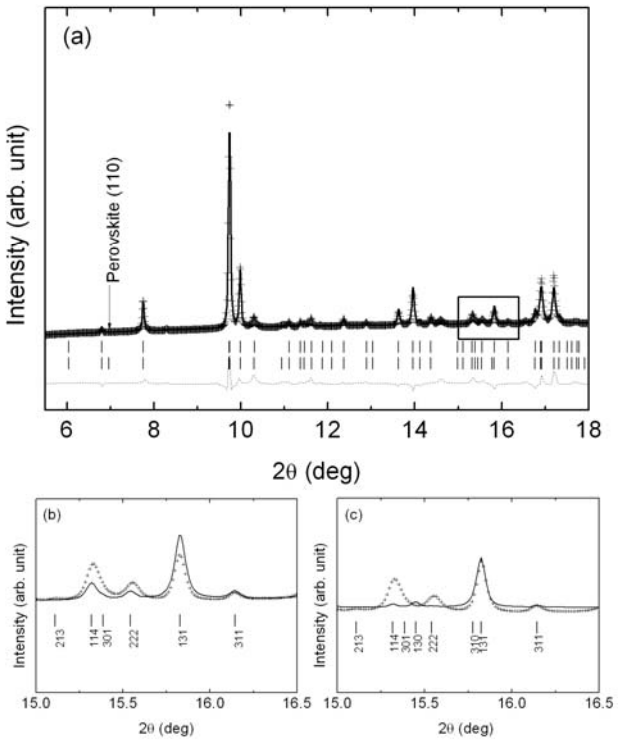

Fig. 1. (a) Powder X-ray diffraction patterns obtained by the Rietveld method (GSAS). Tick marks represent the calculated positions of the diffraction peaks of the Rh_2O_3(II) phase (upper) and orthorhombic perovskite (lower). (b) Enlargement of the square part in (a) fitted by Rh_2O_3(II) and (c) fitted by orthorhombic perovskite structure.

References

[1] J. P. Remeika and M. Marezio, Appl. Phys. Lett. **8**, 87 (1966).

[2] C. T. Prewitt, R. D. Shannon, D. B. Rogers, and A. W. Sleight, Inorg. Chem. **8**, 1985 (1969).

[3] M. P. Pasternak, G. K. Rozenberg, G. Y. Machavariani, O. Naaman, R. D. Taylor, and R. Jeanloz, Phys. Rev. Lett. **82**, 4663 (1999).

[4] S. Ono, K. Funakoshi, Y. Ohishi, and E. Takahashi, J. Phys., Condens. Matter **17**, 269 (2005).

[5] J. F. Lin, O. Degtyareva, C. T. Prewitt, P. Dera, N. Sata, E. Gregoryanz, H. K. Mao, and R. J. Hemley, Nature Mat. **3**, 389 (2004).

Elastic properties of $BaCe_{1-x}Y_xO_{3-0.5x}$ perovskite: Effect of oxygen vacancy and pressure-induced softening

Jianzhong ZHANG (LANSCE-Division, Los Alamos National Laboratory, jzhang@lanl.gov), Baosheng LI (Mineral Physics Institute and Dept. of Geosciences, Stony Brook University, bli@notes.cc.sunysb.edu), Yusheng ZHAO (LANSCE-Division, Los Alamos National Laboratory, yzhao@lanl.gov), Donald J. WEIDNER (Mineral Physics Institute and Dept. of Geosciences, Stony Brook University, donald.weidner@sunysb.edu), Alex NAVROTSKY (Dept. Chemical Engineering and Materials Science, University of California, Davis, anavrotsky@ucdavis.edu))

Dense and polycrystalline specimens of $Ba(Ce_{1-x}Y_x)O_{3-0.5x}$ perovskite (x = 0, 0.05, 0.15) were studied using ultrasonic interferometry at ambient and high pressures, in conjunction with synchrotron X-ray diffraction [1]. The experiments were performed in a cubic anvil apparatus installed at the beamline X17B1 of NSLS, BNL. A dual mode Lithium Niobate transducer (10 degree Y-cut, 30 MHz for S wave and 50 MHz for P wave) mounted at the back of the WC anvil enabled us to collect travel time data for both P and S waves in a single experiment. A glass buffer rod was inserted into the boron epoxy cell assembly between the WC anvil and the sample, with gold foils (2 micron thickness) placed at the interface to enhance the mechanical coupling.

Compressional and shear wave velocities were collected at ambient conditions (bench-top) and at high pressures up to 8 GPa. Our results show that the presence of 2.5% oxygen vacancy has no measurable effect on the elastic bulk modulus. The shear modulus, however, decreases by approximately 5% in $BaCe_{0.85}Y_{0.15}O_{2.925}$ perovskite. The differences between Y^{3+} doped cerate and Al^{3+} doped silicate suggest that the effect of oxygen vacancy on the elastic properties could be system-dependent and may also be sensitive to distribution of oxygen vacancies within structures of the parent compounds. At room temperature, the compressional bulk modulus increases with increasing pressure, as expected for most polycrystalline materials. The shear moduli in all three samples of $Ba(Ce_{1-x}Y_x)O_{3-0.5x}$ perovskite, however, show a negative dependence on pressure over a pressure range of ~2-8 GPa (Fig. 1). This behavior is regarded as unusual because the ultrasonic measurements were carried out on polycrystalline specimen. Softening of transverse acoustic phonons, however, is known to be an important precursor to structural transformations. This phenomenon has also been used widely to explain or predict the pressure- or temperature-induced first-order phase transitions. The softening of the *C*44 shear mode, for example, plays a crucial role in pressure-induced *B*1/*B*2 phase transitions. In this regard, the shear-mode softening in $Ba(Ce_{1-x}Y_x)O_{3-0.5x}$ perovskite probably indicates the destabilization of the perovsite structure, that is, being associated with the phase transition previously observed at 22 GPa using Raman spectroscopic study [2].

References

[1] Li, B.,Kung, J., Liebermann, R.C. (2004) Phys. Earth Planet. Inter. **143–144**, 558–574.

[2] Loridant and G. Lucazeau, (1999) J. Raman Spectr. **30**, 485-492.

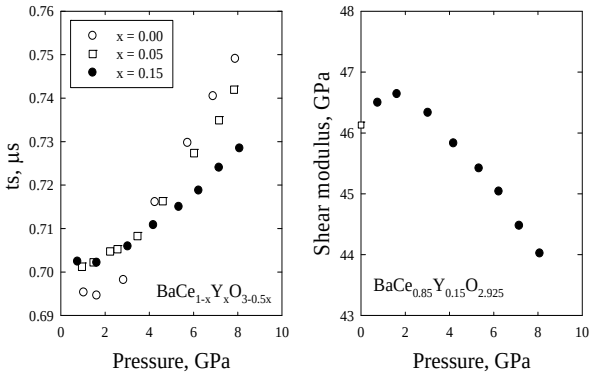

Fig. 1. (Left) Shear-wave travel times as a function of pressure from three independent experiments. (Right) Calculated shear modulus for $BaCe_{0.85}Y_{0.15}O_{2.925}$ perovskite.

Graphic derivations of high *P-T* thermo-mechanics for polycrystalline materials

Yusheng ZHAO (LANSCE-Division, Los Alamos National Laboratory, USA, yzhao@lanl.gov) and Jianzhong ZHANG (LANSCE-Division, Los Alamos National Laboratory, USA, jzhang@lanl.gov)

The diffraction profile is a convolution function of instrument response, grain size distribution, and crystal lattice deformations along the diffraction vector (e.g., [1-2]). In the high-pressure experiments, the microstrain and grain size reduction (crushing) is the dominant factor for peak width broadening in microcrystalline materials when under severe deviatoric stress conditions. In this paper, we present a graphic approach to derive thermomechanical properties of polycrystalline materials under high *P-T* conditions. This method examines the peak width variation and is based on a general definition of overall strain $\Delta d/d$. We also develop a correction routine using diffraction-elastic-ratio to deal with the severe surface strain and/or strain anisotropy in nanocrystals, such that the significant data scatterings can be straightened in a physically meaningful way. Our approach of microstrain can identify "micro/local" yield at the grain-to-grain contacts due to high stress concentration and "macro/bulk" yield and the corresponding yield strength for the plastic deformation over entire sample.

Figure 1 is the plot of $\Delta d^2_{obs.}/d^2$ versus $d^2(P,T)$ for nano-Ni based on the equation

$$\Delta d^2_{obs.}/d^2 = \left(\varepsilon^2 + \Delta d^2_{ins.}/d^2\right) + \left(\kappa/L\right)^2 \cdot d^2(P,T)$$

and synchrotron X-ray diffraction data. Noticeably, the observed raw data (open black circles) scatter significantly and these scatterings are augmented as pressure increases. By applying correction, $DER^2 = (E_{hkl}/E_{200})^2$, the corrected data (solid blue circles) can be readily fit to a straight line and hence allow us to derive the apparent strain and grain size information unambiguously. This correction also allows us to effectively eliminates/minimizes the possible effects of changes in diffraction elasticity associated with the nano-scale and the pressure/temperature effects on the individual elastic moduli. The examples of strain derivation from this approach for micron and nano Ni are shown in Figure 2, which is a graphic de-convolution of all kinds of contributions to the apparent stress. Figure 2 also shows that a complete high-*T* annealing to a true stress-free state provides the instrument baseline for the thermo-mechanics characterization.

References

[1] Gerward, L., Morup, S., Topsoe, H. (1976) Particle size and strain broadening in energy-dispersive X-ray powder patterns. J. Appl. Phys. **47**, 822-825.

[2] Weidner, D.J., Wang, Y., and Vaughan, M.T. (1994) Yield strength at high pressure and temperature. Geophysics Research Letters **21**, 753–756.

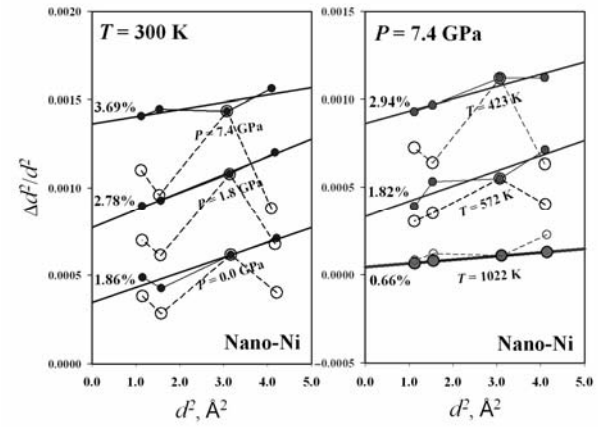

Fig. 1. The plot of $\Delta d^2_{obs.}/d^2$ versus $d^2(P,T)$ for nano-Ni.

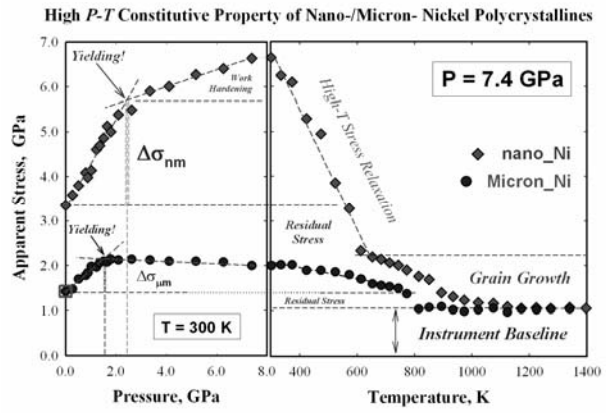

Fig. 2. Apparent stresses for nano-Ni and micron-Ni plotted as functions of pressure and temperature.

Mineral Physics

Magnetic transition and sound velocities of Fe_3C at high pressure

Lili GAO (University of Illinois at Urbana Champaign, USA., liligao2@uiuc.edu)
Bin CHEN (University of Illinois at Urbana Champaign, USA., binchen2@uiuc.edu)
Jingyun WANG (University of Illinois at Urbana Champaign, USA., jwang11@uiuc.edu)
Henry P. SCOTT (Indiana University South Bend, USA., hpscott@iusb.edu)
Michael LERCHE (APS, Argonne National Laboratory, USA.; Carnegie Institution of Washington, lerche@aps.anl.gov)
Jiyong ZHAO (APS, Argonne National Laboratory, USA., jzhao@aps.anl.gov)
Wolfgang STURHAHN (APS, Argonne National Laboratory, USA., sturhahn@aps.anl.gov)
Fang HUANG (University of Illinois at Urbana Champaign, USA., fhuang1@uiuc.edu)
Yang DING (APS, Argonne National Laboratory, USA.; Carnegie Instinttion of Washington, yding@hpcat.aps.anl.gov)
Craig LUNDSTROM (University of Illinois at Urbana Champaign, USA., lundstro@uiuc.edu)
Jay BASS (University of Illinois at Urbana Champaign, USA., jaybass@uiuc.edu)
Jie LI (University of Illinois at Urbana Champaign, USA., jackieli@uiuc.edu)

1. Introduction

Carbon is among the leading candidate light elements in the Earth's core. Fe_3C (cementite) has the lowest carbon content among all known Fe-C compounds and has been proposed to be a major component of the inner core (Wood, 1993). A critical test of this proposal requires knowledge on the density and velocity of Fe_3C. At ambient conditions, Fe_3C is ferromagnetic. A pressure-induced transition from the magnetic phase to a non-magnetic phase has been predicted on the basis of ab-initio calculations (Vočadlo et al., 2002) and observed in previous studies; however, there is controversy about the transition pressure. In order to evaluate Fe_3C as a major inner core component, we investigate pressure-induced magnetic transition in Fe_3C using an independent method and measure the compressional and shear wave velocities of Fe_3C.

2. Experimental method

In this study, we have carried out synchrotron Mössbauer spectroscopy (SMS) and nuclear resonant inelastic X-ray scattering (NRIXS) studies on synthetic ^{57}Fe-enriched Fe_3C up to 52 GPa at room temperature at the undulator beamline 3-ID of the Advanced Photon Source (APS), Argonne National Laboratory. The Fe_3C sample was synthesized by heating ^{57}Fe-enriched Fe and C mixture with atomic ratio of 3.03:1 at 1273K and 2 GPa for 72 hours using a piston-cylinder apparatus at University of Illinois at Urbana-Champaign. High pressures up to 52 GPa were generated using a panoramic diamond anvil cell, and rubies were used to measure the pressures.

3. Results and discussion

Our synchrotron Mössbauer spectroscopy results revealed a loss of magnetism in Fe_3C below 9.3 GPa, consistent with the measured value of 10 GPa from an X-ray magnetic circular dichroism study (Duman et al., 2005), but lower than the reported value of 25 GPa from an X-ray emission spectroscopy investigation (Lin et al., 2004). Combining the phonon density of state derived from NRIXS data and existing equation of state of Fe_3C (Scott et al., 2001, Li et al., 2002), we have also derived the compressional wave velocity V_p and the shear wave velocity V_s of Fe_3C at 1 bar for comparison with seismic observations. The V_p and V_s are shown in Fig. 1. Our results support Fe_3C as a candidate of a possible major inner core component.

References

[1] Dodd et al. (2003) Phys. Stat. Sol. (a), 198(2): 272-281

[2] Duman et al. (2005) Phys. Rev. Lett., 94: 075502

[3] Li et al. (2002) Phys. Chem. Miner., 29(3): 166-169

[4] Lin et al. (2003) Geophys. Res. Lett., 30: 11 1-4

[5] Lin et al. (2004) Earth Planet. Sci. Lett., 226(1-2): 33-40

[6] Lin et al. (2004) Phys. Rev. B, 70: 212405

[7] Mao et al. (2001) Science, 292(5518): 914-916

[8] Mao et al. (2004) Geophys. Res. Lett., 31: L15618

[9] Scott et al. (2001) Geophys. Res. Lett., 28: 1875–1878

[10] Vočadlo et al. (2002) Earth Planet. Sci. Lett., 203: 567-575

[11] Wood (1993) Earth Planet. Sci. Lett., 117(3-4): 593--607

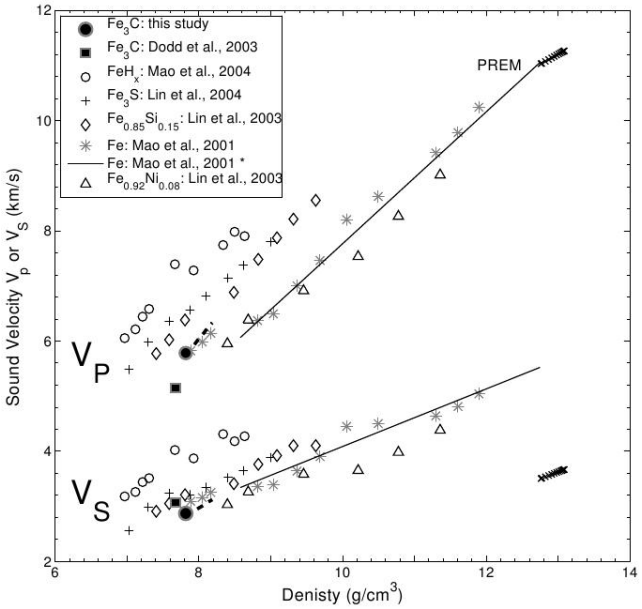

Fig. 1. Sound velocities V_p and V_s. Dashed lines are the extrapolated V_p and V_s of Fe_3C assuming a constant Poisson's ratio of 0.34 at 300K.

Effect of cation ordering on the elastic properties of spinel $MgAl_2O_4$

Barbara LAVINA (UNLV and GSECARS, U.S.A, lavina@cars.uchicago.edu), Stanislav SINOGEIKIN (HPCAT and CIW, U.S.A., ssinog@hpcat.aps.anl.gov), Przemyslaw DERA (GSECARS, U.S.A, dera@cars.uchicago.edu), Lauren BORKOWSKI (UNLV and GSECARS, U.S.A, borkowski @cars.uchicago.edu), Xiaoyu ZHANG (University of Arizona, U.S.A., zhangxy@email.arizona.edu), Vitali PRAKAPENKA (GSECARS, U.S.A, prakapenka@cars.uchicago.edu), Robert T. DOWNS (University of Arizona, U.S.A., rdowns@u.arizona.edu), Malcom NICOL (UNLV, U.S.A., nicol@physics.unlv.edu)

1. Introduction

Spinel is an important rock forming mineral and material with many technological applications, therefore its physical and especially elastic properties have been extensively investigated. In order to constrain the earth's mineralogical models it is critical to know the effect of various parameters such as pressure, temperature, and composition on physical properties of minerals. It turns out that cation ordering can also have appreciable effect on the elastic properties. Spinel shows a remarkably large variation in ordering as a function of temperature, pressure and chemical composition. Moreover, the kinetic barrier makes the ordering-disordering process very slow for the laboratory time scale below ~600˚C, and virtually no ordering-disordering happens below ~400˚C, therefore the ordering state, reflecting thermal history and synthesis conditions, can be easily quenched. The influence of ordering on the elastic properties of spinel has been addressed in several experimental [1-5] and theoretical [6-7] studies. Here we present experimental measurements of the effect of ordering on sound velocities and elastic moduli at two defined ordering states. Ordering is estimated from the inversion parameter, which, for AB_2O_4 stoichiometry, is the amount of B cations in the tetrahedral site.

2. Experiment

The investigated sample is a natural highly ordered spinel from Lake Baikal, Russia. Its crystal chemistry has been determined through single-crystal diffraction and electron microprobe analyses. Disordered crystals have been prepared by thermal treatments under buffered atmosphere; three different crystals from the same rock sample have been equilibrated at 900, 800 and 700°C and then quenched. The predicted change in ordering state has been assessed through Raman spectroscopy with a Thermo Nikolet Almega microRaman system. Oriented (1 1 1) platelets of one untreated sample and one sample equilibrated at 900°C have been polished and single-crystal Brillouin scattering measurements were carried out at ambient conditions. The Brillouin system (13-BMD, GSECARS) includes a Nd:YVO_4 532nm laser and a Sandercock-type Fabry-Pérot interferometer (TFP-1) [8].

3. Results and discussion

Microprobe analyses and single crystal diffraction showed the sample is homogeneous, with cell parameter 8.0907(7) Å and composition $Mg_{0.946}Fe^{2+}_{0.054}Al_{1.996}Fe^{3+}_{0.004}O_4$; the calculated cation distribution leads to the following crystal chemical formula $^{IV}(Mg_{0.81}Fe^{2+}_{0.05}Al_{0.14})$ $^{VI}(Mg_{0.13}Fe^{2+}_{0.01}Al_{1.86})O_4$, with an inversion parameter of 0.14. The unit cell parameter (density) and inversion parameter of the quenched samples behave as predicted according to published experimental trends for synthetic $MgAl_2O_4$ [9]. The Raman spectra for the untreated and quenched spinels are shown on Fig. 1. The thermal treatment results in a remarkable peak broadening and the appearance of new features [3-4] such as a new peak at 727 cm^{-1}.

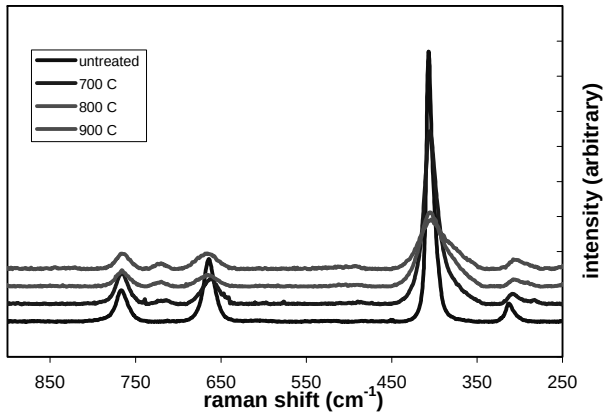

Fig. 1. Raman spectra of spinel at different ordering degrees (532 nm, 10 minutes exposure time).

The acoustic velocities measured on the (1 1 1) single crystal platelet of an untreated natural single-crystal and a crystal quenched at 900°C as a function of Chi angle are shown in Fig. 2. A small but significant difference is observed for one of the transverse acoustic modes. Calculated aggregate adiabatic bulk modulus of the two crystals (Ks(nat)=198.3GPa, Ks(dis)=199.7GPa) is identical, within experimental

uncertainty, whereas the shear modulus is ~2% smaller for the disordered sample. This is opposite to the theoretically predicted behavior [7]. The elastic anisotropy [10], quite high in spinel compared to other cubic structures, is 6% larger in the disordered sample. Both the calculated aggregate velocities (Vp(nat)=9.706, Vs(nat)=5.432, Vp(dis)=9.679, Vs(dis)=5.373 Km/s) show a small decrease with disorder, the longitudinal velocity decreases by 0.3%, the transverse by 1%.

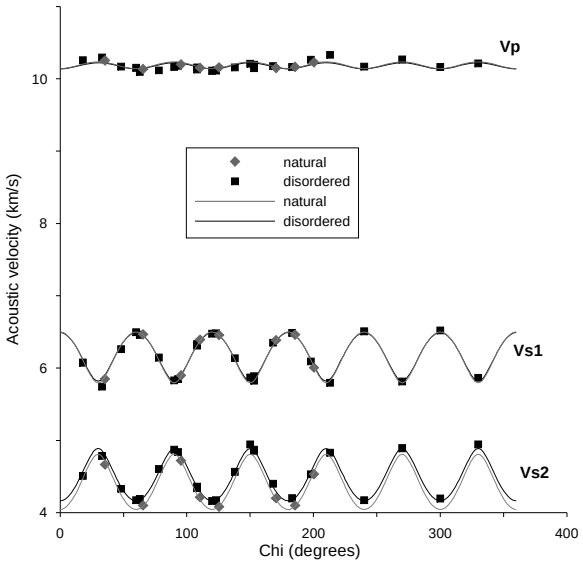

Fig. 2 Acoustic velocities, longitudinal (top) and transverse(bottom) of the natural, ordered, and quenched, disordered, crystals.

Aknowledgements

Support from NSF and DOE (BES and NNSA) are gratefully acknowledged.

References

[1] Yoneda, A (1990) J. Phys. Earth, 38, 944.

[2] Cynn, H., Sharma, S.K., Cooney, T.F., and Nicol, M. (1992) Physical Review B, 45(1), 500-502.

[3] Askarpour, V., Manghnani, M.H., Fassbender, S., and Yoneda, A. (1993) Physics and Chemistry of Minerals, 19(8), 511-519.

[4] Cynn, H., Anderson, O.L., and Nicol, M. (1993) Pure and Applied Geophysics, 141(2-4), 415-444.

[5] Suzuki, I., Ohno, I., and Anderson, O.L. (2000) Harmonic and anharmonic properties of spinel MgAl2O4. American Mineralogist, 85(2), 304-311.

[6] Da Rocha, S., and Thibaudeau, P. (2003) Journal of Physics-Condensed Matter, 15(41), 7103-7115.

[7] Li, L., Carrez, P., and Weidner, D. (2007) American Mineralogist, 92(1), 174-178.

[8] Sinogeikin, S., Bass, J., Prakapenka, V., Lakshtanov, D., Shen, G., Sanchez-Valle, C., Rivers, M. (2006) Rev. Sci. Instr., 77, 103905

[9]Andreozzi, G.B., Princivalle, F., Skogby, H., and Della Giusta, A. (2000) American Mineralogist, 85(9), 1164-1171.

Effect of hydrogen and carbon on the melting temperature of iron

Yoichi NAKAJIMA (Tokyo Institute of Technology, Japan, ynakajim@geo.titech.ac.jp), Koichi SAKAMAKI (Tokyo Institute of Technology, Japan), Eiichi TAKAHASHI (Tokyo Institute of Technology, Japan), Yuh FUKAI (Chuo University, Japan), Toshihiro SUZUKI (Institute for Research on Earth Evolution, Japan Marine-Earth Science and Technology, Japan), Ken-ichi FUNAKOSHI (Japan Synchrotron Radiation Research Institute, Japan)

1. Introduction

The Earth's core consists of mainly Fe-Ni alloy. Seismological and experimental studies show that the Earth's outer core is 10% less dense than pure iron (e.g., [1]), which indicating the presence of light elements in the core such as hydrogen, carbon, oxygen, silicon and sulfur (e.g., [2]). The nature of the light element is the key of issue to understand the temperature of the core. Previous studies on the temperature regime of the core have been discussed based on mainly the Fe-O-S system (e.g., [3]). Although hydrogen and carbon are also the possible candidates of the core component, their effects on the melting temperature of iron at high-pressures are unclear. Therefore, we carried out a series of melting experiments on FeH and Fe_3C using a Kawai-type multi-anvil apparatus with an X-ray radiation at SPring-8 synchrotron.

2. Experimental and results

In situ X-ray diffraction experiments were conducted using a Kawai-type multi-anvil SPEED Mk. II installed at the beamline BL04B1 at SPring-8 synchrotron in Japan. The diffracted X-ray of the sample was collected at $2\theta = 6°$ using an energy dispersive spectrometer. In order to prevent the effect of crystal grain growth, the multi-anvil apparatus was oscillated during X-ray diffraction measurements.

In the experiments on FeH, a mixture of sponge-like iron and MgO powder in 2:3 atomic ratios was used as a starting material. The sample material was packed into a NaCl container with $LiAlH_4$ which was separated from the sample by a thin MgO disk. Hydrogen was supplied by thermal decomposition of $LiAlH_4$. An MgO octahedron (doped with Cr_2O_3) was used as a pressure medium. A mixture of powdered TiC and diamond (5:1 in atomic ratio) was used as a heater with a cylindrical $LaCrO_3$ thermal insulator. The temperature was measured by a W5%Re-W26%Re thermocouple. The pressure cell was compressed using tungsten carbide anvils. A mixture of MgO and NaCl was placed between the NaCl capsule and thermocouple, and the pressure was determined by an MgO pressure scale [4]. The experimental pressure range was between 10 and 20 GPa.

During heating under high-pressures, hydrogenation of iron was observed by volume change. Hydrogen concentration of FeH_x was estimated from the excess volume compared to pure Fe. It was found that FeH_x in the present study at pressures between 10 and 20 GPa are nearly stoichiometric FeH. The phase boundary between ε'- (low-temperature phase) to γ-FeH_x (high-temperature phase) was observed in this study. The melting temperature of γ-FeH was determined by the abrupt change in the X-ray diffraction patterns of crystal to liquid. The melting temperatures were determined to be 1473, 1473, 1493, 1573 and 1593K at 10, 11.5, 15, 18 and 20 GPa, respectively (Fig. 1).

In the experiments on Fe_3C, The starting material Fe_3C was synthesized at 1.8 GPa and 1423K using a piston-cylinder apparatus installed at the Magma Factory, Tokyo Institute of Technology, Japan. Powdered mixture of synthesized Fe_3C and MgO (2:1 in mole ratio) was used as the starting material, which was encapsulated into an MgO container. Powdered mixture of MgO and Au was used as pressure markers, which was separated from the starting material by 0.2 mm thick MgO plate to avoid chemical reaction. $LaCrO_3$ heater was used and the temperature was monitored by a W5%Re-W26%Re thermocouple. Pressure was determined from the unit cell volume of Au [5].

High-pressure experiments on Fe_3C were performed between 20 and 28 GPa. In the diffraction sequences during heating experiments, the peaks of Fe_3C disappeared, and the new peaks identified as those of Fe_7C_3 were observed with halo caused by liquid. Finally, the Fe_7C_3 peaks disappeared, and only the halo pattern was observed. Based on these observations, the incongruent melting of Fe_3C to Fe_7C_3 plus liquid is estimated to occur at 1848 and 1948K at 19.7 and 27.0 GPa, respectively (Fig. 1). The melting temperatures of Fe_3C determined by our experiments are 700K lower than that of the previous estimation based on thermodynamic calculation [6]

3. Discussion

Our experimental results show a possibility that the hydrogen and carbon lower the melting temperature of iron dramatically. The melting temperatures of FeH and Fe_3C are 1593 and 1848K at 20 GPa,

respectively. Those melting temperatures are less than 2260K at 20 GPa of pure Fe calculated by Anderson and Isaak [7] (Fig. 1). Using Lindemann's melting law (e.g. Anderson and Isaak, 2000), we extrapolated the melting curves for γ-FeH and Fe_3C obtained in our experiments to the core pressure. In the extrapolations we use the equations of state for γ-FeH and Fe_3C determined from our unpublished data set. Those melting temperatures are estimated to be ~2600 and ~2900K at the core-mantle boundary (CMB), respectively. In the presence study, we have demonstrated that hydrogen and carbon have a profound effect in lowering the melting temperature of iron. If a large amount of hydrogen and carbon are dissolved in the Earth's core, it is considered that the temperature of the outer core could be much lower than the previous estimation based on the melting temperatures of Fe, FeO and FeS [2].

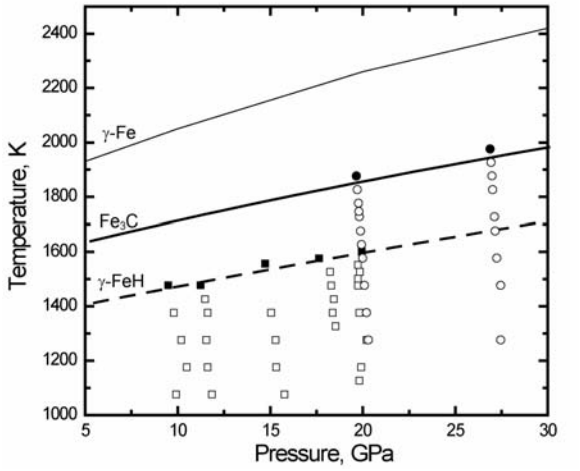

Fig. 1. Experimental results and melting curves for FeH and Fe_3C. Open and solid squares are γ-phase and melt of FeH, respectively. Open and solid circles are solid Fe_3C and Fe_7C_3 + melt, respectively. Melting curves for γ- FeH (broken line) and Fe_3C (Bold line) are determined in this study. The melting curve for γ- Fe (thin line) is calculated by Anderson and Isaak [6].

References

[1] Birch, F. (1952) J. Geophys. Res., 57: 227-286.

[2] Poirier, J.-P. (1994) Phys. Earth Planet. Inter., 85: 319-337.

[3] Boehler, R. (1996) Geochem. Cosmochem. Acta, 60: 1109-1112.

[4] Jamieson, J. C., Fritz, J.N., and Manghnani, M.H. (1982) In: S. Akimoto and M.H. Manghnani (Editors). High Pressure Research in Geophysics. CAPJ, Tokyo, 27-48.

[5] Anderson, O.L., Isaak, D.G., and Yamamoto, S. (1989) J. Appl. Phys., 65: 1534-1543.

[6] Wood, B.J. (1993) Earth Planet. Sci. Lett., 117: 593-607.

[7] Anderson, O.L., and Isaak, D.G. (2000) Am. Miner., 85: 376-385.

Density changes of pyrolite and MORB near the 660 km seismic discontinuity by in-situ X-ray diffraction measurements and chemical composition analyses

Takeshi SANEHIRA* (Geodynamics Research Center, Ehime University, Japan, sanehira@cars.uchicago.edu), Tetsuo IRIFUNE (Geodynamics Research Center, Ehime University, Japan, irifune@dpc.ehime-u.ac.jp), Toru SHINMEI (Geodynamics Research Center, Ehime University, Japan, shinmei@sci.ehime-u.ac.jp), Hiroaki OHFUJI (Geodynamics Research Center, Ehime University, Japan, ohfuji@sci.ehime-u.ac.jp), Yuichiro SUEDA (Geodynamics Research Center, Ehime University, Japan, WD_700_14@hotmail.com), Toru INOUE (Geodynamics Research Center, Ehime University, Japan, inoue@sci.ehime-u.ac.jp), Fabrice BRUNET (Laboratorie de Géologie, Ecole Normale Supérieure, France, brunet@mailhost.geologie.ens.fr), Ken-ichi FUNAKOSHI (Japan Synchrotron Radiation Research Institute, Japan, funakosi@spring8.or.jp),

* Present address: GeoSoilEnviroCARS, the University of Chicago, USA, sanehira@cars.uchicago.edu)

1. Introduction

Pyrolite is a hypothetical rock composition for the Earth mantle and MORB (Mid-Oceanic Ridge Basalt) constitutes oceanic lithosphere and subducts into the mantle. Mineral assemblages and density changes in these rocks under high P and T conditions have been investigated by many authors (e.g., [1-2]) on the basis of quench experiment using multi-anvil (MA) and/or diamond anvil cell (DAC) apparatus.

In such previous studies, densities for pyrolite and MORB as a function of depth have been determined according to the procedure as follows. Firstly, mineral assemblage of pyrolite was determined on the basis of quench experiment using MA and/or DAC. Then, mineral proportions and densities at ambient conditions for individual phases in these rocks were determined. Finally, densities for individual phases under high pressure and high temperature were determined using equations of states for individual phases.

However, thermoelastic parameters for minerals should change as functions of pressure, temperature and chemical composition changes. These dependences have not been well known yet. Thus, direct unit cell volume measurement of individual phases under high pressure and high temperature using in-situ X-ray diffraction measurement, in addition to the chemical composition analyses for these high pressure phases, should be needed to constrain more accurately density changes of these rocks.

In this study, we developed the cell assembly with "multi-sample chamber," combined with in-situ X-ray diffraction measurements. This technique was applied for carrying out direct unit cell volume measurement of individual phases identified in pyrolite and MORB by in-situ X-ray diffraction measurements under simultaneously high pressure and high temperature. We will discuss some implications for density changes and the cross over in pyrolite and MORB at the depths near the 660 km seismic discontinuity.

2. Experimental

In-situ X-ray diffraction measurements combined with multi-anvil apparatus were conducted using SPEED-1500 installed at SPring-8, BL04B1 beamline [3]. Tungsten carbide anvils with 2.5 and 3-mm truncation sizes (TEL = 2.5, 3 mm) were adopted as second stage anvils. Semi-sintered (Mg, Co)O and ZrO_2 were used as pressure media. Three sample chambers made of graphite in LaCrO3 furnace were prepared. These sample chambers were separated by Au foils each other. The central capsule contained a mixture of MgO, Au and NaCl, in 50:1:50 volume ratios, for pressure determination. Pressure was mainly derived from the equation of state for gold proposed by [4].

Temperature was estimated by a W97Re3-W75Re25 thermocouple and no correction of the pressure effect on the e.m.f. was made. The hot junction of thermocouple was located in adjacent to the central chamber. Starting materials of Pyrolite and MORB glass were contained in the two other chambers. These chemical compositions have already been reported by the previous studies [5], [6].

An energy-dispersive method was adopted for X-ray diffraction measurements with a white X-ray beam, which has a size of 50 μm by 200 or 100 μm with horizontal and vertical slits, respectively. The value of 2θ was fixed to ~6°. The press load was increased first up to a target value and then temperature was increased to 1873K and maintained for ~ 4-5 hours at 1873K, which is enough for the attainment of chemical equilibrium. X-ray pattern was collected

several times up to 3000 seconds during this time. A final X-ray pattern was collected at ambient conditions. Lattice parameters of individual phases were mainly refined using the Le Bail whole-pattern fitting method [7] available in the GSAS-EXPGUI software package [8], [9].

After in-situ X-ray diffraction experiments, the recovered samples were invented on an epoxy resin and polished. Chemical composition analyses of the coexisting phases were made using scanning electron microprobe (SEM) equipped with EDS detector. Focused ion beam from the Ga emission source was also directed onto the polished samples invented on an epoxy resin to prepare thin foil specimens for ATEM using the focused ion beam apparatus (FIB). An analytical transmission electron microscopy (ATEM) equipped with EDS detector was also used for chemical composition analyses for the thin foil specimen of the run product.

3. Results and discussion

Fig. 1 shows density changes for pyrolite and MORB as a function of depth. Density jump for the post-spinel transformation in pyrolite composition was estimated to be ~9%, which is comparable to that predicted by PREM [10]. We also constrained density changes in pyrolite near the 660 km seismic discontinuity, which was consistent with those for PREM model, though there is still pressure scale uncertainty near the 660 km seismic discontinuity. Density changes for MORB were less dense than those for pyrolite at the depths of ~610-720 km, and ultimately denser than surrounding mantle again below ~720 km due to formation of Mg-perovskite in MORB. Density difference (Pyrolite-MORB) at two different pressures and temperature of 1873K, corresponding to the depths of ~610-720 km, were evaluated to be 0.25 (2) g/cm^3 at 22.6 (1) GPa and 0.27 (2) g/cm^3 at 23.5 (1) GPa on the basis of present density measurement for these rocks at simultaneous P-T conditions. Thus, present density measurement of both rocks yielded basaltic crust is stagnant above the depths corresponding to the post-spinel transformation, which was consistent with some discussions in the earlier studies (e.g., [1]).

References

[1] Irifune, T., Ringwood, A.E. (1993) Earth Planet. Sci. Lett., 117, 101-110.

[2] Kesson, S.E., Fitz Gerald, J.D., Shelley, J.M. (1998) Nature, 393, 252-255.

[3] Utsumi, W., Funakoshi, K., Urakawa, S., Yamakata, M., Tsuji, K., Konishi, H., Shimomura, O. (1998) Rev. High Press. Sci. Tech., 7, 1484-1486.

[4] Tsuchiya, T. (2003) J. Geophys. Res., 108, B10, doi:10.1029/2003JB002446.

[5] Irifune, T. (1994) Nature, 370, 131-133.

[6] Irifune, T., Ringwood, A.E. (1987) In: Manghnani, M.H., Syono, Y. (eds) High-Pressure Research in Mineral Physics. AGU, Washington, DC, pp 231-242.

[7] Le Bail, A. (1992) In: Prince, E., Stalick, J. K. (eds) Accuracy in Powder Diffraction II, Special Publication 846, NIST, Geithersburg, Maryland, pp 213.

[8] Larson, A.C., Von Dreele, R.B. (2000) Los Alamos National Laboratory Report. LAUR: 86-748.

[9] Toby, B.H. (2001) J. Appl. Crystallogr., 34, 210-213.

[10] Dziewonski, A.M., Anderson, D.L. (1981) Phys. Earth Planet. Inter., 25, 297-356.

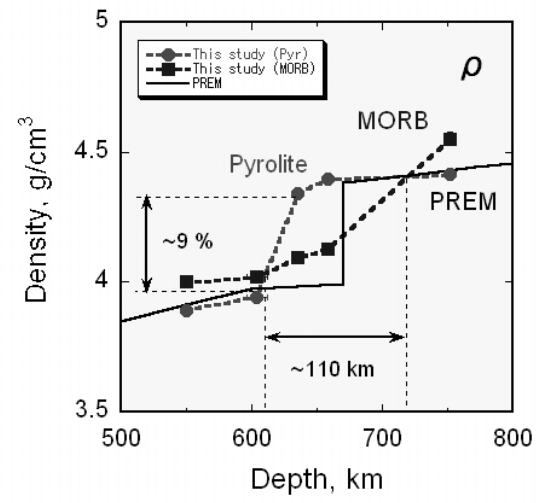

Fig. 1. Density changes for pyrolite and MORB determined by present study as a function of depth.

Room temperature equation of state for Fe_2P

Henry SCOTT (Indiana University South Bend, USA, hpscott@iusb.edu) and
Nana BOATENG (Indiana University South Bend, USA, boatosei@yahoo.com)

1. Introduction

The density, elasticity and structural stability of iron and iron alloys are areas of long-standing interest in planetary science due to the known ubiquity of iron-rich cores in planetary bodies, and the observation that Earth's core is ~10% less dense than pure iron [1]. Furthermore, iron-nickel meteorites often contain inclusions of iron carbide, sulfide and phosphide minerals [2], which has led to considerable interest in C, S and P (as well as many other elements) as potential "light" constituents of planetary cores [3].

As part of our ongoing investigation of Fe_3P, known as schreibersite when found in iron meteorites, we have measured the room-temperature bulk modulus (K_{T0}) of Fe_2P to 8 GPa using synchrotron X-ray diffraction coupled with diamond anvil cells (DACs). Our motivation is to investigate systematics in the Fe-P system due to our previous observation that Fe_3P has a discontinuity in volumetric compression near 8 GPa and a first-order structural transformation above ~15 GPa [4].

2. Experimental

Diamond anvils with 350 μm culets were used to compress samples contained in stainless steel gaskets. The gasket material, initially 250 μm thick, was pre-indented to about 80 μm in thickness, and a 120 μm diameter hole was drilled to construct sample chambers. A methanol, ethanol and water solution was prepared with a volumetric ratio of 16:3:1 and used as a pressure-transmitting medium in all experiments. Pressure-induced shifts in ruby fluorescence were used as a means to indirectly measure sample pressure.

Powder X-ray diffraction patterns were collected using the Advanced Photon Source synchrotron X-ray source at Argonne National Lab. Data were collected in two experimental runs: one was at sector 16 ID-B of HPCAT, and the other was at sector 13 BM-D of GSECARS. The GSECARS data were also used in our previous Equation of State (EoS) measurements for Fe_3P (some Fe_2P was present), but the HPCAT measurements were collected specifically to expand our data on Fe_2P.

We used the same mixed-phase starting material (both Fe_3P and Fe_2P) from Alfa Aesar as in our previous Fe_3P EoS study [4], but examined the bulk material rather than individually selected grains. In our previous study, we had limited success preferentially selecting pure Fe3P grains and did not attempt to select pure Fe2P grains for this work because the phases are too intimately mixed. Accordingly, our data contain information from both phases. The ambient-pressure diffraction pattern of this material shows excellent agreement with previously published lattice parameters for both phases (e.g., ICSD #44-345 for Fe_2P and #43-365 for Fe_3P).

3. Results and discussion

Powder diffraction patterns were collected in two experimental runs reaching pressures of 8 GPa. Due to the mixed-phase nature of our starting material, and the dominance of Fe_3P, we were only able to unambiguously identify two peaks from the hexagonal Fe_2P structure in the high-pressure diffraction patterns in either run: [11-1] and [-230]. To reduce fitting parameters, we imposed a constant c:a ratio of 0.490 based on the ambient pressure value. Notably, a constant ratio over this pressure range is consistent with our previous observations on tetragonal Fe_3P.

A second-order fit (i.e., dK/dP fixed at 4) to the Birch-Murnaghan EoS produced a K_{T0} of 140 ± 4 GPa. This value is 12% lower than that of Fe_3P, and will be used to assess elasticity systematics in iron phosphide phases and potentially other A_xY systems as well.

References

[1] Anderson, W.W. et al. (1994) J. Geophys. Res., 99: 4273-4284.

[2] Wasson, J. (1974) Meteorites: Classification and Properties, Springer, New York.

[3] Li J. and Fei Y. (2003) In Treatise on Geochemistry, The Mantle and Core, Vol. 2 (ed. R. W. Carlson) pp. 521-546. Elsevier.

[4] Scott, H.P. et al. (2007) Geophys. Res. Lett., 34: L06302, doi:10.1029/2006GL029160.

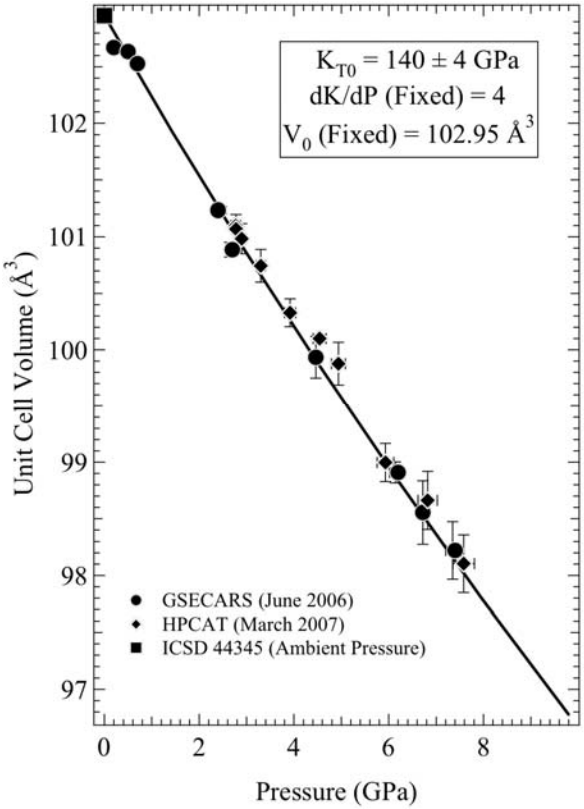

Fig. 1. Room temperature equation of state for Fe_2P. Data from two experimental runs are included and are labeled accordingly. The bulk modulus, K_{T0}, was determined from a second-order fit to the Birch-Murnaghan equation of state.

Density and Fe-Mg partitioning changes in pyrolite to 50 GPa

Toru SHINMEI (GRC, Ehime Univ., Japan, shinmei@sci.ehime-u.ac.jp)

1. Introduction

Pyrolite has been considered to present the Earth's mantle composition. Therefore, detailed studies of the phase relations and mineral physics properties in pyrolite over a wide pressure and temperature condition are required in order to understand the mineralogy and dynamics of the entire mantle. Many experimental investigations for pyrolite have been performed so far, however, the pressure conditions are limited up to 30 GPa. In this study, we have conducted in situ X-ray diffraction experiments to clarify the phase relations, Fe-Mg partitioning and density changes in pyrolite under the lower mantle conditions by using a combination of a multianvil apparatus and synchrotron radiation.

2. Experimental

High pressure and high temperature in situ X-ray diffraction experiments were performed using a Kawai-type apparatus (SPEED-Mk.II) at SPring-8. In order to generate higher pressures equivalent to the lower mantle conditions, sintered-diamond cubes with truncated edge length of 1.5 mm were used as second stage anvils. A glass of pyrolite composition was used as a starting material for the present X-ray diffraction measurements. Pressure was determined from the gold using the equations of state for gold [1,2]. Starting material and pressure marker were directly put into semi-sintered MgO or graphite capsule. WC plus diamond powder cemented by epoxy resin or $LaCrO_3$ sleeve were used as heater, and temperature was measured by a $W_{97}Re_3$-$W_{75}Re_{25}$ thermocouple. The incident X-ray beam was directed to the sample via incident slits of 0.05 mm in horizontal width and 0.1 mm in vertical width. The diffracted X-ray was collected through receiving slits of 0.3 mm in horizontal width and 2.0 mm in vertical width. A collimator with 0.05 mm in horizontal slit was also used to acquire the diffracted X-ray. Experiments were conducted by the energy dispersive method using a white X-ray source and diffracted X-ray was detected by a Ge solid-state detector with a fixed 2θ angle of 6.0°. The pressure conditions were 28 to 47 GPa and temperatures were 1873 to 2073K, and run durations at constant temperature were 2 to 4 hours.

3. Results and discussion

An example of the X-ray diffraction profile for the pyrolite sample at 36.5 GPa and 2073K is shown in Fig. 1. The presence of $MgSiO_3$-rich perovskite (MgPv), $CaSiO_3$-rich perovskite (CaPv) and ferropericlase (Fp) were confirmed from the X-ray diffraction profile. This mineral assemblage is consistent with previous studies, and the calculated bulk densities of pyrolite are close to those in PREM. We also observed the Fe-Mg partition coefficient between MgPv and Fp, $K_D=(Fe/Mg)_{MgPv}/(Fe/Mg)_{Fp}$, significantly decrease from 0.8 to 0.5 with increasing pressure in this above range.

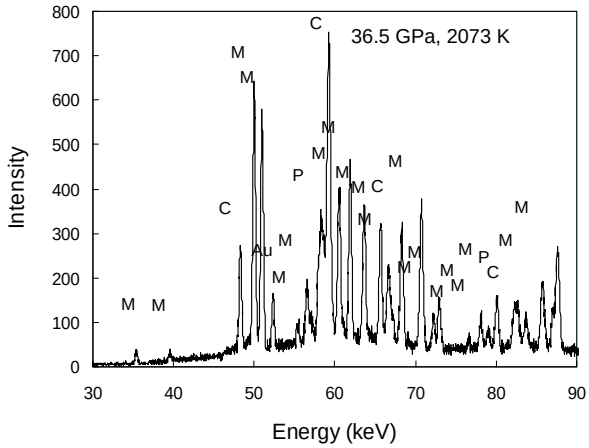

Fig. 1. In situ X-ray diffraction pattern of pyrolite at 36.5 GPa and 2073K. M: Mg-rich Pv, C: Ca-rich Pv, P: ferropericlase, Au: gold.

References

[1] Anderson, O.L et al. (1989) J. Appl. Phys., 65: 1534-1543.

[2] Tsuchiya, T. (2003) J. Geophys. Res., 108: 2462, doi:2410.1029/2003JB002446.

Combined in situ synchrotron X-ray diffraction and ultrasonic interferometry study of ε-FeSi at high pressure and temperature

Matthew L. WHITAKER (Department of Geosciences & Mineral Physics Institute, Stony Brook University, Stony Brook, NY 11794-2100) Wei LIU, Qiong LIU, Liping WANG, Baosheng LI (Mineral Physics Institute, Stony Brook University, Stony Brook, NY 11794-2100)

1. Introduction

It has long been accepted that the core of the Earth, as well as those of other planetary bodies, is predominantly made up of metallic iron (or an iron-nickel alloy), but several studies have shown that metallic Fe is too dense to be the sole element in the Earth's core; particularly the solid inner core [i.e., 1,2]. This indicates that there must be some amount of one or more light elements in the core, and in order to assess which elements these might be, and in what possible proportions, we must study the physical properties of iron-light element alloys under extreme conditions and compare them with the information gained from seismic studies on the Earth's interior. This study focuses on one such alloy: ε-FeSi.

2. Experimental

The starting FeSi material was purchased in powdered form from Alfa Aesar. Powder diffraction conducted on this starting powder revealed that the powder was pure homogeneous ε-FeSi in composition. This powder was then vigorously ground by hand in using an agate mortar and pestle for approximately 30 minutes; the resulting fine powder had an average grain size on the micron scale.

This fine powder was then tightly packed into a gold capsule, dried at 150°C for 2 hours, and then the capsule was pressure sealed to ensure no readsorption of moisture. This capsule was then placed inside a standard 14/8 octahedral cell assembly and prepared for a hot-pressing experiment in a Walker-type 1000-ton uniaxial split- cylinder apparatus. The sample was hot-pressed at 700°C and 7 GPa for exactly one hour.

The hot-pressed sample was analyzed using beamline X17B2 at the National Synchrotron Light Source at Brookhaven National Laboratory to check for any possible heterogeneity in composition or grain size, none of which were found. The *in situ* experiment was conducted in the DDIA-type SAM85 press installed at beamline X17B2 at the NSLS. A schematic of the experimental setup is shown in Fig. 1. The cell assembly used in the experiment is shown in Fig. 2. The ultrasonic measurements were conducted using a dual-mode transducer that was capable of generating frequencies from 20 to 70 MHz.

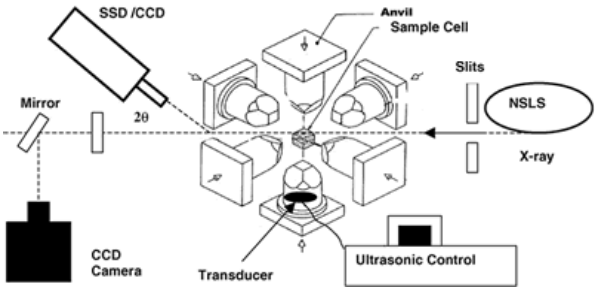

Fig. 1. Schematic diagram of the experimental setup used at beamline X17B2 at the NSLS for this study (after [3]).

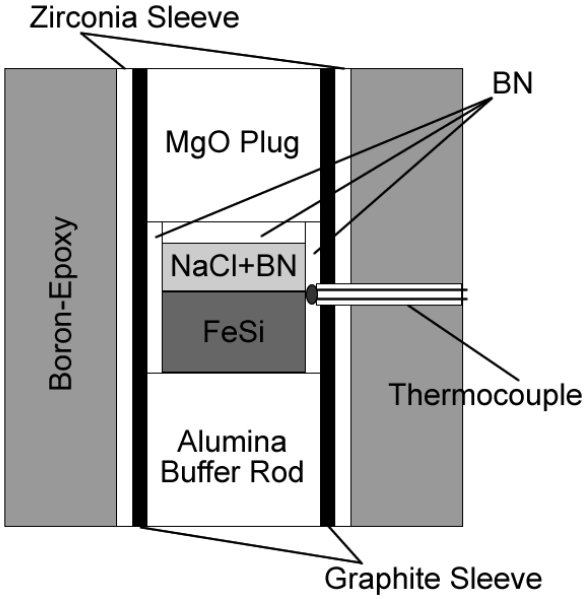

Fig. 2. Schematic diagram of the experimental cell assembly used in this study. The NaCl + BN is a powdered mixture in 10:1 proportions to prevent significant grain growth during the experiment. A 1mm-thick disc of Au foil is placed above and below the sample and at the bottom of the buffer rod to smooth all contact surfaces.

The cell assembly was placed inside the SAM85 press, and brought up to the maximum oil pressure of 60 tons at room T, stopping every five tons along the way to collect data. Then, 10 cycles of data were collected by heating, cooling, and decreasing the pressure. At each desired set of

conditions, an X-ray image of the sample was taken using the CCD camera shown in Fig. 1, ultrasonic data was collected, and an X-ray diffraction pattern for both the NaCl pressure calibrant and the FeSi sample were collected. A typical sample X-ray image is shown in Fig. 3.

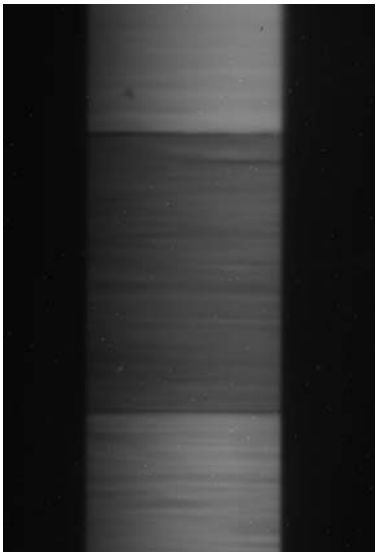

Fig. 3. X-ray image of sample collected at 15 tons of oil pressure during initial cold compression. Black areas to left and right are anvils. Dark gray area (center) is the FeSi sample. Light area above sample is NaCl; light area below is buffer rod. Dark lines top and bottom of sample are Au foil discs.

3. Results and discussion

Over 70 data sets were collected during this experiment, each one at a unique set of temperature and pressure conditions following a saw-tooth pattern typical of this type of experiment. The conditions under which each data set was collected is shown in Fig. 4. Note that in all of the following plots, the pressure used is that obtained via cell refinement of the NaCl pressure calibrant.

By determining the length of the sample in pixels at the end of the experiment when the press is opened, and then measuring the absolute length of the sample after the experiment, we can calibrate the pixel to length ratio, and thereby determine the absolute length of the sample at all P-T conditions (Fig. 5). We use the pulse echo overlap (PEO) technique to determine the two-way travel times of P and S waves going through the sample; the results along cold compression are shown in Fig. 6. From the lengths and travel times, we can then directly obtain the P and S wave velocities for the solid FeSi sample. We use the X-ray data to determine the cell volume of the sample, which can give us a handle on the compressibility of the sample material through equation of state analysis. More details about the experiment, as well as the results of the bulk and shear moduli, and their pressure and temperature dependence derived from these data, will be presented at the workshop.

References

[1] Jephcoat, A. & Olson, P. (1987) Nature 325: 332-335.

[2] Mao, H.K., et al. (1998) Nature 396: 741-743.

[3] Li, B., Kung, J. & Liebermann, R.C. (2004) PEPI 143-44: 559-574.

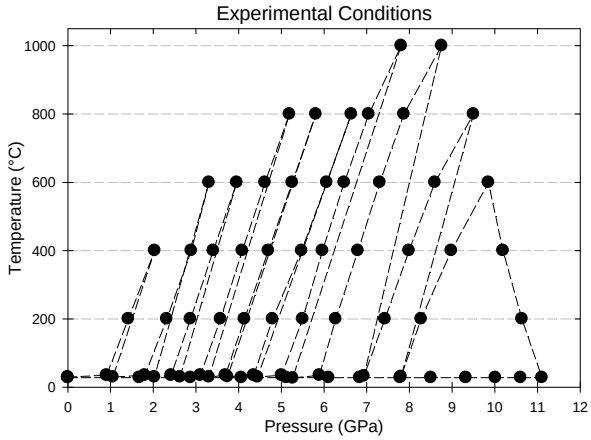

Fig. 4. Plot showing all of the conditions at which data were collected for this study.

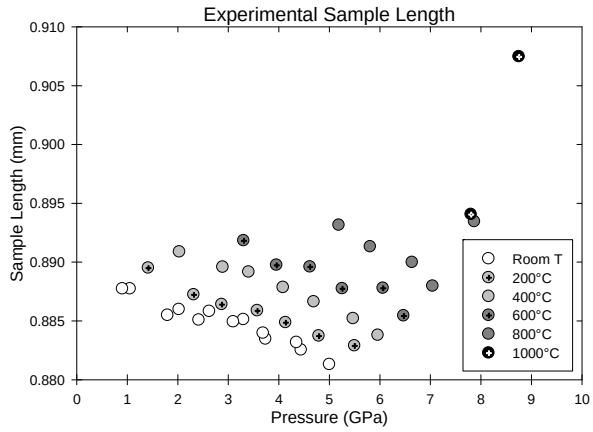

Fig. 5. Plot of the sample length obtained at each data point as a function of pressure. Data is organized in sets by T.

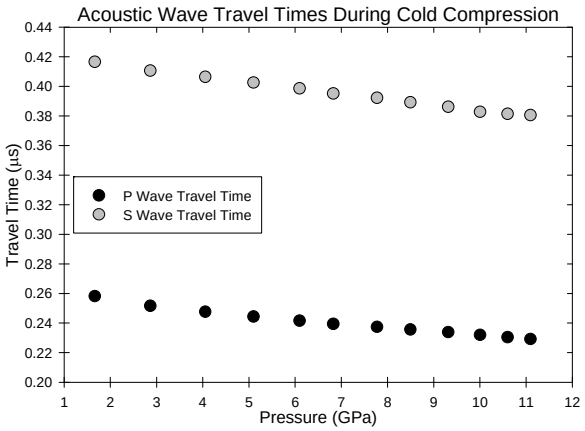

Fig. 6. Plot of P and S vave 2-way travel times in the FeSi sample as a function of pressure during cold compression.

New Techniques

Vibrational spectroscopic analysis of CO_2 fluids at high pressure

Masashi ARAKAWA (Univ. of Tokyo, Japan, arakawa@eqchem.s.u-tokyo.ac.jp), Hiroyuki KAGI (Univ. of Tokyo, Japan, kagi@eqchem.s.u-tokyo.ac.jp), and Junji YAMAMOTO (Kyoto Univ., Japan, jyama@bep.vgs.kyoto-u.ac.jp; Woods Hole Oceanographic Inst., jyamamoto@whoi.edu)

1. Introduction

In the earth's interior, fluids with various origins exist. These fluids are confined in mantle-originated minerals as so-called fluid inclusions. Typical fluid inclusions are several micrometers in diameter. Major components of fluid inclusions are CO_2, H_2O, and CH_4 depending on their origin. Above all, CO_2 fluid inclusions are most frequently observed in mantle-originated rocks.[1,2]

Carbon isotopic compositions ($^{13}C/^{12}C$) of carbon-bearing materials on the earth vary by their origin. For example, carbon from the deep earth (mantle) is rich in ^{13}C; by contrast, biogenic carbon generally has less ^{13}C as a result of biological isotope fractionation, which occurs primarily during photosynthesis.[3,4] Therefore, carbon isotopic compositions serve as a fingerprint that is useful for clarification of the origin and global circulation of CO_2.

We investigated the applicability of micro-Raman spectroscopy for determining carbon isotopic compositions ($^{13}C/^{12}C$) of minute CO_2 fluid inclusions in minerals. This method is nondestructive and has sufficiently high spatial resolution (1 μm) to measure each fluid inclusion independently.

2. Experimental

Isotopically substituted $^{13}CO_2$ gas was prepared by heating amorphous carbon (99% ^{13}C) with CuO. Carbon dioxide samples with various $^{13}C/^{12}C$ ratios were prepared by mixing $^{13}CO_2$ with CO_2 from a tank (15 MPa, 3 m^3, $\delta^{13}C_{PDB}$ = –31.52 ± 0.14‰). Each CO_2 fluid was introduced into a high-pressure cell (PC-400MS; Syn Corp.); high-density CO_2 fluids were prepared in the cell, and Raman spectra were measured. The carbon isotopic compositions of the obtained CO_2 fluids were determined using a mass spectrometer (delta S; Finnigan MAT GmbH) and calibration of Raman spectra for isotopic measurements was achieved.

The present method was applied to natural CO_2 fluid inclusions and the carbon isotopic compositions were estimated by the Raman peak intensity ratios. The peak intensities of Raman spectra of CO_2 were determined precisely using the least-squares peak fitting method with the Solver function (Excel; Microsoft Corp.).

3. Results and discussion

Raman spectra of CO_2 have $^{12}CO_2$-origin Fermi diad peaks at about 1285 cm^{-1} and 1388 cm^{-1} ($\nu^{[12]}_-$ and $\nu^{[12]}_+$) and a $^{13}CO_2$-origin peak at about 1370 cm^{-1} ($\nu^{[13]}_+$); the peaks at 1265 cm^{-1} and 1408 cm^{-1} are hot bands of $^{12}CO_2$ (Fig. 1).

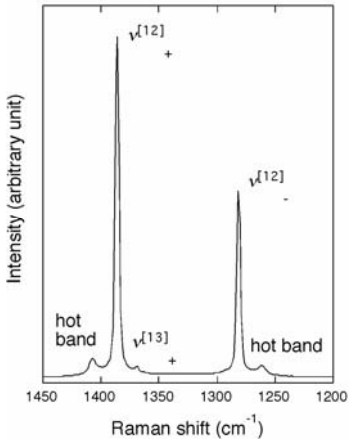

Fig. 1. Raman spectrum of CO_2 ($\delta^{13}C_{PDB}$ = -31.52 ± 0.14‰, 24.1 MPa). The weak peak at 1370 cm^{-1} ($\nu^{[13]}_+$) is from $^{13}CO_2$. Two peaks at 1286 cm^{-1} and 1389 cm^{-1} ($\nu^{[12]}_-$ and $\nu^{[12]}_+$) are a Fermi dyad of $^{12}CO_2$; the peaks at 1265 cm^{-1} and 1408 cm^{-1} are hot bands of $^{12}CO_2$.

The relationship between carbon isotopic compositions and peak intensity ratios of $\nu^{[12]}_+$ and $\nu^{[13]}_+$ was calibrated, and the peak intensity ratio ($I^{[13]}_+/I^{[12]}_+$) were linearly correlated with the carbon isotopic composition of CO_2, which is expected when mixing two isotopic components (Fig. 2). Considering several factors affecting the peak intensity ratio, the error in obtained carbon isotopic composition was 2% (20‰). The reproducibility of intensity ratio at the same experimental environment was 0.5% (5‰). Within the analytical error, we can distinguish biogenic CO_2 from abiogenic CO_2.[5]

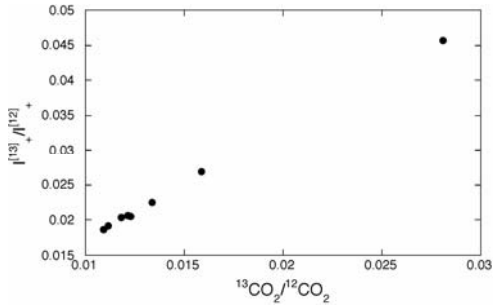

Fig. 2. Peak intensity ratio vs. carbon isotopic composition of the CO_2 fluid measured at 38.0 MPa and 22°C. The intensity ratio ($I^{[13]}_+/I^{[12]}_+$) showed a linear correlation with the carbon isotopic composition of CO_2, which is expected when mixing two isotopic components.

We applied this method (micro-Raman mass spectrometry) to determine the carbon isotopic composition of a natural fluid inclusion. One of the studied fluid inclusions (Fig. 3) contained in a mantle-derived xenocryst found in the lava of a seamount near the Japan Trench.[6] Because of the mantle-origin, it was presumed that this fluid inclusion has a $^{13}C/^{12}C$ value higher than that of biogenic CO_2. For comparison, CO_2 from the tank with an isotopic composition of $\delta^{13}C_{PDB} = -31.52 \pm 0.14‰$ was pressurized to the density of the fluid inclusion. The carbon isotopic ratio of the fluid inclusion, as estimated by the peak intensity ratios ($I^{[13]}_+/I^{[12]}_+$), was $\delta^{13}C_{PDB} = -14.8 \pm 6.7‰$. Carbon isotopic composition of CO_2 inclusions (Fig. 4) contained in upper mantle-derived ultramafic xenoliths sampled in Far Eastern Russia[7] were also determined using this method.

Micro-Raman spectroscopy also provides density information of CO_2 fluid in mantle derived minerals, and the depth where the host mineral and fluid inclusion were equilibrated in the mantle can be calculated using the equation of state of CO_2.[8,9] It is possible to determine density and carbon isotopic composition of CO_2 inclusions simultaneously and independently using the present spectroscopic method.

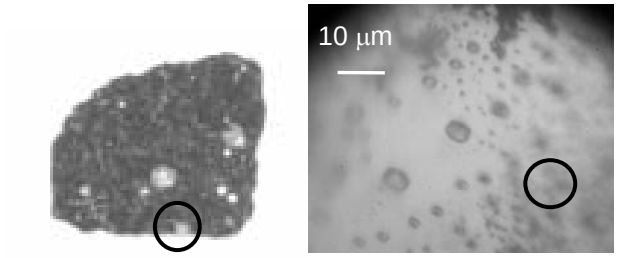

Fig. 3. Fluid inclusion contained in a mantle-derived xenocryst found in the lava of a seamount near the Japan Trench.

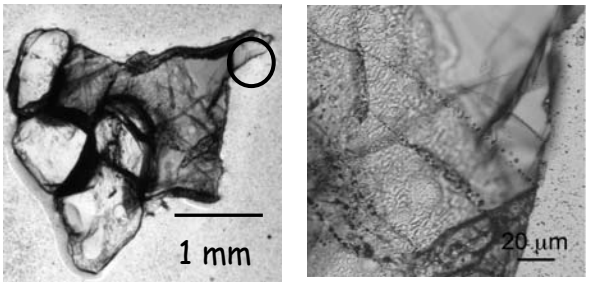

Fig. 4. CO_2 inclusions contained in upper mantle-derived ultramafic xenoliths sampled in Far Eastern Russia.

References

[1] Roedder E. (1965) *Am. Mineral.* **50**: 1746-1782.

[2] Andersen T., and Neumann E. R. (2001) *Lithos* **55**: 301-320.

[3] T. Chacko, D. R. Cole, and J. Horita (2001) "Equilibrium oxygen, hydrogen and carbon isotope fractionation factors applicable to geologic systems", in *Stable Isotope Geochemistry* **43,** J. W. Valley and D. R. Cole, Eds. (The Mineralogical Society of America, Washington, DC), pp. 1-62.

[4] D. J. Des Marais (2001) "Isotopic evolution of the biogeochemical carbon cycle during the Precambrian", in *Stable Isotope Geochemistry* **43,** J. W. Valley and D. R. Cole, Eds. (The Mineralogical Society of America, Washington, DC), pp. 555-578.

[5] Arakawa M., Yamamoto J., and Kagi H. (2007) *Appl. Spectrosc.* **61**: 701-705.

[6] Hirano N., Takahashi E., Ymamoto J., Abe N., Ingle S. P., Kaneoka I., Hirata T., Kimura J. I., Ishii T., Ogawa Y., Machida S., and Suyehiro K. (2006) *Science* **313**: 1426-1428.

[7] Yamamoto J., Kaneoka I., Nakai S., Kagi H., Prikhod'ko V. S., Arai S. (2004) *Chem. Geol.* **207**: 237-359.

[8] Kawakami Y., Yamamoto J., and Kagi H. (2003) *Appl. spectrosc.* **57**: 1333-1339.

[9] Yamamoto J., and Kagi H. (2006) *Chem. Lett.* **35**: 610-611.

Elastic wave velocity measurements under the condition of lowermost mantle transition region

Yuji HIGO (JASRI, JAPAN, higo@spring8.or.jp), Yoshio KONO (GRC, Ehime Univ., Japan, kono@sci.ehime-u.ac.jp), Toru INOUE (GRC, Ehime Univ., Japan, inoue@sci.ehime-u.ac.jp), Tetsuo IRIFUNE (GRC, Ehime Univ., Japan, irifune@dpc.ehime-u.ac.jp)

1. Introduction

Variations of seismic wave velocities (Vp and Vs) as a function of depth are the most fundamental information to assess the materials in the deep Earth interior. Elastic wave velocities of minerals have been measured by various methods, such as ultrasonic interferometry, Brillouin scattering, ultrasonic resonance, etc., but none of these methods have achieved the measurements under conditions of the mantle transition region. We have developed techniques of combined ultrasonic and *in situ* X-ray observations to precisely measure the elastic wave velocities in sintered aggregates of high-pressure phases at simultaneous high pressure and high temperature. As a result, we succeeded in such measurements for representative mantle minerals at pressures to ~21 GPa and temperatures to ~1700K, equivalent to the P-T conditions of the lowermost mantle transition region.

2. Experimental

Combined in situ X-ray and ultrasonic measurements under high pressure and high temperature were conducted at SPring-8 (BL04B1), using a 1500-ton multianvil press (SPEED-1500). Travel times for both P- and S-waves passing through the sample were measured by the ultrasonic interferometry developed by [1], while the sample length under pressure and temperature was determined from the X-ray image of the sample using a high-resolution CCD camera. At the same time, X-ray diffraction data both from the sample and the pressure marker were acquired, and the produced pressure and the phases present were monitored throughout the run.

3. Results and discussion

As the velocity is basically defined by the sample length divided by the travel time, we can determine the Vp and Vs as a function of pressure and temperature from the observed data sets. Fig. 1 shows an example of such variations for the ringwoodite sample, which shows both of these velocities increase with pressure but significantly decrease upon increasing temperature. From these data we are able to derive elastic moduli and their pressure/temperature derivatives quite precisely, which can be used to tightly constrain the mineralogy and chemistry of the mantle transition region, which have been controversial for many years. Further extension of the pressure and temperature conditions toward those of the lower mantle is currently being pursued, which should yield comprehensive understanding of the constitution of the whole mantle.

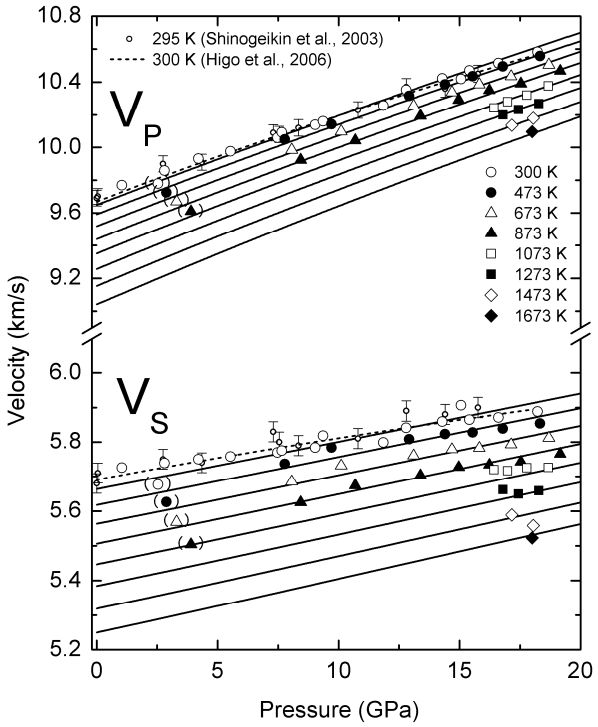

Fig. 1. P and S wave velocities of $(Mg_{0.91}Fe_{0.09})_2SiO_4$ ringwoodite at high pressure and high temperature.

References

[1] B. Li, et al. (2004) Phys. Earth Planet Inter., 143: 559-574.

[2] S. V. Sinogeikin et al. (2003) Phys. Earth Planet Inter., 136: 41-66.

[3] Y. Higo et al. (2006) Phys. Earth Planet Inter., 159: 276-285.

The study of binary chemical reactions at high pressure and high temperature using an imaging system and laser heated diamond anvil cell

Simon CLARK (ALS, LBNL, USA, smclark@lbl.gov), Jason KNIGHT (ALS, LBNL, USA, JWKnight@lbl.gov), Martin KUNZ (ALS, LBNL, USA, MKunz@lbl.gov), Wendel CALDWELL (ALS, LBNL, USA, SanderCaldwell@gmail.com), Michael WALTER (Dept. of Earth Sciences, University of Bristol, UK, M.J.Walter@bristol.ac.uk), Oliver LORD (Dept. of Earth Sciences, University of Bristol, UK, Oliver.Lord@bristol.ac.uk) and David WALKER (Lamont Doherty Earth Observatory, University of Columbia, USA, dwalker@ldeo.columbia.edu)

1. Introduction

Understanding the reactivity between solids and liquids at high pressures and temperatures is important for our understanding of the structure of the Earth and its evolutionary history. For example, debate about the nature of the D″ layer has raged for the last 20 or 30 years. Experiments by Knittle and Jeanloz [1] showed that reaction takes place between liquid iron and Mg-perovskite at high-pressure and temperature. This suggests the possibility of material transfer across the core-mantle boundary, and a possible mechanism for the formation of the D″ layer. These experiments were done in diamond anvil cells (DAC) with laser heating but with samples quenched to room temperature and pressure before evaluation. Other quenching studies have shown artifacts [2] can be introduced during cooling and depressurization. The *in situ* study of these systems at high pressures and temperatures is notoriously difficult due to the small size of the sample inside the DAC and the complex nature of melt-solid systems. Here we present a method of studying melt-solid interactions using an X-ray imaging method. Preliminary results for FeS and FeO will be used to illustrate our method.

2. Experimental

A system for making X-ray shadowgraph images of DAC samples at high pressure and during laser heating has been developed on beamline 12.2.2 of the Advanced Light Source at the Lawrence Berkeley National Laboratory. Figure 1 contains a schematic diagram of the system. A flat field of X-rays large enough to bath the entire field of a DAC sample (~150 μm diameter) by rapidly oscillating the second crystal of a two crystal monochromator or a toroidal mirror in the vertical plane. X-rays travel through the sample and are converted to visible light using a cadmium tungstate phosphor.

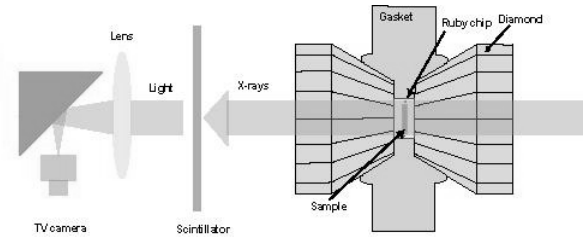

Fig. 1. Schematic diagram showing experimental arrangement of the imaging system.

An Apogee U series digital camera is used to record images. We find that we can record images of sufficient signal to noise ratio with a few seconds exposure time. Sample assemblies consisting of spatially separated reactants, for example Fe and FeO, are fabricated and loaded into the DAC between an inert pressure media. These are pressurized and then heated on the boundaries between materials till melting occurs and a liquid phase can be imaged. The optical density of the images of the melt can be used to determine the X-ray transmission density of the melt that maps onto melt chemistry.

3. Results and discussion

We have studied Fe-FeS as described above as part of our validation of this method. At 5 GPa we found a Fe-FeS saturated liquid with 75 wt% Fe in agreement with the literature value [3]

References

[1] Knittle and Jeanloz *Science* **251** 1438-1443 (1991).

[2] O'Neill, Canil and Ruby *J. Geophys. Res. Solid Earth* **103** 12239-12260 (1998).

[3] Usselman *American Journal of Science* **275** 278-303 (1975).

High pressure diamond anvil cell studies using synchrotron micro-tomography and high energy X-ray scattering techniques

Haozhe LIU (Harbin Institute of Technology, China), Luhong WANG (Harbin Institute of Technology, China), Xianghui XIAO (Advanced Photon Source, Argonne National Laboratory, USA), Peter LEE (Advanced Photon Source, Argonne National Laboratory)

Although two-dimensional imaging, i.e., synchrotron X-ray radiography, is used in a routine way for high pressure diamond anvil cell (DAC) experiments, "volume imaging," i.e., X-ray tomography, will offer us more information regarding volume measurement and shear deformation under high pressure. A recent technical development effort on micro-tomography study using DAC in a radial geometry will be presented. One major application for DAC tomography will be relative density measurement for amorphous materials, metallic glasses, and liquid or melt in DAC under pressure, which will provide better information for the density of non-crystalline materials under pressure than routine X-ray radiography. We will demonstrate preliminary studies on DAC tomography for amorphous selenium, zinc oxide, gold and nickel polycrystal samples under pressure.

Using synchrotron high energy X-ray scattering to reach a large Q range through the limited opening in the DAC, the structural evolution for non-crystalline materials was studied. The project on polyamorphism will undoubtedly broaden our horizons and perspectives of the states of matter in general, and may have a significant impact on existing theories about the structure, formation, and evolution of amorphous materials. The procedure of the pressure-induced amorphous state to crystalline state is another interesting subject. By combining high-energy X-ray diffraction with the time-resolved area detector, we not only could accurately measure the structural factors evolution of amorphous materials under pressure, but also could record the time dependence of the crystallization procedure. These will provide new insight on the nature of crystallization, provide new invitation for electronic theoretical studies of the phase stability and competition in time and spatial domains, and improve our understanding of the kinetic process of the common pressure induced crystallization. A couple of cases, including metallic glasses and amorphous Se, will be presented.

Concept of a new large volume D-DIA, "MADONNA"

Norimasa NISHIYAMA (GRC Ehime Univ, Japan, nishiyama@sci.ehime-u.ac.jp), Tetsuo IRIFUNE (GRC Ehime Univ, Japan, irifune@dpc.ehime-u.ac.jp), Kouhei WADA (GRC Ehime Univ, Japan, kou-wada@sci.ehime-u.ac.jp), Yoshinori TANGE (GRC Ehime Univ, Japan, tan@sci.ehime-u.ac.jp)

1. Introduction

Deformation-DIA (D-DIA) is a new deformation apparatus which has a potential to let us carry out quantitative deformation experiments at conditions corresponding to mantle transition zone (Wang et al., 2003). D-DIA is a modification of DIA apparatus which has six anvils to squeeze the cubic space. In the case of D-DIA, there are two small hydraulic rams (differential rams) behind the top and bottom anvils. Thus, these two anvils can be moved independently under pressure produced by the main ram. This mechanism makes it possible to perform deformation experiments. D-DIA combined with synchrotron radiation enables us to perform simultaneous stress and strain measurements during deformation (e.g., Uchida et al., 2004) and, for example, stress-strain curves of hcp-iron at prescribed pressures, temperatures, and strain rates were observed in its stability field (Nishiyama et al., 2007). Previous deformation experiments using D-DIA have been performed at pressures of 1 – 10 GPa routinely and there have been experimental difficulties for experiments at conditions corresponding to mantle transition zone (pressures between 14 and 23 GPa). Anvils with truncated edge length (TEL) of 2 mm are required to generate pressures above 15 GPa (Yagi and Akimoto, 1976). In this case, the size of the sample camber can be 0.5 mm in diameter and 0.6 mm in height (Nishiyama et al., 2007). There is no room to place thermal insulator to achieve homogeneous temperature distribution of the sample, and a capsule to control the water content and oxygen fugacity of the sample. In order to perform deformation experiments at pressures corresponding to the mantle transition zone and under the controlled sample environment, a D-DIA apparatus with larger sample volume is required.

2. MADONNA

"MADONNA" (Fig. 1) is a D-DIA apparatus installed in Geodynamics Research Center, Ehime University. The maximum load of the main ram is 1500 tons (15 MN), which is about ten times larger than that of a previous D-DIA apparatus. Therefore, the sample volume of MADONNA can be larger than that of previous D-DIA apparatuses. MADONNA has a system to measure displacements of all the six anvils and the differential rams' pressures or displacements can be controlled with main ram load. There are two purposes for MADONNA. The first is to accomplish homogenous compression, which means keeping cubic symmetry for the pressure cavity during compression. This can be good for 6-8 experiments with sintered diamond anvils as the second stage. The second is to carry out quantitative deformation experiments at conditions corresponding to the mantle transition zone. Some preliminary results of the homogeneous compression for the 6-8 system and deformation experiments will be shown in the session.

Fig. 1. A photo of "MADONNA."

References

[1] Wang et al. (2003) J. Appl. Phys., 42: 3239-3244.

[2] Ucida et al. (2004) Rev. Sci. Instrum., 74, 3002-3011.

[3] Nishiyama et al. (2007) Geophys. Res. Lett., in press

[4] Yagi and Akimoto (1976) J. Appl. Phys., 47, 3350.

Development of spectroscopic three-dimensional stress imaging technique around mineral inclusions in diamond

Shoko ODAKE (Univ. Tokyo, Japan, odk@eqchem.s.u-tokyo.ac.jp), Satoshi FUKURA (Univ. Tokyo, Japan, fukura@eqchem.s.u-tokyo.ac.jp), Hiroyuki KAGI (Univ. Tokyo, Japan, kagi@eqchem.s.u-tokyo.ac.jp)

1. Introduction

Most natural diamonds trap the mantle minerals and/or fluids as inclusions during its formation in the Earth's interior. Diamond is chemically and physically stable; it is able to store the mantle material from deep part of earth to the Earth's surface. One of the aims of our current researches is to determine the depth origin of diamond formation from the residual stress around mineral inclusions. When inclusions and host diamond form at some initial temperature and pressure, the inclusions pressure may be assumed to be the same as the confining pressure acting upon the host diamond. Subsequently the diamonds come up to the Earth's surface, the pressure inside the inclusion is expected to be different from that in the host diamond because compressibilities and thermal expansivities of the inclusions and diamond are different (Fig. 1). If the remnant pressure around the inclusion of diamond and initial temperature are obtained, we can estimate the depth where inclusions were trapped inside diamond.

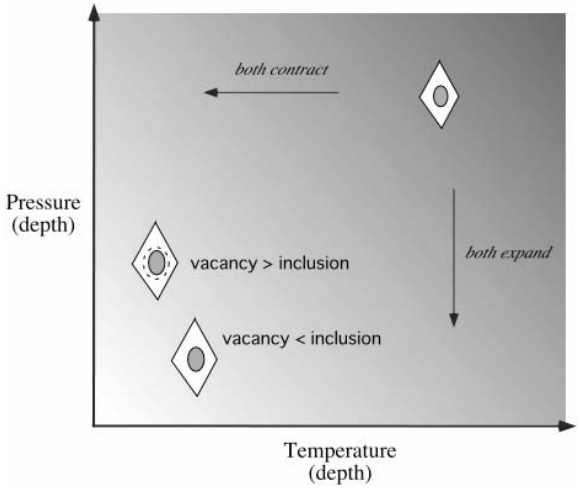

Fig. 1. Schematic illustration showing the volume change of host mineral and inclusion during ascent from the deep Earth to the surface of the Earth.

Residual stress exists in the host diamond around the inclusions. Residual stress of diamond can be measured using micro-Raman spectroscopy, as Raman peak of diamond shifts to higher wavenumber when pressure is applied (2.2 cm^{-1}/GPa along the <111> direction according to Grimsditch et al. (1978)). The Raman technique is useful because it is non-destructive and can be applied to inclusions embedded inside of diamonds. Two-dimensional Raman mapping of diamond samples have disclosed the stress distribution around mineral inclusions (e.g., Nasdala et al., 2005). Due to the anisotropic elastic properties of minerals, however, three-dimensional Raman mapping is necessary for detailed and precise estimations of stress distributions. In the present study, we aimed at three-dimensional visualization of stress distribution using micro Raman spectroscopy.

2. Experimental

Raman spectra of diamond were measured using a confocal Raman microscope equipped with an automatic X-Y-Z stage. High spectroscopic resolution is required for measuring subtle difference (c.a. 0.1 cm^{-1}) in Raman shift corresponding to residual stresses distributing in diamond. Furthermore, high stability of spectrometer is also required because it takes long time to obtain three-dimensional mapping. Our previous studies revealed that time-change of peak position of Raman spectra contained the periodic oscillation with amplitude 0.15 cm^{-1} synchronizing with the room temperature regulation (Fukura et al., 2006). In the present study, neon emission lines as the wavenumber standard were introduced into the spectrometer using a bifurcated optical fiber to achieve real-time wavenumber correction.

Figure 2 shows a photomicrograph of the studied sample, which was sampled from Internationalnaya pipe (Russia) and contains one olivine and three chromite inclusions. The sample was polished to optical grade and Raman spectra were acquired for a volume containing a couple of inclusions by scanning three dimensionally.

3. Results and discussion

By digitizing the Raman shift of diamond, stress distribution around the inclusions was visualized three-dimensionally (Fig. 3 and Fig. 4).

The stress distributions around the two mineral inclusions were determined independently and difference in the maximum pressure between olivine and chromite were revealed.

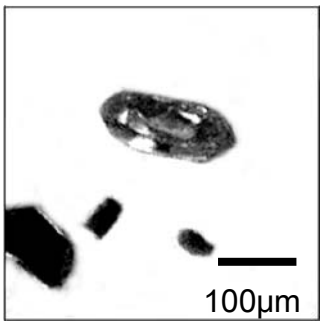

Fig. 2. Photomicrograph of scanned area including one olivine and three chromite inclusions.

By measuring residual stresses around at least two mineral species with different bulk modulei and thermal expansivitivties, the confining pressure and temperature can be estimated. Using the obtained maximum residual pressures, initial confining temperature and pressure were estimated by solving equation modified after Barron (2005) (see Fig. 5). The obtained P-T value was in the stability field of diamond.

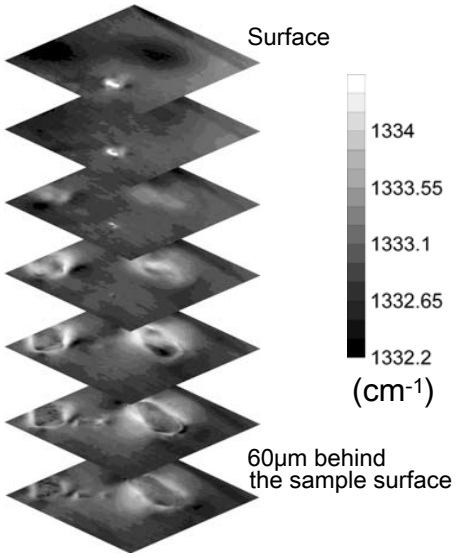

Fig. 3. Stacked Raman maps of diamond containing mineral inclusions from sample surface to interior.

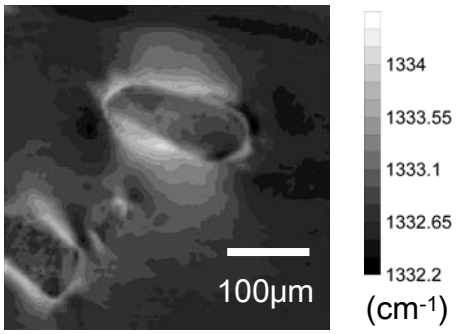

Fig. 4. Two-dimensional Raman map of diamond 50 μm underneath the diamond surface, picked up from Fig. 3.

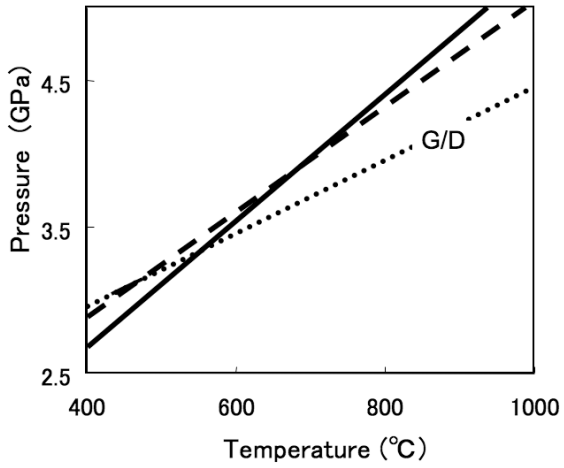

Fig. 5. Calculated zero volume difference lines for olivine (solid) and chromite (dashed) inclusions in diamond, related to the graphite / diamond transition (G/D).

References

[1] Grimsditch, M.H. et al., (1978) Physical Review B, 18: 901-304.

[2] Nasdala, L. et al., (2005) American Mineralogist, 90: 745-748.

[3] Fukura, S. et al., (2006) Applied Spectroscopy, 60: 946-950.

[4] Barron, L.M., (2005) The Canadian Mineralogist, 43: 203-224.

Gas loading system

Mark RIVERS (University of Chicago, USA, rivers@cars.uchicago.edu), Clayton PULLINS (University of Chicago, USA, pullins@cars.uchicago.edu), Vitali PRAKAPENKA (University of Chicago, USA, prakapenka@cars.uchicago.edu)

1. Introduction

We have designed and built a new system to load gases at high pressure into diamond anvil cells. The gases are used either as a quasi-hydrostatic pressure medium to surround the sample, or as the sample itself. Being able to have samples under hydrostatic stress (very small strain) is critical for both power and single crystal diffraction experiments.

The gases can be loaded at pressures up to 29000 PSI, which is high enough so that the densities become comparable to the densities of the liquid phase. The system was largely funded by the COMPRES high-pressure consortium which is managed by SUNY Stony Brook. The design and assembly were done at GSECARS. All of the high-pressure components are commercially purchased.

The system will be located at Sector 13, but it will be made available to anyone who wants to use it. This includes scientists running experiments on other APS sectors, or registered APS users who want to load cells to use in their home laboratories or elsewhere.

The system we have constructed builds on the experience from existing systems at the Geophysical Laboratory at the Carnegie Institution of Washington, the CHESS synchrotron at Cornell University, and the Lawrence Livermore National Laboratory. Our system is designed to be very easy to safely use, because a PLC prevents incorrect operation of all valves. In addition the system provides optical access for a ruby fluorescence pressure measurement system, so that the user can accurately determine when the cell has sealed and reached the desired pressure. Our system also accommodates a wide range of diamond anvil cell designs, rather than being restricted to a single type of diamond cell.

Based on discussions held at a workshop at the APS in April 2006 , the following key system design goals were identified:

- Able to load many kinds of cells.
- Closure mechanism (motor driven screws) closes a clamping device, not the cell itself.
- Easy to add new cell designs, just a different clamp or different spacers.
- Optical access.
- Vacuum pump to clean system before loading.
- No electrical parts except pressure transducers in high-pressure enclosure.
- Allows flammable gas operation in future.
- Easy to operate safely.

The system includes the following key safety features:

- All high-pressure components are supplied from vendors, pressure tested. No locally machined high-pressure components.
- Gas loaded from lecture bottle to limit total mass (energy) that can be compressed in pressure vessel.
- Interlocked heavy-duty enclosure (3/8" aluminum, ¾" plywood). All high-pressure components contained inside enclosure.
    - Protects against user forgetting to load cell or filler parts.
- Pressure meters on both low and high pressure systems which will vent before rupture disk fails
- Gas-operated valves and motor operated drives for remote operation
- PLC for interlock control and computer for routine operations control

The system is currently completely constructed and awaiting safety approval from the APS for use to begin operation.

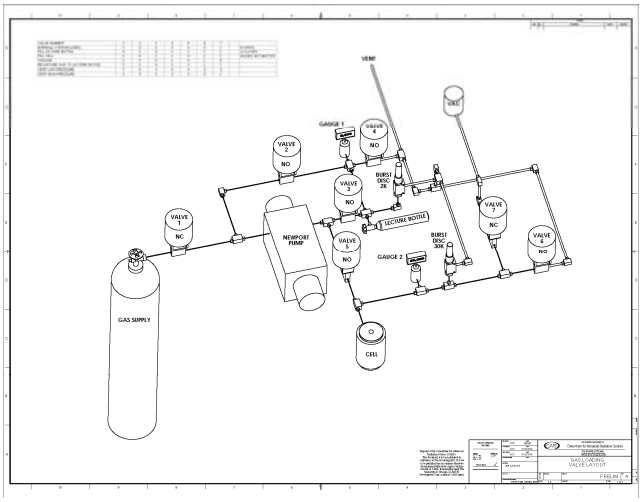

Fig. 1. Schematic layout of gas loading system.

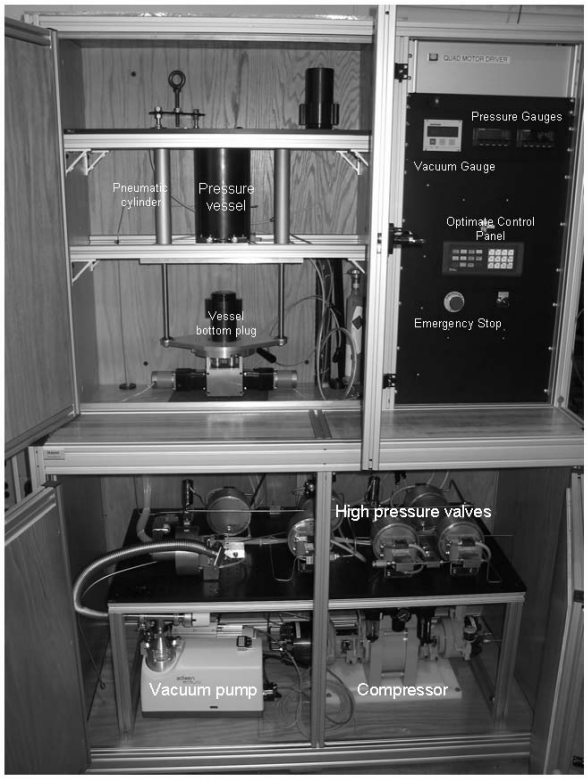

Fig. 2. Annotated photograph of gas loading system

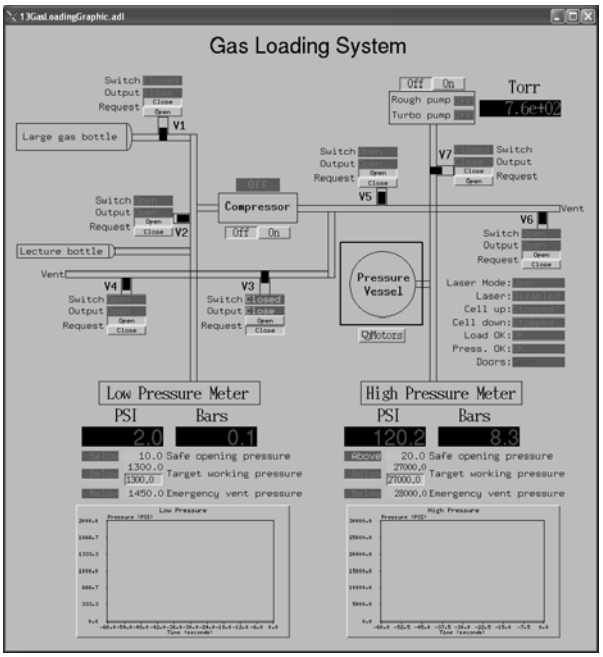

Fig. 3. Computer control screen for gas loading system

Johnson noise thermometry at high pressure

Takeshi SANEHIRA (GeoSoilEnviroCARS, University of Chicago, USA, sanehira@cars.uchicago.edu), Yanbin WANG (GeoSoilEnviroCARS, University of Chicago, USA, wang@cars.uchicago.edu), Ivan C. GETTING (University of Colorado-Boulder, USA, Getting@colorado.edu), Norimasa NISHIYAMA* (GeoSoilEnviroCARS, University of Chicago, USA, nishiyama@sci.ehime-u.ac.jp), John LABENSKI (BAE Systems, USA, john.labenski@baesystems.com), Mark L. RIVERS (GeoSoilEnviroCARS, University of Chicago, USA, rivers@cars.uchicago.edu),

*Present address: Geodynamics Research Center, Ehime University, Japan

1. Introduction

Temperature measurements using thermocouples under high pressure have been facing with a well-known problem: the unknown pressure dependence of the thermocouple e.m.f. Johnson Noise Thermometry (JNT) technique, on the other hand, is based on a physical phenomenon which is pressure independent. A combination of JNT measurements with temperatures obtained from thermocouples may provide a quantitative measure of the pressure effect on e.m.f., thereby solving a long-standing problem of temperature measurements under high pressure.

Johnson noise is expressed as a mean squared voltage, $\langle E \rangle^2$, which is related to the resistance (R) of an open-circuit resistor and the absolute temperature (T), by the following (Johnson-Nyquist) equation [1], [2]:

$$\langle E \rangle^2 = 4kTRB$$

where k is Boltzmann's constant and B is the bandwidth of frequency over which Johnson noise is measured. The Johnson Noise Thermometer constructed by Ivan Getting and John Hall uses two amplifiers (A and B) to collect the Johnson noise voltage, E_A and E_B, each having its own random noise E_a or E_b, in addition to the Johnson noise voltage E:

$$E_A = E + E_a$$

$$E_B = E + E_b$$

These outputs are measured as time series and multiplied point by point and averaged (numerically correlated). Since the product of any two random noise signals averages to zero, $C = (1/N)\Sigma(E+E_a)(E+E_b) = (1/N)\Sigma(E^2+EE_a+EE_b+E_aE_b) = E^2$.

This technical development will now be extended to higher pressures in this study. We report the first Johnson Noise Thermometry (JNT) measurements at pressure and temperature at Sector 13 of the GeoSoilEnviroCARS, IDD beamline, the Advanced Photon Source.

2. Experimental

Fig. 1 shows the cell assembly for JNT measurement and a picture of the probe resistor. The cell assembly consists of a soft-fired pyrophyllite pressure medium and graphite furnace, along with MgO and BN disks and sleeves. The MgO and BN components were fired at 900-1100 ^oC overnight to remove volatiles from moisture and adhesives used to mount them before assembling these parts. In previous tests we determined that these volatiles contaminated the cell and corrupted the electronic signals at high temperatures. Probe resistors were built on polished faces of sapphire disks, 5 mm in diameter and 1 mm thick by vapor deposition of metals (Ti and Pt). A mask was used to produce a serpentine-like metal ribbon 400 nm thick. Two pairs of thermocouples (WRe26%-WRe5%) were used to make four-wire probe resistance measurements and to obtain temperature measurements at each end of the probe resistor.

Unused electronics, which affects the JNT signal, inside the experimental station were turned off to avoid signal contamination for the JNT measurements. Harmonics of the 60 Hz sinusoidal heater power source were present in the JNT signals, however. They occurred at frequencies below about 20 kHz. The contamination increased with increasing electrical power during heating. A numerical notch filter was used to reduce these harmonics from 600 to 9000 Hz with notch bandwidths of 5 or 10. The original time series also passed through a second numerical filter, which is a fourth or tenth order high pass filter with a corner frequency of 20 kHz.

3. Results and discussion

We have carried out one test run using 1000 tons press in the IDD 13 hutch. A target load of 20 tons was applied prior to the first temperature excursion. A total of four heating cycles were made with Johnson noise observations during both increasing and decreasing temperatures. After the first heating cycle, we increased the load to 25 tons for the second and third heating cycles to obtain a better furnace

contact between the upper and lower guide block of the DIA apparatus. The final heating cycle was made at a load of 35 tons. Based on later pressure calibrations with X-ray diffractions, pressures were estimated to be ~0.1–0.2 GPa at these loads.

Using the filtering described above we obtained the measurements of Johnson noise without significant contamination to ~ 600K. This behavior was also shown in the relationship between JNT output and the product of probe resistance and temperature (Fig. 2). Above this temperature, the apparent probe resistor resistance decreased noticeably over a temperature range of about 100K and then increased again. This behavior is physically unrealistic and resulted in a non-linear relationship between the output of Johnson noise measurements and the product of probe resistance and temperature (Fig. 2). These anomalous results were reproducible in all four heating cycles.

We also conducted the JNT measurement up to ~1 GPa, combined with in-situ X-ray diffraction measurement to determine the pressure dependence of thermocouple e.m.f. Including the results for the test run and two runs by in-situ X-ray diffraction measurement, recent results and next some improvements in the future will be discussed.

References

[1] Johnson, J. B. (1928) Phys. Rev., 32, 97-109.

[2] Nyquist, H. (1928) Phys. Rev., 32, 110-113.

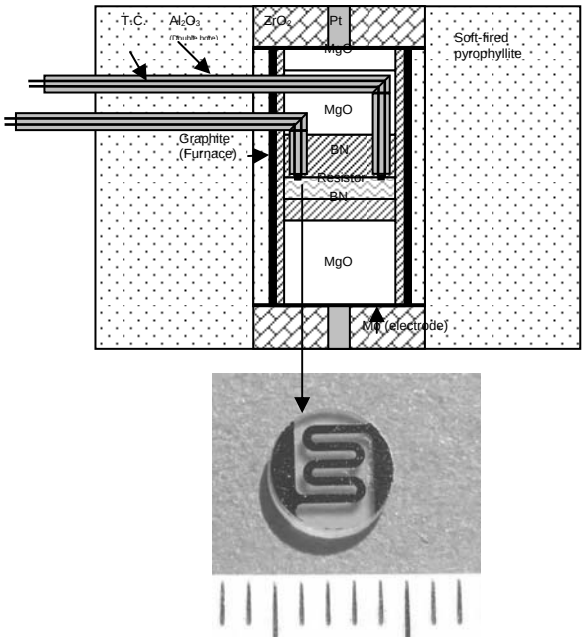

Fig. 1 Schematic illustration of the cell assembly for JNT test experiment (top). All cell parts must be fired at 900-1100^{o}C overnight, to remove glue and other organic residues, which tend to evaporate under modest temperatures and alter the electromagnetic (EM) character of the cell. Probe resistors (bottom) are multilayer metal deposition built on a polished face of a sapphire disk.

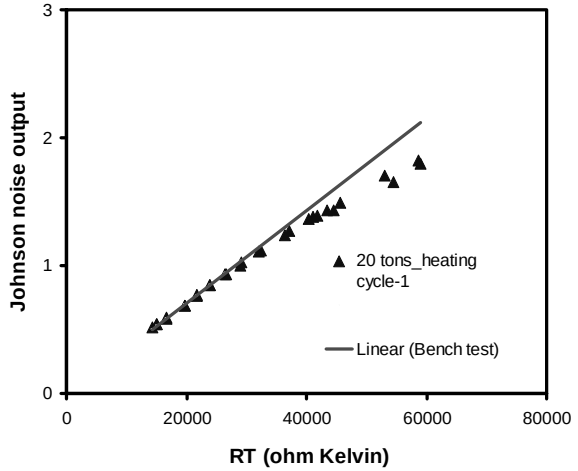

Fig. 2. An example of JNT signals (triangles) obtained in the 16/12 mm cell at 20 tons (P ~ 0.2 GPa), plotted against the product of probe resistance times absolute temperature. Red line is the bench test result at 300K, by varying probe resistance.

Development of high-pressure and high-temperature X-ray tomography technique: Application to sessile drop interfacial energy measurement

Satoru URAKAWA (Okayama Univ., Japan, urakawa@cc.okayama-u.ac.jp), Hidenori TERASAKI (Tohoku Univ., Japan, terasaki@mail.tains.tohoku.ac.jp), Ken-ichi FUNAKOSHI (JASRI, Japan, funakosi@spring8.or.jp), Norimasa NISHIYAMA, (Ehime Univ., Japan, nisiyama@sci.ehime-u.ac.jp), Takeshi SANEHIRA (Univ. Chicago, USA, sanehira@cars.uchicago.edu), Yanbin WANG (Univ. Chicago, USA. wang@cars.uchicago.edu)

1. Introduction

X-ray tomography is a powerful tool to image three-dimensional shape of sample confined in the high-pressure cell [1]. Application of X-ray tomography to the high-pressure study yields the opportunity to measure the physical properties of the planetary forming materials which have never examined under pressure. One of those properties is interfacial energy of molten iron alloy, which controls the aggregation and separation of molten iron-alloy from liquid or crystalline silicate during core-formation. In order to measure the interfacial energy of molten iron-alloy, we have developed the technique of the high-pressure sessile drop method by means of X-ray tomography.

2. Experimental

X-ray tomography experiments were conducted at 13BMD of APS, using the tomography module driven by 250 ton uniaxial press [1]. High pressure is generated by a cupped or a toroidal type opposite anvils apparatus and the sample cell assembly used is shown in Fig. 1. The sample is a powder mixture of iron and iron sulfide or nickel and nickel sulfide, which is enclosed by (Na,K)-disilicate.

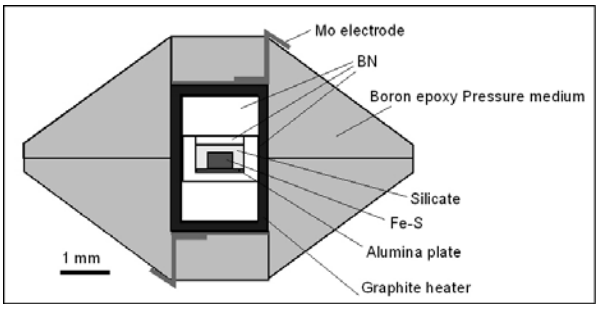

Fig. 1. Schematics of high-pressure cell assembly.

Using a monochromatic X-ray, shadowgraph images were collected from all directions by rotating the high pressure apparatus and then were reconstructed into 3D tomography image. X-ray tomography experiments were performed at the pressure up to 2 GPa and the temperature up to 1500K. We used a new designed plastic gasket by which the anvil gap is kept as wide as few mm even at high pressure, because it is necessary to use large sample of mm size for the sessile drop method (Fig. 2).

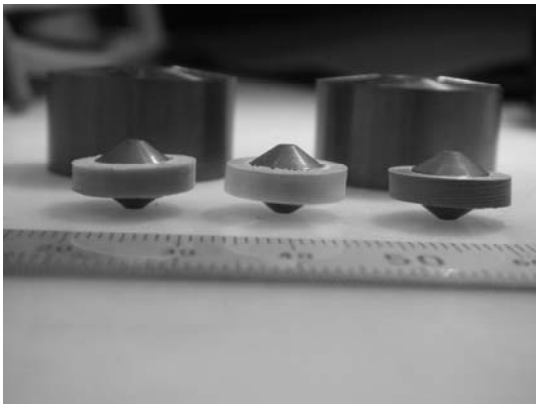

Fig. 2. High pressure cell with three kinds of plastic ring gaskets.

3. Results and discussion

A field of view corresponding to the anvil gap was significantly increased by using the plastic ring gasket, although the gasket decreased an efficiency of pressure generation. Therefore, the entire image of the sample was successfully obtained during the tomography data collection at high pressure and temperature. Tomography images of Fe-S droplet at 1.8 GPa and 1273K are shown in Fig. 3. Fe-S liquid is quite spherical in shape because of its high interfacial tension and small size. The cross section without internal structure indicates that the Fe-S liquid was a homogeneous during heating.

In order to obtain the larger sample volume, we have used another type of cell; toroidal anvil cell with a diameter of 15 mm center hole of the WC anvil. The composite plastic ring gasket was used as shown in Fig. 4. The cell was compressed to 40 ton which corresponds to ~1 GPa. The gasket worked well and kept a field of view still wide at 40 ton.

References

[1] Wang YB et al. (2005) Rev. Sci. Instr., 76: Art. No. 073709.

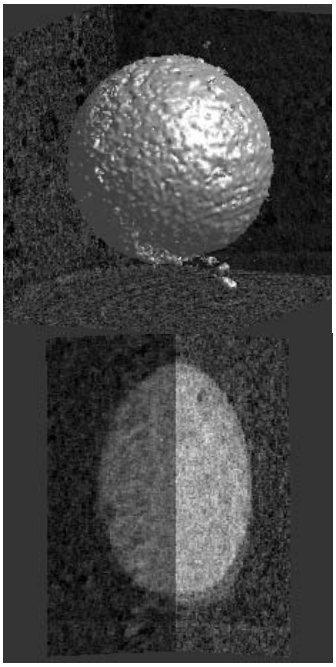

Fig. 3. (Left) 3-D tomography image of $Fe_{60}S_{40}$ droplet at 1.8 GPa and 1273K. (Right) Cross section of the Fe-S droplet shown in left.

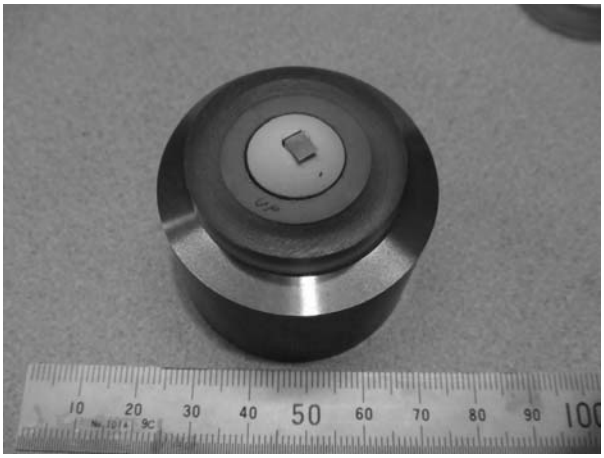

Fig .4. Toroidal cell with composite plastic ring.

Pressure generation and observation of post-perovskite phase in $MnGeO_3$ and $MgGeO_3$ by *in situ* X-ray diffraction using sintered diamond anvils

Eiji ITO (Institute for Study of the Earth's Interior, Okayama University, Japan, eiito@misasa.okayama-u.ac.jp),
Daisuke YAMAZAKI (ISEI, Okayama University, Japan, dy@misasa.okayama-u.ac.jp),
Shuangmeng ZHAI (ISEI, Okayama University, Japan, zhai@misasa-okayama-u.ac.jp)
Anton SHATSKIY (ISEI, Okayama University, Japan, ashatsky@misasa.okayama-u.ac.jp)
Takashi YOSHINO (ISEI, Okayama University, Japan, tyoshino@misasa.okayama-u.ac.jp)
Hiroshi FUKUI (ISEI, Okayama University, Japan, fukuih@misasa.okayama-u.ac.jp)
M. A. Geeth M. MANTHILAKE (ISEI, Okayama University, Japan, geethmm@misasa.okayama-u.ac.jp)
Tomoo KATSURA (ISEI, Okayama University, Japan, tkatsura@misasa.okayama-u.ac.jp)
Ken-ichi FUNAKOSHI (Japan Synchrotron Radiation Institute, Spring-8, Japan, funakosi@spring8.ac.jp)

1. Introduction

The Kawai-type multianvil apparatus (KMA) is widely used in the field of high pressure physics, mineral sciences, material physics, and so on. This type of high pressure apparatus has the advantage of generating uniform pressure over a fairly larger volume compared with diamond anvil cell (DAC). Moreover, the sample can be heated uniformly by an electric resistance furnace embedded in the pressure medium. However, the available pressure in KMA by using conventional anvil material, tungsten carbide (WC), has been limited to ~30 GPa. Sintered diamond (SD) was adopted as the anvil material for KMA, and generated pressure as high as ~40 GPa (Ohtani et al. 1989; Kondo et al. 1993) was achieved, since SD anvils are much harder than WC anvils. More recently, SD anvils with larger dimensions (14 mm edge length; Ito et al. (1998); cf. ~10 mm edge length in the earlier studies) became available, so larger press load can be applied. As a result, pressure higher than 70 GPa can be produced in KMA (Ito et al. 2007).

The most dominant mineral in the Earth's lower mantle is $(Mg,Fe)SiO_3$ perovskite (Pv) and thus its mineral physics behavior is very important in understanding constitution and composition of the lower mantle (e.g., Ringwood 1991). Laser-heated DAC (LHDAC) experiment revealed that $MgSiO_3$ perovskite (*Pbnm*) transforms into a different structure, so-called post-perovskite (PPv) phase (*Cmcm*), at ~120 GPa (Murakami et al. 2004). This discovery has significant implications for the mantle structure and dynamics, but precise phase boundary between Pv and PPv has not been well resolved. Thus further experimental study should be conducted with greater accuracies.

We report the progress in high pressure generation using SD anvils in Kawai-type apparatus, with special emphasis on the technical development for in-situ X-ray diffraction measurements under simultaneous high pressure and temperature conditions towards 1 Mbar. Using this technique, we examined the stability of $MnGeO_3$ and $MgGeO_3$ perovskites at pressures above 60 GPa. $MnGeO_3$ and $MgGeO_3$ are often used as analogue materials for $MgSiO_3$ and were recently demonstrated to adopt the post-perovskite structure at pressure of 50-65 GPa using LHDAC (Tateno et al., 2005; Hirose et al., 2005).

2. Experimental

In-situ high pressure experiments were carried out using SPEED Mk-II installed at BL04B1 SPring-8 (Katsura et al. 2004). We adopted SD cubes as second stage anvils with edge length of 14 mm and truncated corners of 1.5 mm (TEL = 1.5 mm). MgO was used as pressure medium, and pyrophyllite was used as gasket. To obtain the relationship between generated pressure and press load, we acquired X-ray diffraction profiles of gold to calculate pressure with increasing press load every 0.25 MN during in situ X-ray experiments.

For heating experiments, TiB_2+BN+AlN tube was used as a heater because of its high transparency for X-ray, and the sample was enclosed in a graphite capsule. Temperature was monitored by a $W_{97}Re_3$-$W_{75}Re_{25}$ thermocouple with diameter of 50 μm. Fluctuation of temperature was within ±10°C throughout the runs and the pressure effect on emf of thermocouple was ignored. Pressure was determined using the EOS of Au proposed by Anderson et al. (1989). Uncertainties of the pressure determination were mostly within ±0.5GPa.

$MnGeO_3$ and $MgGeO_3$ orthopyroxenes were first synthesized from the mixture of oxides (MnO_2 and GeO_2 for $MnGeO_3$, and MgO and GeO_2 for $MgGeO_3$)

at 700°C for 20 hours in atmosphere. Then we synthesized $MnGeO_3$ and $MgGeO_3$ ilmenites using these orthopyroxenes at 7 GPa and 1200°C for 10 hours using the Kawai-type apparatus at ISEI, Okayama University. X-ray diffraction pattern of the recovered sample showed the transformation reaction was completed and all diffraction peaks were indexed on the basis of the ilmenite structure. Then the synthesized ilmenites were mixed with Au powder as the pressure standard (10:1 in weight), and used as the starting materials for the in situ X-ray observation.

3. Results and discussion

3.1 Pressure generation using SD anvils

Figure 1 summarized the pressure generated using SD anvils. So far we generated highest pressures at room temperature (72 GPa) and high-temperature (1973 K and 74 GPa) in multi-anvil apparatus (Ito et al., 2007). The main problems for higher pressure generation are blow out and subsidence at top of the SD anvils. SD assembly blows out much more frequently than WC assembly, though stress relaxation by heating is an effective preventive method. Subsidence of an anvil causes large pressure decrease, which may avoid by using high quality (harder and uniform) SD anvil.

3.2 PPv of $MnGeO_3$

In the experiment for $MnGeO_3$ (run no. M471), Pv was synthesized at 16.7 GPa and 700°C and subsequent transformation from Pv to PPv was observed at 63.2 GPa and 950°C (Fig. 2). However, the transformation was not observed at 63.7 GPa and 950°C in the different run (run no. M509). In run M509, EoS of Pt proposed by Holmes et al. (1989) was used for pressure calibration. Therefore, the discrepancy of the observed phase may caused by the different pressure scale. The transition pressure (in the run M471) of 63.2 GPa and 950°C is higher than expected phase boundary based on DAC experiments (Tateno et al., 2005).

3.3 PPv of $MgGeO_3$

We observed the PPv of $MgGeO_3$ at 63.0 GPa and 1223K (Fig. 3). The phase boundary between Pv and PPv was also examined over the P-T conditions of 60-74 GPa and 1100-2150K (Fig. 4). However, both the Pv to PPv and the reverse transitions are very sluggish and the precise location of the boundary has not been constrainted.

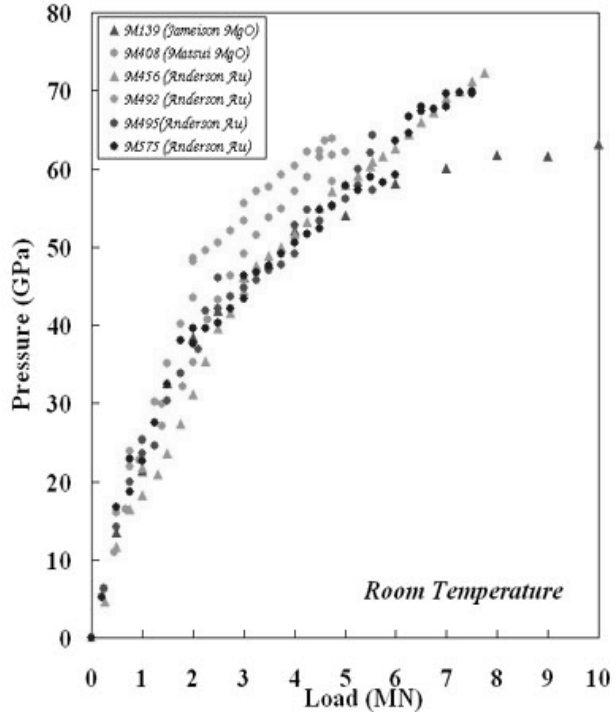

Fig. 1. Pressure generation using SD anvils.

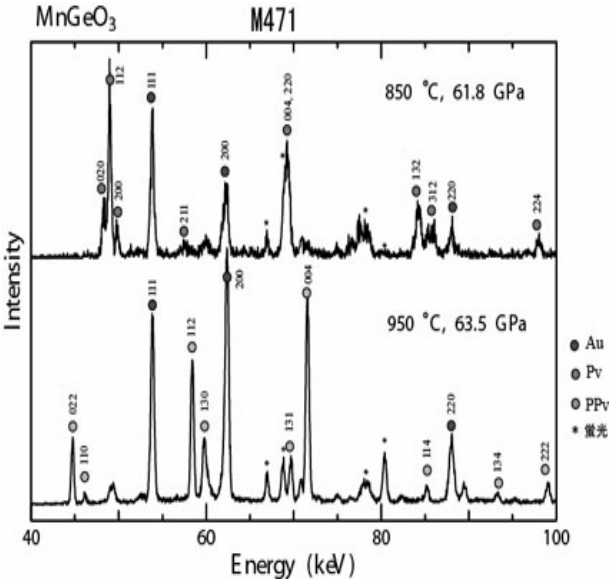

Fig. 2. Diffraction profile in $MnGeO_3$ at high pressures and temperatures.

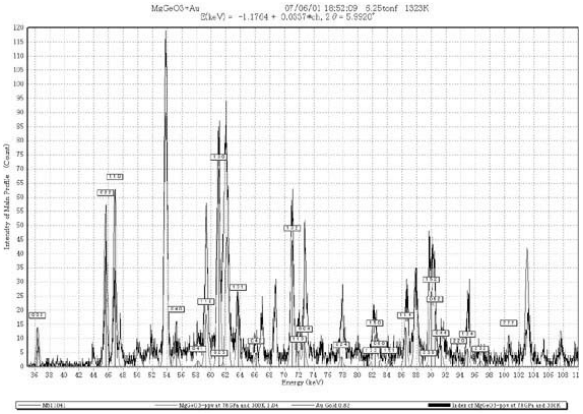

Fig. 3. Diffraction profile in $MgGeO_3$ at high pressures and temperatures.

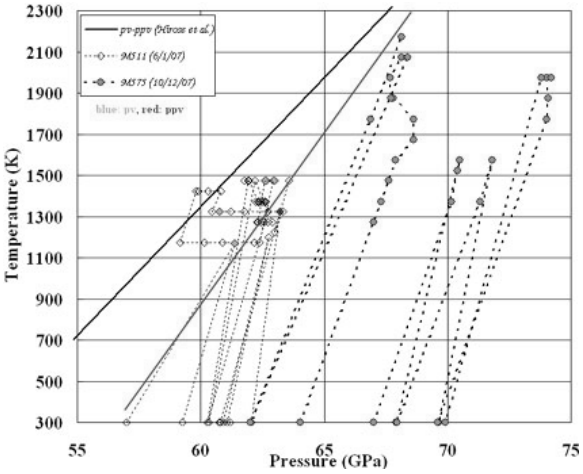

Fig. 4. In situ X-ray observation of Pv and PPv in $MgGeO_3$ at high pressure and temperature conditions.

References

[1] Anderson, O.L., Isaak, D.G. and Yamamoto, S. (1989) J. Appl. Phy., 65: 1534-1543.

[2] Hirose, K., Kawamura, K., Ohishi, Y., Tateno, S. and Sata N. (2005) Am. Mineral., 90: 262-265.

[3] Holmes, N.C., Moriarty, J.A., Gathers, G.R., and Nellis, W.J. (1989) J. Appl. Phy., 66: 2962-2967.

[4] Ito et al., 2007 SPring-8 Experiment Report 2007A.

[5] Ito, E., Kubo, A., Katsura, T., Akaogi, M. and Fujita, T. (1998) Geophy. Res. Lett., 25: 821-824.

[6] Katsura, T., Funakoshi, K., Kubo, A., Nishiyama, N., Tange, Y., Sueda, Y., Kubo, T. and Utsumi, W. (2004) Phys. Earth Planet. Inter., 143-144: 497-506.

[7] Kondo, T., Sawamoto, H., Yoneda, A., Kato, M., Matsumura, A. and Yagi, T. (1993) High Temp.-High Pressure, 25: 105-112.

[8] Murakami, M., Hirose, K., Kawamura, K., Sata, N. and Ohishi, Y. (2004) Science, 304: 855-858.

[9] Ohtani, E., Kagawa, K., Shimomura, O., Togaya, M., Suito, K., Onodera, A., Sawamoto, H., Yoneda, A., Utsumi, W., Ito, E., Matsumoto, A. and Kikegawa, T. (1989) Rev. Sci. Instrum., 60: 922-925.

[10] Ringwood, A.E. (1991) Geochimica et Cosmochimica Acta, 55: 2083-2110.

[11] Tateno, S., Hirose, K., Sata, N. and Ohishi, Y. (2005) Phy. Chem. Miner., doi 10.1007/s00269-005-0049-7.

Nuclear resonant scattering under simultaneous high pressure and high temperature at 3-ID, APS

Jiyong ZHAO (Advanced Photon Source, Argonne National Laboratory), Wolfgang STURHAHN (Advanced Photon Source, Argonne National Laboratory), Michael LERCHE (HP-Sync, Advanced Photon Source, Argonne National Laboratory)

Nuclear resonant scattering (NRS) includes synchrotron Mössbauer spectroscopy (SMS) for the study of hyperfine interactions and nuclear resonant inelastic X-ray scattering (NRIXS) for the study of lattice dynamics. The NRS technique has become a unique tool for high-pressure research because it can be used to study materials with very small amount in quantities (e.g., sample in a DAC at ultra high pressures) with perfect element selectivity (i.e. Mössbauer effort). On the other hand, in the last two decades, the laser heated diamond anvil cell (LHDAC) has been advanced greatly in heating capability, temperature measurement, and other related issues and has been widely used in X-ray diffraction and other studies. Using the LHDAC in the NRS experiment will enable us to study the magnetic and vibrational properties of materials at very high-temperature and high-pressure in a way no other technique could, thus bringing additional impact on relevant scientific research. Combining these two techniques is not straightforward, mostly due to the nature of long counting times for NRS experiments at current beam conditions. For example, a typical collecting time for a meaningful NRIXS spectrum at the 3-ID beamline at the APS is at least 4 to 6 h. So far, most LHDAC systems are only required to provide stable heating conditions on the order of minutes for *in situ* X-ray diffraction experiments. It is thus quite challenging to design an LHDAC system for NRS applications. Furthermore, the use of a high-resolution monochromator with meV bandwidth and avalanche photodiode (APD) timing detectors in NRS experiments requires a stable thermal environment in the experiment hutch and around the DAC. In particular, a heated DAC has to be thermally insulated to minimize the effects on the environment. All of the above conditions have to be taken into account when designing an LHDAC system for NRS studies. Here we describe a new double-sided LHDAC system deployed at 3-ID, APS, for the purpose of NRIXS and SMS studies under simultaneous high-pressure and high-temperature conditions.

The schematic diagram of the heating system at 3-ID is shown in Fig. 1. Figure 2 shows the setup of the NRS experiment at 3-ID. The system has been installed at 3-ID and has been successfully applied for experiments using both SMS and NRIXS techniques on various iron-containing materials. In addition, an on-line diffraction capability has been added to give the structural parameters of the materials under high pressure and high temperature. The details of the beamline and the experimental system will be described during the presentation.

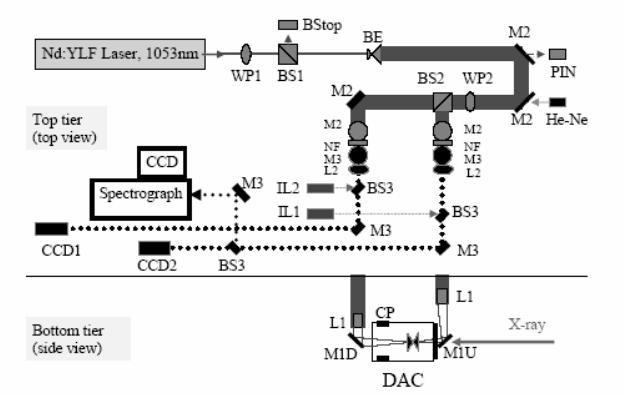

Fig. 1. Schematic of the double-sided LHDAC system at 3-ID, APS. WP1, WP2: waveplate; BS1, BS2: polarizing cube beamsplitter; BS3: 50/50 neutral beamsplitter; BStop: water-cooled beam stop; BE: zoom beam expander; PIN: photodiode; M1: beryllium laser mirror coated with gold or carbon mirror coated with silver; M2: dichroic mirror reflecting (> 99%) vertical polarized laser beam at 1053 nm; M3: Al-coated mirror; L1: apochromatic objective lens with focal length of 100 mm; L2: achromatic lens with 1000 mm focal length; NF: notch filter; CCD1 and CCD2: CCD cameras; CCD-Spectrograph: spectrograph and CCD for temperature measurement; He-Ne: alignment laser; IL1 and IL2: illuminators; CP: cooling plate for DAC.

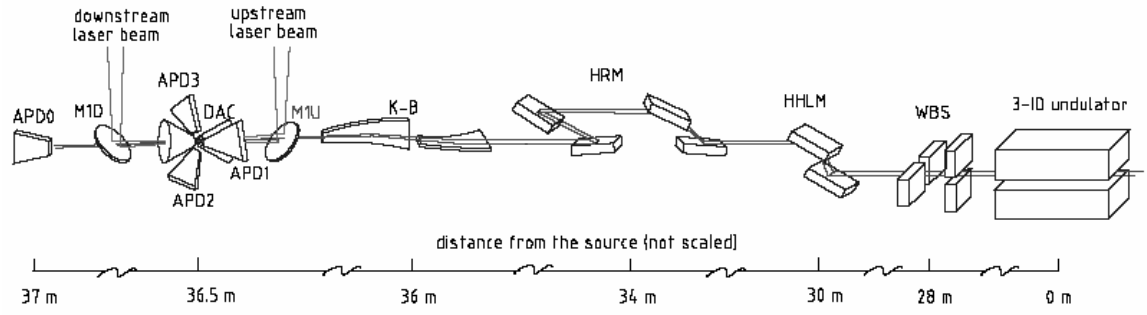

Fig. 2. Experimental setup for NRS under high pressure and high temperature. WBS: white-beam slits; HHLM: diamond high-heat-load monochromator; HRM: high-resolution monochromator; K-B: K-B mirror; M1U and M1D: laser mirrors; DAC: diamond anvil cell; APD: avalanche photodiode detector.

Acknowledgments

We thank Drs. J.F. Lin, G.Y. Shen, H.K. Mao, V. Prakapenka, M. Yue, M.L. River, and J. M. Jackson for their help during our LHDAC system construction and testing. Use of the Advanced Photon Source is supported by the U.S. Department of Energy, Office of Science, Office of Basic Energy Sciences, under Contract No. DE-AC02-06CH11357.

Author Index

ALATAS, Ahmet 54
ALP, Ercan E. 54, 66
AMULELE, George 47
ARAKAWA, Masashi 85
ASAHARA, Yuki 52
BASS, Jay 72
BOATENG, Nana 79
BORKOWSKI, Lauren 38, 45, 74
BROWN, D. 66
BRUNET, Fabrice 78
CALDWELL, Wendel 89
CHEN, Bin 51, 72
CHEN, Jiuhua 65
CLARK, Alisha 27
CLARK, Simon 88
DERA, Przemyslaw 38, 45, 47, 74
DING, Yang 40, 72
DOWNS, Robert T. 38, 47, 74
FIQUET, Guillaume 50
FUKAI, Yuh 75
FUKUI, Hiroshi 99
FUKURA, Satoshi 89
FUNAKOSHI, Ken-ichi 14, 52, 75, 78, 97, 99
GAO, Lili 72
GAUDIO, Sarah 27
GAVRILIUK, A.G. 66
GETTING, Ivan C. 95
HASKEL, Daniel 26
HIGO, Yuji 60, 87
HIRAO, Naohisa 10, 58
HIROSE, Kei 10
HUANG, Fang 72
HUSHUR, Anwar 47
INOUE, Toru 56, 60, 78, 87
IRIFUNE, Tetsuo 14, 30, 32, 56, 60, 78, 87, 90
ITO, Eiji 99
KAGI, Hiroyuki 22, 34, 85, 91
KATSURA, Tomoo 97
KHARLAMOVA, S.A. 66
KIKEGAWA, Takumi 32, 52, 56, 58
KNIGHT, Jason 88
KONDO, Tadashi 58
KONO, Yoshio 60, 87
KUNZ, Martin 88
LABENSKI, John 95
LATHE, Christian 18
LAVINA, Barbara 38, 45, 74
LEE, Peter 89
LEINENWEBER, Kurt 16
LERCHE, Michael 66, 72, 102
LESHER, Charles E. 27
LEU, Bogdan M. 54
LI, Baosheng 69, 82
LI, Jie 51, 72
LIERMANN, Hanns-Peter 45
LIU, Haozhe 89
LIU, Qiong 82
LIU, Wei 82
LORD, Oliver 88
LUNDSTROM, Craig 72
LYUBUTIN, I.S. 66
MANTHILAKE, Geeth 99
MANGHNANI, Murli H. 47
MAO, Ho-kwang 28, 36
MIYAHARA, Masaaki 58
MUELLER, Hans J. 18
MURAKAMI, Motohiko 10
NAGATOMO, Shouhei 34
NAKAJIMA, Yoichi 75
NAVROTSKY, Alex 69
NICOL, Malcom 38, 74
NISHIDA, Keisuke 52
NISHIJIMA, Masahiko 58
NISHIYAMA, Norimasa 13, 35, 90, 95, 97

ODAKE, Shoko 34, 91
OHFUJI, Hiroaki 30, 32, 34, 78
OHISHI, Yasuo 10, 58, 67
OHNISHI, Takeo 30
OHTANI, Eiji 52, 58
OKADA, Taku 32
OKUCHI, Takuo 34
OVCHINNIKOV, S. 66
PRAKAPENKA, Vitali B. 8, 54, 74, 93
PULLINS, Clayton 93
RIVERS, Mark L. 8, 13, 93, 95
SAID, Ayman H. 54
SAKAI, Takeshi 58
SAKAMAKI, Koichi 75
SAKAMAKI, Tatsuya 52
SANEHIRA, Takeshi 13, 78, 95, 97
SATA, Nagayoshi 32, 67
SCHILLING, Frank R. 18
SCOTT, Henry P. 72, 80
SHATSKIY, Anton 99
SHEN, Guoyin 12, 28, 54
SHINMEI, Toru 30, 78, 82
SINN, Harald 54
SINOGEIKIN, Stanislav 66, 74
SOIGNARD, Emmanuel 16
STRUZHKIN, V. 66
STURHAHN, Wolfgang 25, 54, 66, 72, 102
SUEDA, Yuichiro 78
SUGATA, Mitsuru 34
SUMIYA, Hitoshi 30, 34
SUTTON, Steve 8
SUZUKI, Akio 52
SUZUKI, Toshihiro 75
TAKAHASHI, Eiichi 75
TANGE, Yoshinori 14, 90
TERASAKI, Hidenori 52, 58, 97
TOELLNER, T. 66
TSUCHIYA, Taku 67
TSUNO, Kyusei 52
TULK, Chris A. 24
URAKAWA, Satoru 97
VOGEL, Sven C. 35
WADA, Kouhei 90
WALKER, David 88
WALTER, Michael 88
WANG, Jingyun 72
WANG, Liping 82
WANG, Luhong 89
WANG, Yanbin 13, 16, 27, 28, 35, 47, 95, 97
WANG, Yuchang 47
WANG, Yuejian 35
WEHBER, Michael 18
WEIDNER, Donald J. 69
WHITAKER, Matthew L. 82
XIAO, Xianghui 89
YAGI, Takehiko 32
YAMADA, Akihiro 56
YAMAMOTO, Junji 83
YAMANAKA, Takamitsu 36
YAMAZAKI, Daisuke 99
YANG, Wenge 28
YANG, Yunpeng 65
YOSHIMI, Isamu 56
YOSHINO, Takashi 99
YU, Tony 65
YUSA, Hitoshi 67
ZHAI, Shuangmeng 99
ZHANG, Jianzhong 35, 65, 69, 70
ZHANG, Xiaoyu 74
ZHAO, Jiyong 54, 66, 72, 102
ZHAO, Yusheng 35, 65, 69, 70